INTERACTIONS OF MICROMACHINES AND THE FLUID ENVIRONMENT

RAPID MIXING IN MICROMIXERS

by

SECK HOE WONG

A thesis submitted to
The University of Birmingham
for the degree of
DOCTOR OF PHILOSOPHY

Mechanical Engineering Department
School of Engineering
The University of Birmingham
April 2004

ABSTRACT

This Ph.D thesis investigates the mixing performances in a micro T-mixer and a cross-shaped micromixer incorporated with static mixing elements. The micromixers are fabricated on a silicon substrate sandwiched between a glass cover plate and a supporting polystyrene plate. Design calculations and computer simulations are performed to predict the flow properties and mixing performances in the micromixers. The mixing performance is characterized by mixing a commercial blue dye and de-ionized water. The results are further verified by mixing two chemical solutions that produce a distinct colour change when fully mixed. Complete mixing is observed in the micro T-mixers when the Reynolds number in the mixing channel is between 400 and 500. The corresponding times are in the range of one millisecond. Complete mixing is not observed in the cross-shaped micromixers investigated but significant improvement in mixing performance is nevertheless achieved. The rapid mixing in micro T-mixers is largely explained by the asymmetrical flow conditions at the inlets that result in swirling flow in the mixing channel that significantly enhances the mixing performance. The short mixing time achieved by the micro T-mixers makes them suitable for the analysis of fast reactions involving expensive samples.

ACKNOWLEDGEMENTS

My heartiest gratitude goes to my supervisors Dr. Michael Ward and Prof. Phil Prewett who provided me with the much needed guidance throughout my PhD research these three years. I would also like to thank them for the crucial discussions that we have had and the constructive criticisms that they made on my research work, but still giving me the freedom to chart my research direction.

I would also like to express my deepest appreciation to Prof. Christopher Wharton for his assistance in the preparation of dichloroacetyl phenol red (DCAPR) used as an indicator for mixing performance in the micromixers fabricated in this study. The preparation procedures and the measurement of second order rate constant of DCAPR described in Appendix B were carried out by Prof. Wharton.

I would also like to thank Mr. John Greenwood at GE Druck for providing a pressure transducer to be used in the experiments carried out in this research. My special thanks also goes to Mr. Barry Varney for his guidance in using the double sided mask aligner and wafer cutting tools in GE Druck. I also want to thank Mr. Alistair Bell at GE Druck for his assistance in calibrating the pressure transducer used in this research. The assistance from all the staffs at GE Druck while I was there is also very much appreciated.

I would also like to thank Dr. Patrick Bryant for his explanation on the working principle and operation of a Fourier transform and laser infrared spectrometer to me at the beginning of this research work and also for his help in providing me with some of the tools required in the experimental work.

The assistance and willingness of all my colleagues to share their skills in my day-to-day research are also very much appreciated as it has help tremendously in the progress of my research.

Last but not least, I want to thank my wife, my parents, brothers and friends for their continuous support and encouragements without which I could not have been able to achieve this much.

Dedicated to my beloved wife, Pei Kuan

TABLE OF CONTENTS

LIST OF FIGURES

LIST OF TABLES

NOMENCLATURE

Normal symbols

A	Cross sectional area, m^2
a	Width of a channel, m
b	Depth of a channel, m
C	Friction coefficient
c	Concentration of a species, moles/m^3
D	Diffusion constant, m^2/s
D_h	Hydraulic diameter, m
d	Characteristic length of flow in a closed channel, m
δ	Deviation of grey level from mean value across a channel
f	Friction factor
g	Gravitational acceleration, m/s^2
I_m	Intensity of mixing
I_s	Intensity of segregation
K	Loss coefficient
L	Length of a channel, m
P	Wetted perimeter, m
p	Pressure, Pa
Q	Volume flow rate, m^3/s
R_a	Average surface roughness, m
Re	Reynolds number
t	time, s
$\overline{u}$	Mean flow velocity, m/s
u	Velocity component in the X direction, m/s
v	Velocity component in the Y direction, m/s
w	Velocity component in the Z direction, m/s
x	Displacement in the X direction, m
y	Displacement in the Y direction, m
z	Displacement in the Z direction, m

Vectors

B	Body forces acting on a fluid element, m/s^2
V	Velocity vector, m/s

Greek symbols

Δ	Difference
ε	Surface height deviation from the mean plane, m
μ	Dynamic viscosity, Ns/m^2
ν	Kinematic viscosity, m^2/s
ρ	Liquid density, kg/m^3
σ	Standard deviation
ζ	Vorticity, rad/s
Δp_{loss}	Pressure difference due to losses, Pa

Subscripts

i	At the inlet
o	At the outlet

LIST OF PUBLICATIONS

Wong, S.H., Ward, M.C.L. and Wharton, C.W. (2004). 'Micro T-mixer as a rapid mixing micromixer'. *Sensors and Actuators B: Chemical*, 100, 359-379.

Wong, S.H., Bryant, P., Ward, M.C.L. and Wharton, C.W. (2003). 'Investigation of mixing in a cross-shaped micromixer with static mixing elements for reaction kinetics studies'. *Sensors and Actuators B: Chemical*, 95, 414-424.

Wong, S.H. Bryant, P., Ward, M.C.L. and Wharton, C.W. (2002). 'Investigation of mixing in a cross-shaped micromixer with turbulence inducing elements for reaction kinetics studies'. *Proceedings of the 16th European Conference on Solid-State Transducers*, Prague, Czech Republic, 431-432.

INTRODUCTION

1.1 INTRODUCTION

The clinical use of antibiotics since the 1940s has led to the cure for many infections caused by bacteria. Some of these antibiotics work by inhibiting the formation of the bacterial cell wall while others act by disrupting the protein synthesis or disturbing the replication of genetic materials in the invading organism. Although these antibiotics worked well in eliminating infection-causing bacteria in human body, some bacteria managed to mutate and gain resistance to the antibiotics under some circumstances. The issues of bacteria resistant to antibiotics have been emerging ever since the discoveries of antibiotics. But the problem was kept somewhat under control as new classes of antibiotics were discovered in quick successions in the early years (Neu, 1992). The problem is however compounded by the misuse and overuse of antibiotics over the years, which encourages the emergence of antibiotic resistant bacteria. When a patient fails to complete an antibiotic prescription, not all bacteria are eliminated. Those bacteria that survive mutate into something stronger and become resistant to that antibiotic. The same antibiotic that the patient took is no longer effective to cure the infection caused by those bacteria. A new antibiotic needs to be prescribed. The decrease in the rate at which new antibiotics are discovered over the past decade further aggravates the situation. Antibiotic resistant bacteria cause once easily treatable diseases such as pneumonia and tuberculosis to be untreatable while wound infections caused by bacteria resistant to antibiotics create complications in treating patients

in hospitals. Therefore, the discovery of new antibiotics is urgently needed to eliminate these bacteria and stay one step ahead of an outbreak.

There are four major mechanisms which are used by antibiotic resistant bacteria to neutralize the action of antibiotics: (i) by excreting enzymes that modifies or destroys the antibiotic, (ii) by preventing the antibiotic from reaching its target site, (iii) by altering the antibiotic target site and (iv) by acquiring a replacement metabolic step inhibited by the antibiotic (Towner, 1995). One of the enzymes excreted by antibiotic resistant bacteria that break down the β-lactam antibiotics like penicillin is β-lactamases. The understanding in the early events of the reaction between these enzymes and antibiotics is very valuable in the discovery of new antibiotics. This can be studied through spectroscopic methods particularly through Fourier Transform Infrared Spectroscopy (FTIR). Currently, conventional mixers are able to prepare a homogeneous mixture of an antibiotic and a target enzyme for FTIR within microseconds (Regenfuss *et al.*, 1985) and one such mixer is being marketed by Bio-Logic Science Instruments. Only with such a short mixing time can the very early events of the reaction be resolved. Conventional mixers are fine if both antibiotics and enzymes are available in abundance. This is however not the case for the enzymes involved in the study of antibiotic resistance, which are available only in very low concentrations. The use of conventional mixers that are large and which consume a large amount of the reagents in every analysis is uneconomical and is therefore not suitable.

The reaction kinetic studies of target enzymes and antibiotics for drug discovery therefore demand an unconventional mixer that is able to rapidly mix the two reagents for analysis, using only tiny quantities of the reagents. Microfluidics has the advantage of being very small, therefore consuming only a tiny fraction of what would otherwise be consumed by a conventional mixer. The fact that silicon, which is a material much used in microfluidics, is transparent to infrared light making the idea of a silicon micromachined

micromixer incorporated in FTIR analysis even more attractive. Silicon microfabrication techniques provide an ideal technology for the manufacture of such an unconventional mixer mentioned above. The scale and complexity of the required structure, together with the transparency of silicon to infrared light, suggests an application marriage to stopped flow kinetics studies.

1.2 AIM AND OBJECTIVES

The aim of this study is *"to investigate the feasibility of rapid mixing in micromixers intended for fast reaction kinetics studies"*. To fulfil this aim, the micromixer must be able to completely mix two liquids within a millisecond. The amount of the two liquids used shall be in the range of microlitres and the substrate material of the micromixer shall be silicon to ensure its compatibility with infrared spectroscopy.

1.3 THESIS OVERVIEW

This Ph.D thesis consists of ten chapters. The first chapter introduces the readers to the background of the problem arisen from antibiotic resistance in bacteria and the need to produce a rapid mixing micromixer to assist in the discovery of new antibiotics. The aim and objectives of this study are also outlined in this chapter. In the second chapter, the historical background of microfluidics and its economic impacts are described. This is then followed by a review on similar work carried out by other investigators in the search of a high performance micromixer. Many micromixers have been designed and investigated. They can be classified into a two main categories, namely active and passive micromixers. The review is presented according to these categories. In Chapter 3, the fundamental fluid flow theories used in analyzing and characterizing the mixing performance of the micromixers fabricated in this study are described. This is then followed by a description of the three basic processes

making up the mixing mechanism between two liquids. The mixing concepts applied in achieving rapid mixing in this study are also described in the beginning section of Chapter 4.

In this study, the two micromixers intended to be used as rapid mixing micromixers are designed, fabricated and tested. From Chapter 4 to Chapter 7, the design, fabrication and testing procedures of the micro T-mixers and their experimental results are presented. Chapter 4 introduces the design of the micro T-mixer investigated in this study followed by some design calculations and computer simulation work performed to predict its mixing performance. A comparison between computer simulation results and design calculations is also presented. Chapter 5 and Chapter 6 describe the practical aspects of this study where the respective fabrication and testing methods are described in detail. The mixing performance in the micromixers is characterized first by mixing a blue dye and de-ionized water, then by the mixing of two chemicals that give a distinct change in colour when they are completely mixed. The mixing process in the micromixers is observed under a microscope fitted with a video camera that allows images of the mixing process to be capture and analyzed. The images are analyzed by a computer program to determine if complete mixing is achieved based on the colour uniformity of the mixture at the outlet of the micromixers. The mixing performance of the micromixers is characterized by the Reynolds number of flow in the mixing channel so that the mixing performance can be compared with results from other experiments.

Chapter 7 presents the experimental results obtained from the mixing experiments performed in micro T-mixers of different dimensions and compares the mixing performance in the micromixers at various Reynolds numbers in the mixing channel. Further computer simulations are carried out after testing the micromixers to gain better insight in the mixing process in the micromixers. Similar work on the cross-shaped micromixer investigated in this study is collectively described in Chapter 8. The design, simulation, fabrication, testing and

experimental results of a cross-shaped micromixer with static mixing elements introduced in its mixing channel are presented. Chapter 9 presents a discussion on all the results and observations obtained from the two micromixers in the study. Some explanations for the observed mixing performance in the two micromixers are presented and are further supported by computer simulation results. It also compares the results obtained in this study and those obtained by other investigators to distinguish the similarities and differences between the studies. This study is finally concluded in Chapter 10 where the main findings obtained from this study are emphasized. Some possible future work is also presented.

1.4 CLOSURE

This introduction section makes us aware of the urgent need to discover new antibiotics in the guerrilla warfare against the bacteria which are fast gaining resistance to most of the antibiotics already discovered. As the enzymes involved are rare, the need for an unconventional mixer that can rapidly mix minute amount of target enzymes and antibiotics for analysis is vital if the reaction kinetics between enzymes and antibiotics are to be understood to help in drug discovery. A micromixer fabricated using silicon microfabrication technology is considered the most suitable candidate for fulfilling this need. The aim and objectives of this research are outlined followed by an overview of this Ph.D thesis according to each chapter. Although the main motivation of this research is to produce a rapid mixing micromixer for reaction kinetics studies between enzymes and antibiotics, the study of protein folding that can shed light to the cause of a disease also desires a rapid mixing micromixer (Roder and Shastry, 1999). Therefore, this research has the potential of opening up many new possibilities in the field of BioMEMS.

A REVIEW ON MICROFLUIDIC SYSTEMS

2.1 HISTORICAL BACKGROUND OF MICROFLUIDICS

The term *microfluidics* originates from *fluidics* – a hybrid technology introduced in the late 1950s that fused the field of fluid mechanics and control systems. While the conventional fluid flow engineering is mainly concerned with harnessing fluid power economically, fluidics uses fluids both as an informational processing and control medium and as a means of transmitting power. By early 1970's, hundreds of fluidics patents were registered in the United States (Kirshner and Katz, 1975) and logic components in fluidics, equivalent in characteristics to their electronic counterparts, were designed and fabricated. These components can perform logic functions such as OR-NOR gates and AND gates as well as flip-flops and amplifiers. Samples of fluidic components and the working principle of a bi-stable memory fluid logic component are shown in *fig. 2-1*. Depending on the presence of a pulse of air from the either control ports, the confined jet of air from the supply nozzle is deflected to one of the outlet ports signalling one of the two stable states. Wall reattachment of the confined jet assisted by the attachment wall causes the jet to maintain its flow path until another pulse of air is applied to change its state. By connecting these individual fluidic components together, control and actuating systems can be built that respond in the same way as electronic components. Fluidic components have no moving parts, so they are more robust and reliable, simpler and resilient to harsh operating environments. Therefore, fluidics found some applications in the areas of aerospace and automation (Bouteille, 1973).

However, they have a much slower response and they are larger than their electronic counterparts. The popularity and availability of electricity as a source of energy compared to compressed gas also contribute to electronic components being in favour. All these have eventually put an end to the flourishing era of fluidics in the 1960s.

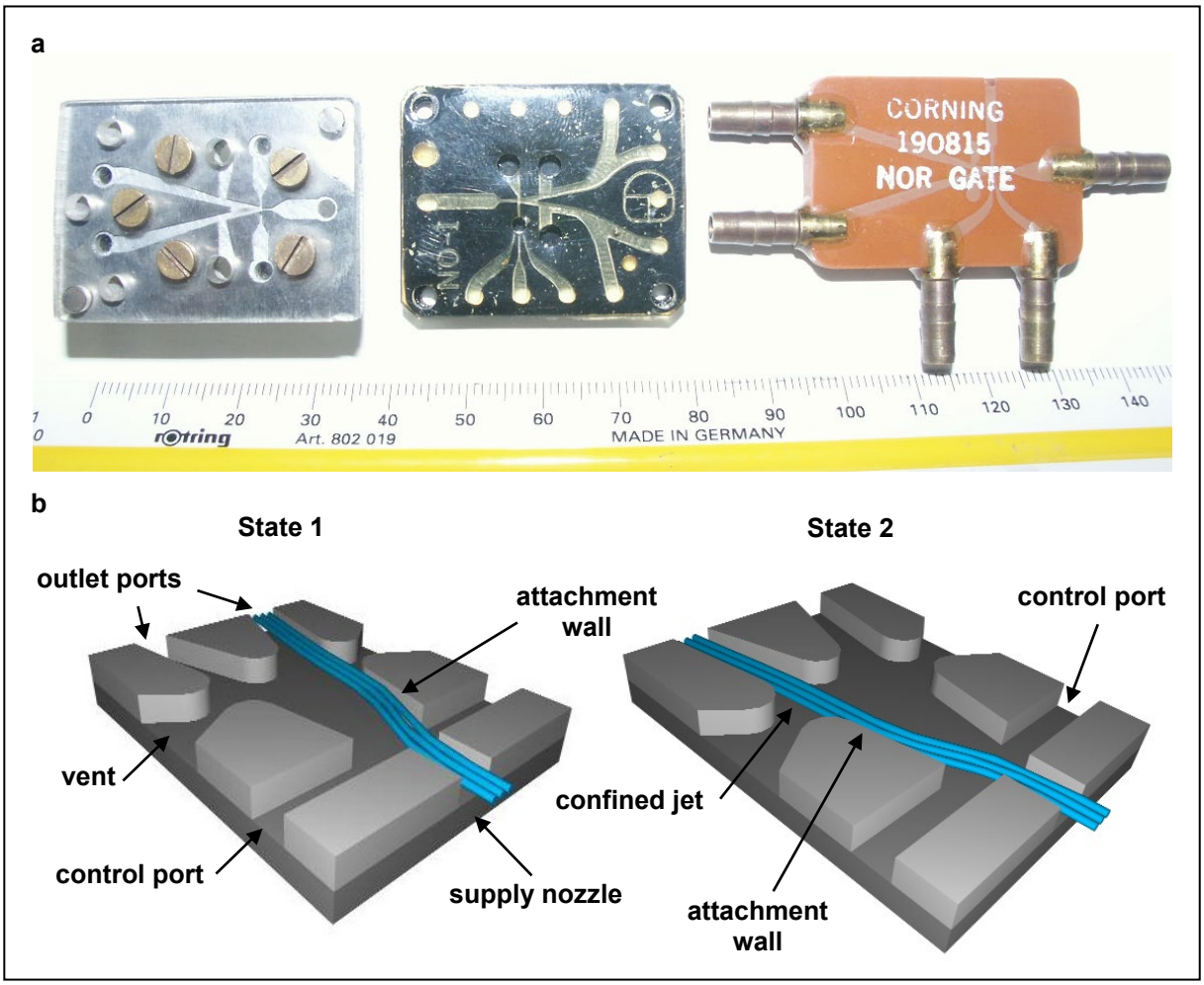

Fig. 2-1 *(a) Samples of some fluidic components (b) A bi-stable memory fluid logic component. The principle of wall reattachment of jets is extensively utilized in the design of fluid logic. Two states are obtainable in the fluid logic component shown above, depending on the control jet.*

In the advent of microelectromechanical systems (MEMS) in the 1980s, silicon microfabricated channels were made with the aim to produce high capacity heat sinks for microprocessor chips (Tuckerman and Pease, 1981). Liquid was used as a medium for heat removal. This marked the beginning of using fluids in MEMS devices. Fluidics reemerged in the early 1990s but has since lacked its originality. A few microscale fluidic components were fabricated but they were just a scale down of their larger ancestors (Zdeblick *et al.*,

1990). Meanwhile, microelectromechanical components for fluid handling continued to be developed for all sorts of applications. As these components also deal with the flow and control of fluid in microscopic systems, they are therefore classified as microfluidic systems. Far from the constraints of the definition for fluidic systems in the 60's, microfluidics encompasses a wide range of operating principles and applications from micro chemical analysis systems that carry out analyses with only minute amounts of samples to arrays of micro-nozzles used in the print head of many commercial inkjet printers.

2.2 AN INTRODUCTION TO MICROFLUIDICS

Microfluidics is defined as everything involving the usage of fluid in the operation of a MEMS device. Microfluidic components are not only some miniaturized versions of valves, pumps, mixers, reaction chambers, etc. that are encountered in chemical engineering processes. They, for example, also involve surface properties modifications for the detection of species in a fluid, enabling biochips with different functionalities to be produced. The possibilities that can be created from microfluidics are literally unlimited. The integration of microfluidic components onto a single chip enables the miniaturization of large equipment into hand-held portable devices. The wide application area of microfluidics has the potential of making a quantum leap in the lifestyle of the general human population, especially in the health care segment. So how exactly does microfluidics do that? The impacts brought about by microfluidics are described here.

There are many tasks which microfluidic devices can accomplish. They can mix as well as separate two species from a mixture. They can cause fluid flow in the devices with a micropump and control the movement of the fluid with a microvalve. They can measure the rate of flow of the fluid in microchannels and also detect the presence or concentration of a particular species in the fluid. They can also provide optimum conditions for chemical

reactions taking place in the devices to produce high yield. They perform these functionalities with high reliability, speed and accuracy but with only a tiny amount of the sample.

The integration of various microfluidic components onto a single chip is very attractive and important as it results in the fabrication of more compact devices, which are able to perform more functions on a single device without the need of conventional interconnections that tend to create more dead volume, slower response and incompatibilities. Names like lab-on-a-chip and micro-total-analysis-system (μTAS) are given to self-contained chips where complete procedures of an analysis can be performed on-board. Some of these products have already reached market, such as a portable blood analyser produced by iSTAT Corporation that is capable of performing a range of blood tests. Disposable cartridges containing microchannels, reservoirs and biochips are used where only a drop of blood is sufficient to carry out the tests. Glucose level and the levels of some minerals in a blood sample can be detected within minutes. The information can be stored to enable trends to be monitored. Such devices are very valuable for paramedics, doctors, as well as for the patients.

While most of the portable clinical diagnostic tools that are currently in the market target health professionals, the potential for these devices to reach the general public is very real. Kricka (2001) predicted that in the near future, health consumers will be able to have access to a range of health diagnostic tools to perform self-diagnosis and as a result revolutionizing the health industry today. Highly complex clinical testing, which is currently performed only in large clinical laboratories will become available in non-laboratory settings with a personal laboratory unit incorporating lab-on-a-chip technology without the need for skilled workers. Test results that are taking days to obtain can be collected within minutes while time and money spent in logistics can be saved. This has a very significant impact on

the cost of health care and the level of health awareness of the public, which can be likened to the impact of personal computers today. This gives an idea of how large the potential market for integrated microfluidic devices can be.

With good integration of microfluidic components, the amount of sample used in performing tests can be greatly reduced. Although this is mainly attributed to the size of the device, the fact that only one device is all that is needed for an entire analysis results in no sample loss that usually happens when transferring samples in conventional analysis. Savings in terms of laboratory space can be realized with the use of integrated micro analytical systems as these systems have the size of a desktop computer. The laboratory space can then be utilized to a better extent while the costs of setting up an advanced clinical laboratory can be reduced.

Wearable or implantable devices such as drug delivery systems for automatically delivering a measured amount of medication according to need can be made possible with microfluidics. With its inherently small size, it can be conveniently carried by patients. Such drug delivery systems are more efficient than the existing administration of drug in high doses that last for a few hours, which may cause wastage and addiction. A micro drug delivery system may consist of a biosensor that analyzes the body fluid of a patient such as blood or sweat to detect the level of drug in his or her body. Depending on the result, the microelectronic control system activates the micropump to deliver drugs from a reservoir and at the same time measures the amount of drug that has been delivered into the body by using a micro flow sensor. In such a feedback system, drugs can be administered according to one's need and the risk of shock to drugs can be reduced.

Of course microfluidics is not just limited to devices for use in medical and health care applications. One of the most successful microfluidic devices in the market is a micromachined micro-nozzle array found in the print head of inkjet printers. Such invention

has delivered affordable colour printing facilities to households and small businesses. Environmental sensors used in the detection of the level of some hazardous particles in the atmosphere or in water samples are also based on microfluidic technology. Microfluidics is also acting as the enabling technology for many researches in life science without which the progress of some scientific advances is dramatically hampered. The potential of microfluidics is only limited by human's imagination. Some economics analysts see huge growth in MEMS companies producing microfluidics chips. Their applications are so numerous and far reaching and their impacts on the world economy in the years to come cannot be underestimated.

2.3 ECONOMIC IMPACTS OF MICROFLUIDICS SYSTEMS

The impact of microfluidic systems on the world economy is going to be profound. The estimated market for microfluidics chips in the year 2000 was reported by MSTNEWS to be 400 million USD and it is forecasted that the revenues from the sales of microfluidic products are to grow by more than 50% a year through 2007 (Rubenstein, 2003). The high predicted growth from the sales of microfluidic system based products reflects the increasing number of applications for microfluidics. In the first generation of products based on microfluidics, it was more to the technology itself taking centre stage. Inkjet print heads being one of the examples. Although a large fraction of the microfluidics' market until recently is contributed by the use of microfluidic components for inkjet printing, it is expected that this proportion is going to decrease as the market for inkjet printing is approaching maturity. The continuous phenomenal growth of microfluidic systems in forecasts is based on the second generation of microfluidic systems where they are acting as the enabling technology for many other fields such as biotechnology, medical applications,

drug discovery and ecological monitoring systems. The vast application area of microfluidics is fueling its rapid growth.

The other reason why microfluidics is expected to see substantial growth is the business model adopted by MEMS companies, which has a “razor and razor blade” analogy. Since contamination of sample must be prevented in microfluidic systems from one analysis to the other, the preferred solution is to produce disposable microfluidics chips, where the chips are high margin consumables to an already installed system. These microfluidics chips are batch produced to ensure low unit cost. The need to replace the used microfluidics components by its users ensures continual demand, thus steady revenue for the manufacturers.

The market for microfluidics diagnostic devices incorporated with biochips has the potential of encompassing the general public besides health care workers. This is also the reason for the upbeat forecasts on the future of microfluidics devices that they enjoy today. If the microfluidics devices for self diagnosis are as common as desktop computers, the economic impacts of microfluidics on the companies producing it and on the world as a whole will be very significant.

2.4 MIXING WITH MICROMIXERS

There is a need to mix two or more liquids together to produce a homogeneous mixture, particularly for drug discovery, medical applications and life science researches. It is a very important sample preparation step prior to a chemical or biochemical reaction taking place in the microfluidic chip. A well mixed sample improves the accuracy of an analysis as it removes the property gradients within the mixture. Conventionally, the amount of chemical or biological samples used by a mixer is often more than sufficient for an analysis to be

performed and for its results to be obtained. This has obviously resulted in inefficiencies and wastage especially in the case for rare and expensive samples.

As such, the need to mix two or more liquids together in the smallest possible amount is crucial because it greatly reduces the cost of analysis with expensive drugs. For example, consider an existing mixer that requires 0.5 ml each from the reagent and sample to produce a homogeneous mixture, a micromixer having a mixing chamber of 100 μm sides will enable one million analyses to be carried out with the same amount!

Other than the issue of the amount of samples used in mixing, the speed of mixing is also very important. In some analyses, it is not only the final reaction products that are important but also the intermediate products. This allows the reaction mechanism to be studied. These intermediate stages can be as short as a few microseconds (Roder and Shastry, 1999). Therefore, in order to detect the various intermediate products and subsequently understand the reaction mechanism, a micromixer that can rapidly mix two or more liquids together is very much desired.

Micromixers based on different functional principles have been investigated in the literature and they can generally be classified into two main categories – active and passive micromixers. In the category of active micromixer, are the mechanical and non-mechanical micromixers. In the category of passive micromixer, there are diffusion micromixers and static micromixers. The work that has been done so far in advancing each type of micromixers is described in the following sub-sections.

2.4.1 ACTIVE MICROMIXERS

Active micromixers are micromixers that require some form of power input to effect mixing besides causing fluid flow. Active micromixers allow the user to have extra control over the rate and degree of mixing, thereby providing an additional degree of flexibility to these

micromixers. The development of active micromixers lags behind passive ones as active micromixers are more complicated in its design and fabrication process. The number of active micromixers that have been produced and tested is fewer than passive ones.

Mechanical micromixers achieve mixing through the use of moving elements. These moving elements cause the fluid to flow in a random manner in a chamber or microchannel. This results in the mixing of two or more species in the fluid. All mechanical micromixers produced so far use external vibration to enhance the mixing of fluids. Yang *et al.* (2001) produced and investigated a mechanical micromixer that mixed two types of liquids. The two liquids were fed by external pressure into a mixing chamber where they were mixed by a vibrating membrane that formed the top of the chamber. This membrane was actuated by a piezoelectric ceramic such as a lead-zirconate-titanate crystal as shown in *fig. 2-2*. The piezoelectric material was excited by a potential difference of 50 V at ultrasonic frequencies. The evaluation of mixing in the chamber was carried out through fluorescence method whereby water and uranine, a water-soluble fluorescein-sodium salt, were mixed together and the extent of mixing was analyzed by a fluorescence microscope. It was observed that there was no linear relation between excitation frequency and mixing ability and mixing efficiency showed no direct relation to the diaphragm displacement. Complete mixing was achieved after about 2 seconds. The area of mixed fluid was found to increase with increasing power input but an increase in power input did not achieve faster mixing.

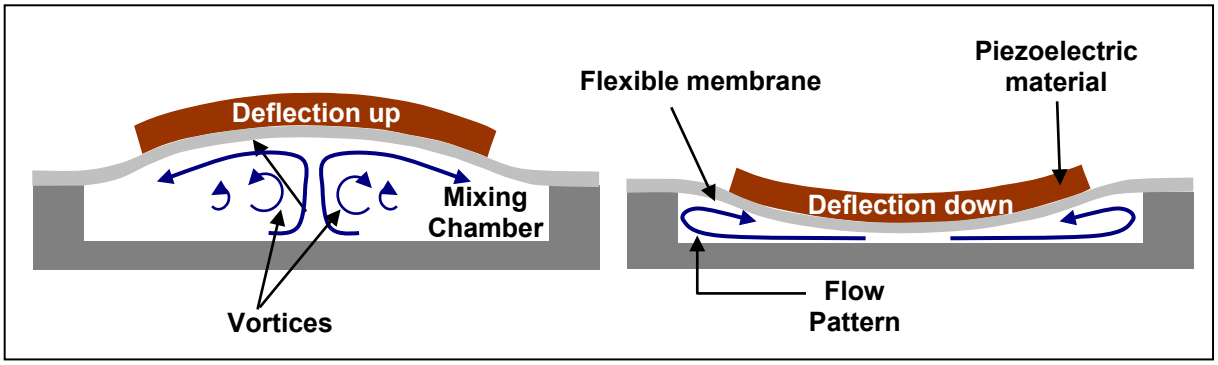

Fig. 2-2 *The sectional view of an ultrasonic micromixer. It consists of a thin membrane above the mixing chamber that causes mixing by ultrasonic vibration from the lead-zirconate-titanate (PZT) crystal.*

Andersson *et al.* (2001), while investigating their valve-less diffuser micropump, discovered that a diaphragm micropump actuated by a piezoelectric disc produced mixing in the chamber. Their micropump has the configuration similar to that shown in *fig. 2-2*. Polystyrene micro-beads were introduced into the pumping chamber where vortex-like flow patterns were observed in the chamber indicating mixing. Mixing in the microscale can also be achieved through surface acoustic waves (SAW) generated from a piezoelectric material. RF power is applied to these devices causing the piezoelectric material to agitate at high frequencies. The SAW propagate to a chamber containing the liquids to be mixed. It was shown by Vivek *et al.* (2000) that the agitation was sufficient to cause significant liquid motion that could lead to mixing. Toegl *et al.* (2003) on the other hand produced a SAW micromixer for mixing DNA samples in gene expression profiling assays.

Mixing can also be achieved in an active micromixer without the use of any moving elements. These micromixers are classified as non-mechanical type micromixers. Bau *et al.* (2001) produced a minute magneto hydro dynamic mixer that can stir an electrolyte solution in a conduit by applying potential difference across pairs of electrodes in the conduit with the presence of a magnetic field. The Lorentz force generated from the interaction of electric current and magnetic field resulted in mixing of species in the solution. By creative arrangement and varying potential differences of the electrodes, the flow of the solution in the conduit could be controlled. Tsai and Lin (2002) also produced an active micromixer that achieved mixing through oscillatory flow of one of the liquids created by a thermal bubble micropump. In the experiment, isopropanol was injected at an angle into the flow of a blue dye by a thermally actuated bubble micropump. The expansion and collapse of bubbles in the micropump created wavy interface between the two liquids. The mixing performance became optimum when the wavelength of the wavy interface is equal or shorter than the diffusion length for the liquids. Niu and Lee (2003) showed the feasibility of producing an active

chaotic micromixer through numerical studies. The operating principle of the micromixer investigated by them was similar to that produced by Tsai and Lin. The micromixer consisted of a microchannel where the two liquids to be mixed were flowing side by side under creep flow. A number of pairs of side channels were connected to both sides of the microchannel. By applying positive and negative pressured on the pairs of side channels, it was shown that stretching and folding of the liquid interface can resulted in chaotic mixing in the microchannel.

2.4.2 DIFFUSION MICROMIXER

Diffusion micromixers belong to the category of passive micromixer. Unlike active micromixers, they need no extra power input apart from that for causing fluid flow. Although mixing by diffusion is not practical in the macroscale, some degree of success has been achieved in the microscale as the distance involved in diffusion is short. Much work has been carried out in producing micromixers that employ diffusion as the means of mixing. This is because of its relatively simple fabrication procedures and operating principles.

According to the fundamental law of diffusion, the time it takes for a molecule to diffuse over a distance x is proportional to the square of x and inversely proportional to the diffusion constant, D, of the diffusing compound.

$$t = \frac{x^2}{D} \tag{2-1}$$

As the distance required by the molecules to travel between two points to achieve complete mixing is much smaller in microfluidics devices, the mixing time, t, is considerably shorter, making diffusion mixing in micromixer much more attractive. To illustrate the speed of mixing attainable with diffusion mixing, consider a micromixer with a diffusion length, x, of 10 μm, and a diffusion constant for a common biological sample of 10^{-11} m^2s^{-1}, the mixing

time is a short 1.6 second. This is sufficient for a simple, easy to manufacture and reasonably fast micromixer for less demanding applications.

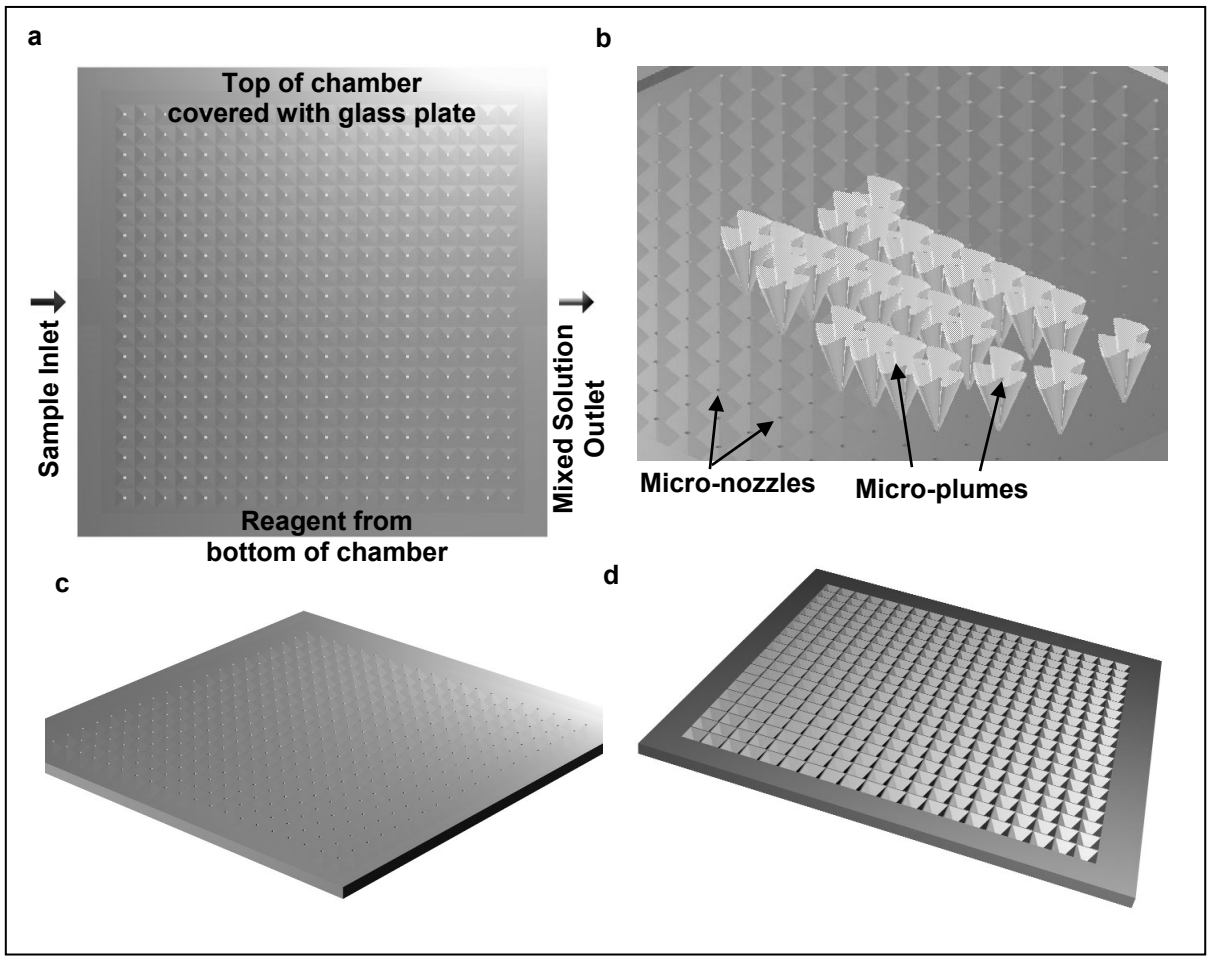

Fig. 2-3 *Mixing by diffusion. a) and b) Micro-nozzles at the bottom of the mixing chamber inject one liquid into the chamber containing another liquid forming many micro-plumes that shorten the diffusion length and hence mixing time. c) and d) show the front and back side of the wet etched micro-nozzles.*

An early work on diffusion micromixer was by Elwenspoek *et al.* (1994) who described some of the microfluidics components that made up an integrated microfluidics system. They did a feasibility study on a micromixer that was based on diffusion theory. They investigated a micromixer consisting of a mixing chamber, the bottom of which had an array of 400 micro-nozzles as shown in *fig. 2-3*. These micro-nozzles were only 20 μm in size and positioned very closely in rows, 10 to 100 μm apart. The mixing chamber above the nozzles was filled with a sample liquid. The other liquid was injected into the sample liquid through the micro-nozzles forming many micro-plumes. As the distance between these

micro-plumes was small, the diffusion length was greatly reduced, resulting in a mixing time of just 1.2 seconds.

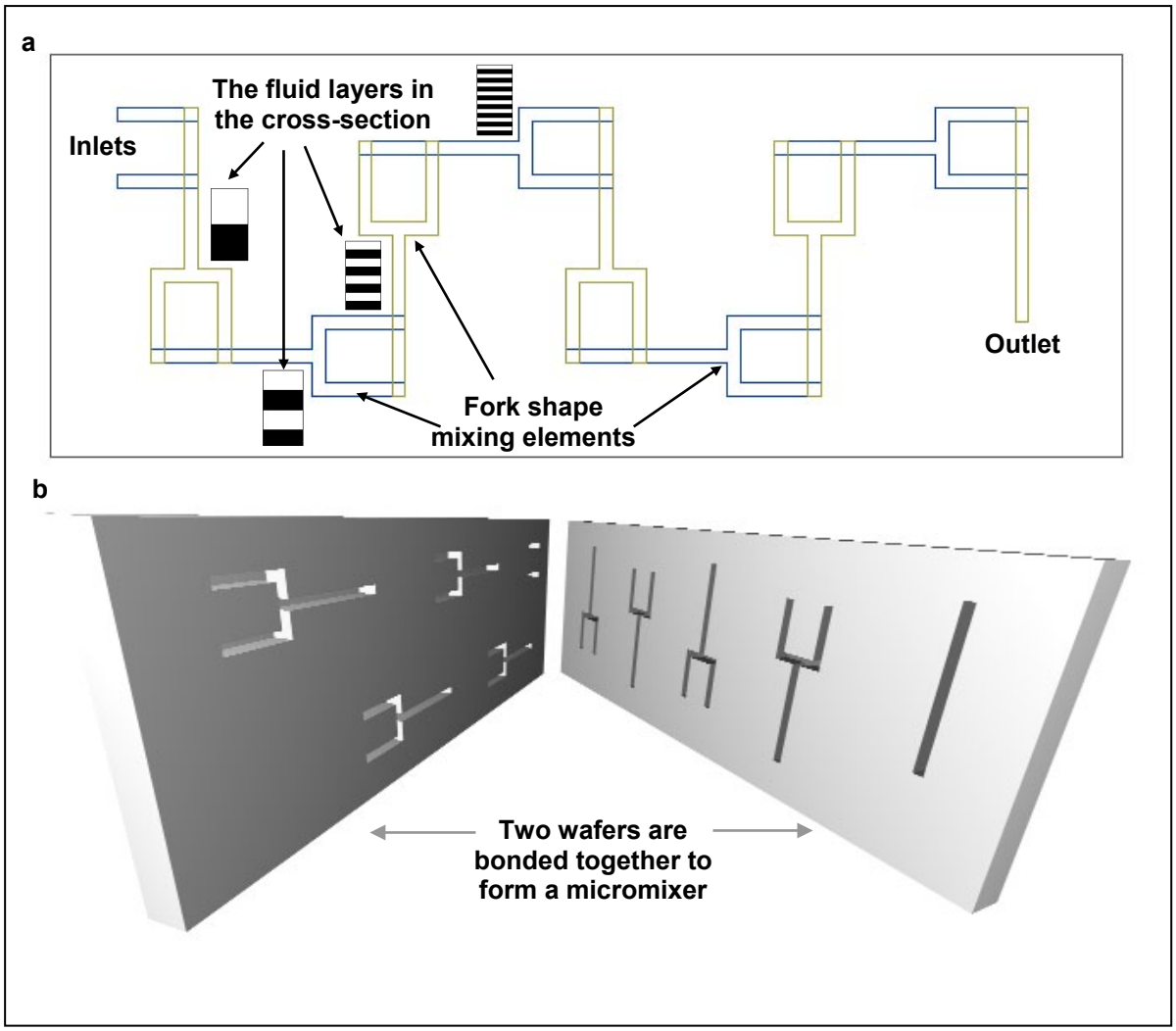

Fig 2-4 *Top view a) and three-dimensional view b) of the mixing unit investigated by Schwesinger et al. The fork shape mixing elements on the two wafers together formed a channel network that effect mixing.*

Schwesinger *et al.* (1996) investigated another type of micromixer often called the 'Möbius-type' mixer that operated on a cut-and-slice principle. In their micromixer, the layers of the two liquids were separated perpendicularly to the boundary layer and reunited again in such a way that twice the number of fluid filaments was formed. The mixing unit that was fabricated consisted of a number of fork-shaped mixing elements. The mixing elements were etched on the surface of two silicon substrates at different positions but formed a network of channels when the two wafers were bonded together as shown in *fig. 2-*

4. The number of mixing elements in a mixing unit determined the degree of mixing achieved.

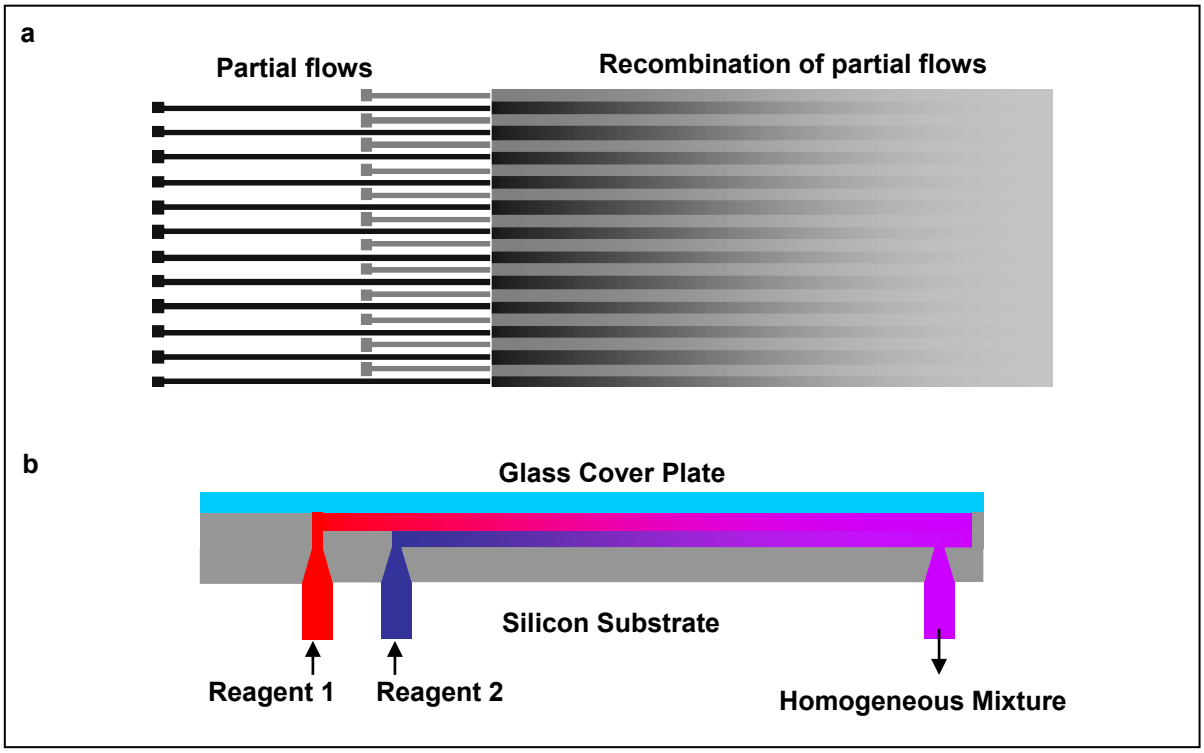

Fig. 2-5 *a) Diffusion mixing is achieved by separation of main flow into a number of partial flows and subsequently recombining them. b) Diffusion mixing is achieved by the lamination of two layers one on top of another.*

Another design of diffusion micromixers adopted by Erbacher *et al.* (1999), Koch *et al.* (1998; 1999a) and Hessel *et al.* (2003) involved separating the main flows of the two different liquids to be mixed into several partial flows, and subsequently recombining them in such a way that on both sides of each of the partial flow were the partial flows of the other liquid to be mixed as shown in *fig 2-5a*. Diffusion occurred at the interfaces between the two liquids during recombination. The diffusion length of these micromixers can be adjusted by varying the width of the partial flows and so varying their mixing times. The mixing performance can also be improved by focusing the recombined stream into a narrower channel (Hessel *et al.*, 2003). Another similar method of diffusion mixing described by Koch *et al.* (1998), Voldman *et al.* (2000) and Hinsmann *et al.* (2001) was the lamination of two

liquid layers one on top of the other as shown in *fig. 2-5b*. The depth of the channel was made very small, at about 10 μm for that produced by Koch *et al.*, so that complete mixing can be achieved within a relatively short time.

Knight *et al.* (1998) fabricated a diffusion micromixer that was shown to mix two liquids in microseconds using only nanolitres of the liquids. The micromixer had fluid channels the shape of a cross. A liquid flowing into the mixer through the microchannel in the middle collided and mixed with another liquid from the two side-channels. A nozzle was incorporated at the junction for focusing the main flow after leaving the microchannel in the middle. The main flow was squeezed by the two side flows into a very narrow layer of less than 2 μm enabling diffusion mixing to take place. A channel width of 10 μm was used resulting in a very low liquid consumption rate of 5 nl/s and a mixing time of 20 μs.

A simple diffusion micromixer developed by Veenstra *et al.* (1999) consisted of a microchannel with two inlets and two outlets. Two different liquids from the two inlets flowed into the microchannel where they mixed by diffusion. The width at the mixing channel of the micromixer was made much narrower, greatly reducing the diffusing distance and hence mixing time. However, it was a compromise between mixing time and pressure drop over the narrow part of the channel. The minimum possible channel width was limited by the maximum pressure drop that can be overcome by the syringe pumps that drove the liquids. The length of the narrow part of the mixing channel was simply determined by the diffusion time and the flow rate of the system. The mixed liquids collected separately from the two outlets were compared by measuring the concentration of the liquids. Complete mixing was considered achieved when the similar concentrations between the two liquids were obtained.

The micromixer designed and fabricated by He *et al.* (2001) was based on the principle of packed-bed mixers. While a packed-bed mixer depended heavily on transchannel coupling, a process by which liquids mixed when adjacent streams merged after passing around particles in the bed, the improved micromixer enhanced lateral mixing by selective void strategy, where a zigzag microchannel was connected by many narrower microchannels across each length between bends. It was found that the mixing of two streams of different liquids that came together was accomplished after a length of only 200 μm in the micromixer, corresponding to a mixing time of 0.67s, compared to 3000 μm under the same conditions in an open channel. Gobby *et al.* (2001) performed computational fluid dynamics simulations for the mixing of oxygen and methanol in a micro T-mixer. The mixing simulated was mainly due to diffusion process as the diffusion constants for gases were much higher than liquid and the Reynolds number of flow in the mixing channel was below 20. Although the mixing in the micro T-mixer simulated by Gobby *et al.* is mainly by diffusion, micro T-mixers have also been used as a static micromixer, which will be described later. Micro T-mixers of various aspect ratios, mixing angles and mixing velocities as well as with a throttling junction were each simulated to investigate their effects on the mixing length in the mixing channel. It was found that increasing the aspect ratio with constant channel width resulted in a non-monotonic influence on mixing length while increasing the aspect ratio with constant hydraulic diameter resulted in a shorter mixing length. The mixing angle was found to have little effect on the mixing length and a lower inlet flow rate resulted in a shorter mixing length. A throttling junction was observed to result in faster mixing.

All the micromixers that mix by diffusion described above do not contain any moving components in them. The fabrication procedures for these micromixers involve simple designs and common process steps that are relatively simple to carry out such as dry or wet

etching and anodic bonding. The ease of fabrication makes these micromixers easily integrated with other microfluidics components such as micropumps and microvalves.

2.4.3 STATIC MICROMIXERS

There is another type of passive micromixer that does not utilise diffusion as the sole means of mixing. Diffusion only plays a minor part in the mixing process. These micromixers are classified as static micromixer, which achieve mixing through induced convection in the flow. Due to the small width of the channels, the Reynolds number of flow in microchannels rarely exceeds 1000. The flow of liquid in microchannels is therefore laminar in most cases. Mixing by turbulence through turbulent flow that is usually encountered in macroscopic static mixers cannot be emulated in static micromixers. Nevertheless, convection and chaotic advection can be induced in the flow of liquid through modification of the geometry of the microchannels. These micromixers achieve mixing through secondary flow, vortices generated as a result of separation of boundary layers or through breaking up, stretching and folding of the liquid. In the rarest case, mixing by turbulence is utilised. A number of micromixers that use these principles to achieve mixing are described here.

One of the earliest efforts to produce micromixers in this category is by Bökenkamp *et al.* (1998) who attempted to achieve rapid mixing with micro T-mixers fabricated on silicon. Two T mixing elements were connected back to back forming a micromixer with three inlets and an outlet. This enabled three samples to be mixed in two stages at the two junctions. A mixing time of 110 μs was achieved by the micro T-mixer for the basic hydrolysis of phenyl chloroacetate into phenol and chloroacetate. It was observed that complete mixing effected by turbulent mixing could only be achieved with a flow rate of above 0.5 ml/s, which was corresponding to a Reynolds number greater than 1000. Relatively large microchannels with cross-sectional dimensions of 500 μm were used in their

micromixers in order to achieve high Reynolds number of flow required by mixing with turbulence. This together with the work presented by Gobby *et al.* represents the two extremes within which a micro T-mixer can operate, depending heavily on the velocity of flow in the micro T-mixer. When liquids instead of gases are to be mixed and when smaller microchannels are used in a micro T-mixer, mixing is effected between the two extremes where convection plays a major role in the mixing process as demonstrated by Kockmann *et al.* (2003), Engler *et al.* (2003) and Hoffmann *et al.* (2003). Kockmann *et al.* and Engler *et al.* carried out numerical studies on mixing in a micro T-mixer and Y-shaped micromixers. Kockmann *et al.* highlighted the three regimes of flow in the mixing channel, namely strictly laminar flow, vortex flow and engulfment flow depending on the Reynolds number of flow in the mixing channel. Reynolds numbers of flow of up to 310 were simulated. It was shown that at high flow velocity, break up of symmetry in the flow field occurred resulting in the so-called engulfment flow at the junction, which is characterized by some fluid from one side reaching beyond the centreline of the micro T-mixer to engulf the fluid from the other side. It was shown that improved mixing performance was achieved with engulfment flow. Engler *et al.* also highlighted the improvement of mixing as a result of asymmetrical flow conditions at the inlets of the micro T-mixer. Hoffmann *et al.* carried out computer simulations and experimental work on mixing in T-shaped mixers with trapezoidal cross section. They based their observations of mixing on the three regimes of flow highlighted by Kockmann *et al.* From their computer simulations, they showed that improved mixing performance could be obtained with engulfment flow.

Besides micro T-mixers, micromixers based on the secondary flow and vortices generated when liquid flows past a bend have also been investigated. Mengeaud *et al.* (2002) carried out computer simulations and experimental study on the mixing process in a planar zigzag microchannel. It was found that at low Reynolds number of flow, the two liquids

flowing side by side mixed only by diffusion. But at higher Reynolds number, the inertia of the liquids resulted in the separation of boundary layer after each bend and the recirculation phenomenon that was accompanied by boundary layer separation induced transverse velocity components that help species transport across the channel. It was shown that significant improvement in mixing performance was obtained when subsequent bends were located at the point of reattachment of the separated boundary layer and a Reynolds number of flow greater than 80. Yi and Bau (2003) also carried out investigations on bend-induced mixing in microchannels with the use of a mapping method. Two-dimensional map was constructed to project the displacement of particles at a cross section before the bend to a cross section after the bend. This map was applied repeatedly to simulate the mixing induced after a number of bends. Mixing in planar and three-dimensional configurations of bends as shown in *fig 2-6* was simulated and it was found that mixing performance was better in three-dimensional configuration as the symmetry that was present in the planar configuration was eliminated. This resulted in a more efficient stirring of the mixture. Reynolds numbers of flow of up to 40 were simulated and achieved experimentally. Effective mixing was only observed at a Reynolds number of flow of more than 10 and at higher Reynolds number, chaotic advection was predicted through Poincaré maps and complete mixing was observed after a few evolutions of the three-dimensional bends. Similar micromixers based on the same principle had also been investigated by Liu *et al.* (2000) and Beebe *et al.* (2001) who fabricated and tested micromixers in the form of three-dimensional serpentine microchannel. The presence of chaotic advection in the serpentine microchannel was suggested and improved mixing performance at a Reynolds number greater than 10 was observed.

Park *et al.* (2004) investigated micromixers that mixed liquids by stretching and folding the liquid interface and by breaking up the liquid mixture. Two micromixers were fabricated based on the two principles of mixing mentioned. One of them mixed by

stretching and folding liquid interfaces through the rotation of liquid as a result of flowing in a multi-segmented microchannel as shown in *fig. 2.7*. The other micromixer fabricated by them achieved mixing by alternately breaking up and merging the liquid mixture in addition to the stretching and folding processes. It was found that the additional break-up process resulted in a better mixing than with just stretching and folding processes.

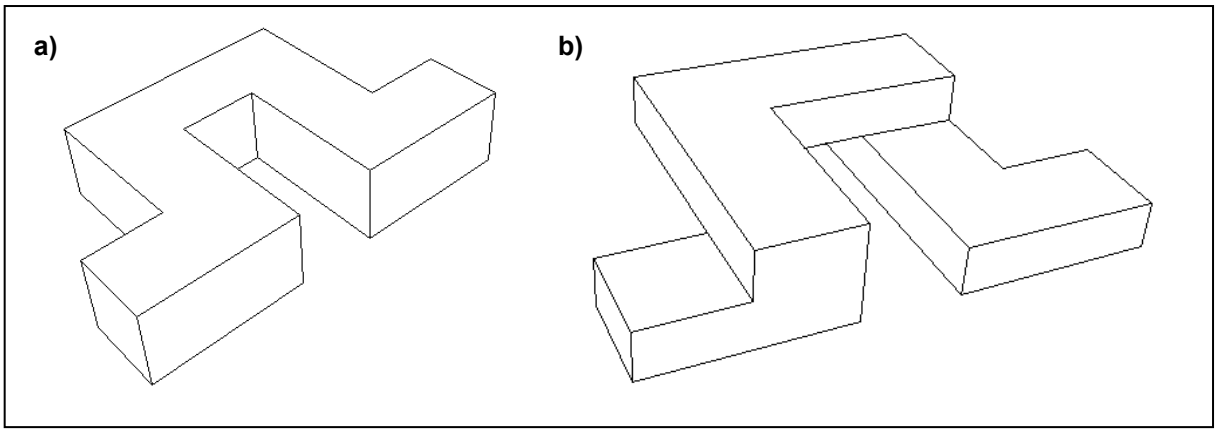

Fig. 2-6 *The tortuous microchannels used by Yi and Bau, Liu et al. and Beebe et al. for generating mixing by chaotic advection. (a) shows the planar configuration while (b) shows the three-dimensional configuration.*

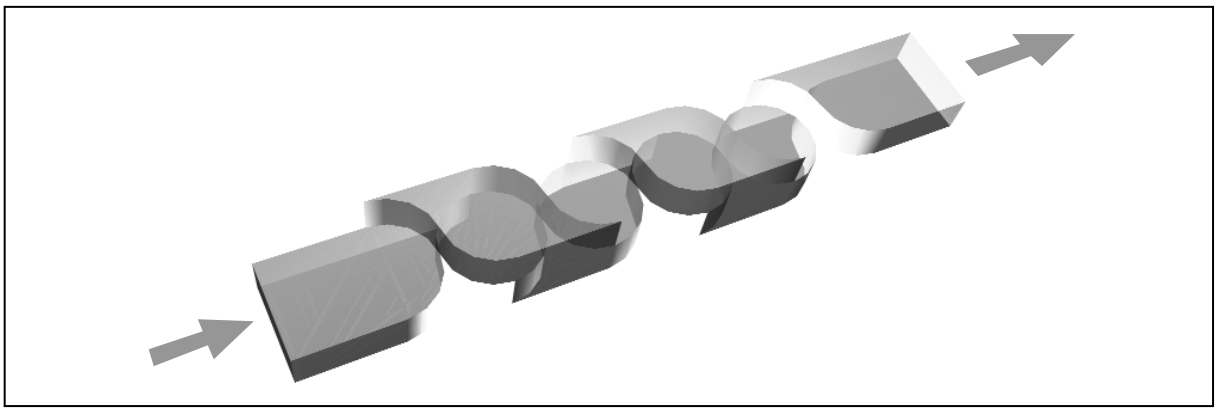

Fig. 2-7 *The multi-segmented microchannel mixes liquids by stretching and folding of liquid interface created through rotation when the liquid mixture travels from one segment to the next.*

Static micromixers, like diffusion micromixers, also have very simple fabrication process, but unlike diffusion micromixers, do not depend solely on diffusion process to achieve mixing. Static micromixers generate lateral velocity components in the mixing channel by various means to achieve mixing apart from the naturally occurring diffusion

process. This has resulted in more efficient micromixers that can achieve mixing more rapidly than is possible with diffusion micromixers.

2.5 RAPID MIXING MICROMIXER

The micromixers in the three categories described in the last section demonstrate the varieties of principles available for achieving mixing in the microscale. Most of these micromixers are able to achieve complete mixing within seconds, with the exception of a few, which manage to achieve this in under a second. As described in Chapter 1, reaction kinetics studies of fast reactions involving expensive reagents require micromixers that can achieve complete mixing within milliseconds. *Table 2-1* shows a summary of the mixing times achieved by the micromixers that have been fabricated and tested by the investigators described in this chapter.

Investigators	Mixing time (s)	Type
Bökenkamp *et al.* (1998)	110×10^{-6}	Static
Elwenspoek *et al.* (1994)	1.2	Diffusion
He *et al.* (2001)	0.67	Diffusion
Hessel *et al.* (2003)	$\sim 10 \times 10^{-3}$	Diffusion
Koch *et al.* (1998)	~ 1	Diffusion
Knight *et al.* (1998)	20×10^{-6}	Diffusion
Veenstra *et al.* (1999)	4.0	Diffusion
Voldman *et al.* (2000)	2.1	Diffusion
Hinsmann *et al.* (2001)	100×10^{-3}	Diffusion
Yang *et al.* (2001)	~ 2	Active, Mechanical

Table 2-1 *The mixing times of the micromixers in the literature described in this chapter are summarized along with the types of micromixers which they have been classified.*

Although active micromixers allow extra control over the rate of mixing, there is still no active micromixer that can demonstrate rapid mixing so far. Active micromixers are also more difficult to fabricate and integrate with other microfluidic components. Generally, passive micromixers are easier to fabricate and integrate with other microfluidic components and some diffusion and static micromixers have already shown very promising results. Of all the micromixers that demonstrate complete mixing in milliseconds, those investigated by Bökenkamp *et al.* and Hessel *et al.* are relatively large resulting in a higher rate of consumption of reagents. This is not attractive for reaction kinetics studies where expensive reagents are involved. The micromixer fabricated by Hinsmann *et al.* is more relevant to this study because the micromixer is intended for time resolved infrared spectroscopy of chemical reactions. The mixing time that was achieved was also fairly short at 100 ms. But it would be more desirable if faster mixing could be achieved so that the reaction kinetics of fast reactions can be better resolved. The micromixer investigated by Knight *et al.* on the other hand has too low a flow rate which makes it unsuitable for infrared spectroscopy. The designed flow rate of their micromixer is just 5 nl/s with the mixture produced from a microchannel of 10 μm wide. A sufficient amount of homogeneous mixture is required within milliseconds in order for spectroscopic measurements to be performed. Furthermore, the short mixing time achieved by Knight *et al.* is based on mixing of disproportionate amount of reagents. The width of the stream of one liquid in the middle is very much thinner than the other liquid on both sides to achieve small diffusion distance. The effect of this could be a wrong impression of fast mixing as the concentration of the liquid with smaller flow rate decreases rapidly to below the limit detectable by the acquisition system, although complete mixing has not been achieved. An example illustrating the extreme case can be demonstrated by mixing a drop of ink with a bucket of water. Even though the molecules of

ink have not travelled to the entire volume of water, the concentration difference between mixed and unmixed liquids can no longer be detected.

It is therefore apparent that there is a "window" between the micromixers investigated by Bökenkamp *et al.* and Hessel *et al.* and that fabricated by Knight *et al.*, where a micromixer with intermediate channel dimensions and flow rates has not been looked into. It is intended in this study to investigate the feasibility of rapid mixing in static micromixers and characterizing the performance of these micromixers that fall into this "window" of channel dimensions and flow rates. The cross-sectional dimensions of the micromixers investigated in this study are mostly in the range of tens of micrometers while the flow rates are in the range of μl/s.

2.6 CLOSURE

A detailed introduction to microfluidics has been presented in this chapter, where historical background, benefits and impacts of microfluidics have been discussed. This is then followed by a detailed review of all the micromixers that have been investigated so far. All these provide us with an insight on the progress that has taken place in this field and show us the areas which our understanding is lacking or the specifications which we have not been able to achieve. This has prompted an investigation of mixing in static micromixers with flow rates falling in the range of μl/s and having cross-sectional dimensions of tens of microns.

FUNDAMENTAL THEORIES

3.1 FUNDAMENTAL FLUID FLOW THEORIES

The theory of fluid flow in microchannel is central to the operation of microfluidic devices. It is therefore imperative that there is a good understanding on the fluid flow theory, especially for flows in microchannels, when designing microfluidics devices. Unfortunately, whether the well-developed theories for fluid flow in macro-sized pipes widely found in fluid mechanics text books are adequate to predict fluid flow behaviour in microchannels are still open to debate. Numerous works have been carried out by many investigators to look at liquid flow in microchannels. While some observed no anomaly in the liquid flow in microchannels, others reported deviations of flow behaviour from that predicted by the existing theories. Urbanek *et al.* (1993), Wang and Peng (1994), Peng and Peterson (1995; 1996) all observed anomalies in the liquid flow and heat transfer behaviour in microchannels that cannot be accounted for by the experimental errors. The friction constant, which is a dimensionless parameter that is associated with the cross-sectional shape of the microchannel, was found to be higher than the already established values. A higher friction constant results in a lower flow rate than would otherwise exist for an applied pressure gradient. They also suggested early onset to turbulent flow in microchannels based on their experimental data. Other investigators like Mala *et al.* (1997a; 1997b; 1998), Yang and Li (1998), Yang *et al.* (1998), Papautsky *et al.* (1999) and Ren *et al.* (2001a; 2001b) have attributed the anomalies in practical observations to effects associated to microscale and

constructed models to account for the anomalies. Among the explanations for the anomalies are surface roughness of microchannels, interfacial electrokinetic effects due to the surface charges on the walls of microchannels and the deviation of liquid properties from Newtonian liquid to micropolar liquid (Eringen, 1966). Xu *et al.* (2000) on the other hand found no anomalies in the flow of liquid in microchannels and demonstrated the possibility of incorrect measurements by other investigators. Judy *et al.* (2002) carried out comprehensive and detailed experiments on liquid flow in microchannels and found that no distinguishable deviation from the conventional theories was observed throughout their experiments.

It can therefore be seen that there is still no widely accepted conclusion of whether the conventional fluid flow theories can be applied with good accuracy to predict liquid flow in microchannels. Furthermore, the models that have been suggested by some investigators are complicated to use, not to mention if the suggested microscopic effects are actually causing the most deviation in experimental observations of liquid flow in microchannels. In any case, only one microscopic effect was considered by each investigator who showed to account for the deviation from conventional theories without considering other microscopic effects. While there is still no well accepted explanation for the anomalies observed in the liquid flow in microchannels, the conventional theories for liquid flow in macro-sized pipes continue to be used for analysing liquid flow in microfluidic devices in many occasions. Nevertheless, the deviation of liquid flow behaviour in microchannels is not very significant and the conventional theories can generally be applied to liquid flow in microchannels without much loss of accuracy.

In the following sub-sections, a number of aspects in the conventional theories that are used in analysing and characterizing the mixing problem, as well as explaining the experimental observations and mixing mechanisms in this study are described.

3.1.1 REYNOLDS NUMBER

Reynolds number, Re, is one of the most common dimensionless parameter encountered in fluid dynamics for characterizing fluid motion. It is defined by equation 3-1 for any fluid in motion.

$$\mathrm{Re} = \frac{\rho \bar{u} d}{\mu} \tag{3-1}$$

For fluid flow in a closed channel, its hydraulic diameter is often used as the characteristic length in the computation of the Reynolds number. The hydraulic diameter, D_h, is defined by

$$D_h = \frac{4A}{P} \tag{3-2}$$

Qualitatively, the Reynolds number is the ratio of inertia force to viscous force in the flowing fluid. Very low Reynolds number, typically less than one, indicates creeping flow where the viscous forces in the fluid are dominant over inertia forces. No formation of eddies in the flow is possible. At moderate Reynolds number, typically less than 2300, the flow is considered laminar where the fluid motion is made up of many non-intersecting layers of fluid in motion. Each layer exerts its influence onto the adjacent fluid layer. As the influence of viscous forces is significant in this regime of flow, any eddy formation is quickly damped so that the flow reverts back to laminar flow. At high Reynolds number of more than 4000, the flow is considered turbulent with the continuous formation of many eddies in the flow. At Reynolds number between 2300 and 4000, there is transition flow where the flow is very sensitive to small perturbations and it oscillates between laminar and turbulent flow depending on the perturbations. The Reynolds number of flow in microchannels of hydraulic diameter of below 100 μm rarely exceeds 2300. As such, liquid flow in microchannels is usually laminar even at moderate to high applied pressures. This is very much due to the small dimensions of the channel cross-section. As turbulent flow is not achievable in microfluidic, rapid mixing by means of generating turbulence through turbulent flow is not

usually possible. Other means of mixing is therefore adopted when designing micromixers to perform fast mixing.

It should also be noted that even though the Reynolds number of flow is low, the liquid flow velocity in microchannels can be very high. Flow velocity of several meters per second is easily attainable and higher velocity is possible. This creates a very high velocity gradient in the microchannels and therefore a very high shear stress at the channel wall and also between liquid layers. There is a fundamental difference between two flows at the same Reynolds number but flowing in channels of very different cross-sectional dimensions. To illustrate an example, consider a flow in a macro-sized channel having a hydraulic diameter, D_{h1}, of 0.3 m and another flow in a microchannel with a hydraulic diameter, D_{h2}, of 300 μm. With the density and viscosity of the liquid being the same and the two flows are both at the same Reynolds number, it can be shown that the flow velocity in the microchannel is three orders of magnitude greater than that in the macro-sized channel, given by the ratio of D_{h1}/D_{h2}. Assuming a parabolic velocity profile typical across a laminar flow, the velocity gradient in the microchannel at any point across the flow is six orders of magnitude greater than that in the macro-sized channel at the corresponding points. This is equal to the square of the ratio D_{h1}/D_{h2}. Consider a two-dimensional flow in the x-y plane along a channel, the vorticity about the z-direction, ζ_z, given by $\partial v/\partial x - \partial u/\partial y$ is a function of the velocity gradient. The vorticity generated in a flow in microchannels is therefore far greater than that generated in a flow in the macro-scale at the same Reynolds number. This has profound implications in the viability of generating vortices in microchannels which will be discussed later in this study. Reynolds number is also a very useful parameter in characterizing the flow of liquid in microchannels. It allows investigators to associate their experimental observations to a common platform so that the observations obtained from different studies can be compared.

3.1.2 NAVIER-STOKES EQUATIONS

The most fundamental theory that is widely used to predict fluid flow is one implied by the continuity and Navier-Stokes equation. For incompressible flow, they have the following forms.

$$\nabla \cdot \mathbf{V} = 0 \qquad \text{Continuity equation} \qquad (3\text{-}3)$$

$$\frac{\partial \mathbf{V}}{\partial t} + (\mathbf{V} \cdot \nabla)\mathbf{V} = -\frac{1}{\rho}\nabla p + \nu \nabla^2 \mathbf{V} + \mathbf{B} \qquad \text{Navier-Stokes equation} \qquad (3\text{-}4)$$

Equation 3-3 is derived from the principle of conservation of mass while equation 3-4 is derived from the Newton's Second Law. The terms on the right-hand side of equation 3-4 represent the total external and body forces acting on an element of fluid while the terms on the left-hand side represent the resultant rate of change of momentum of the fluid element. The external forces acting on the fluid elements are implied by $-\nabla p/\rho$ and $\nu\nabla^2\mathbf{V}$ terms. The $-\nabla p/\rho$ term accounts for the forces due to pressure applied onto the fluid elements. The $\nu\nabla^2\mathbf{V}$ term on the other hand accounts for the effects due to the fluid viscosity. The body forces that are acting on the fluid elements are collectively represented by **B**. Examples of body forces are the weight of the fluid element or the electrical body force acting on the fluid elements in an electric field.

The Navier-Stokes equation in the form of equation 3-4 is a nonlinear partial differential equation, which is very difficult to be solved analytically. Numerical methods and iterations have to be employed in solving the equation, therefore making it more suitable to be solved by computers with established computational fluid dynamics software. Nevertheless, Navier-Stokes equation can be simplified to a one-dimensional differential equation under certain flow conditions so that it can be attempted analytically. When considering the flow of liquid in microchannels, a number of assumptions can be made to simplify the Navier-Stokes equation without significant loss of accuracy. Weight of the fluid

elements can be neglected in the analysis of liquid flow in the microscale as its effect is much weaker than the other external forces acting on the fluid. For steady, incompressible flow of Newtonian fluids in a rectangular microchannel as shown in *fig. 3-1*, one can assume that the mean flow velocities in the *y* and *z* directions denoted by *v* and *w* respectively are negligible compared to that in the *x* direction along the channel. For steady flow in a microchannel with uniform cross-section, the velocity in the *x* direction, denoted by *u*, does not change along the channel. Applying these assumptions, the Navier-Stokes equation is simplified to a two-dimensional equation.

$$\frac{\partial^2 u}{\partial y^2} + \frac{\partial^2 u}{\partial z^2} = \frac{1}{\mu}\frac{\partial p}{\partial x} \tag{3-5}$$

By solving equations 3-5, the velocity profile across the width and depth of the microchannel can be found. This allows a relationship between the volume flow rate through the channel, *Q*, and the pressure gradient along the channel, d*p*/d*x*, to be obtained. Equation 3-5 can be further simplified for the case of a rectangular microchannel with very low aspect ratio by approximating it to the flow between two parallel plates, where the velocity component *u* does not change in the *z*-direction, to give equation 3-6, which can be easily solved for laminar flow.

$$\frac{\mathrm{d}^2 u}{\mathrm{d}y^2} = \frac{1}{\mu}\frac{\mathrm{d}p}{\mathrm{d}x} \tag{3-6}$$

A common relationship between volume flow rate and pressure gradient for steady laminar flow in a closed channel derived from the Navier-Stokes equation is given by equation 3-7.

$$Q = -\frac{2AD_h^{\,2}}{\mu \mathrm{C}}\frac{\mathrm{d}p}{\mathrm{d}x} \tag{3-7}$$

C is a dimensionless constant called the friction constant described in Section 3.1 that is equivalent to the product of the friction factor, *f*, and the Reynolds number, Re. The details of the derivation of equation 3-7 are given in Appendix A.

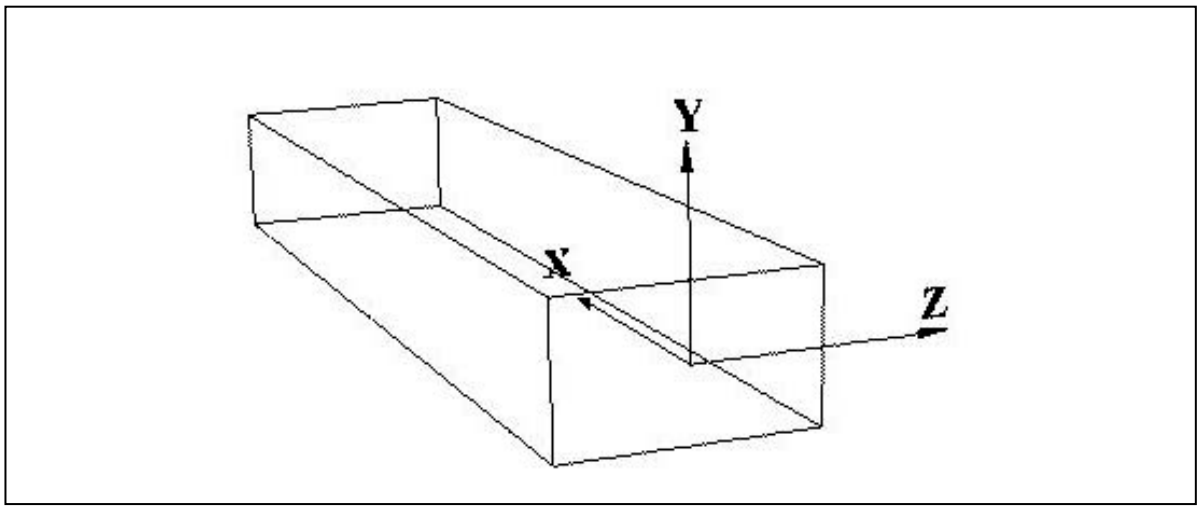

Fig. 3-1 *An illustration of a microchannel with a rectangular cross-section. The orthogonal axes show the directions of X, Y, and Z considered when simplifying the Navier-Stokes equation.*

3.1.3 DIFFUSION-CONVECTION EQUATIONS

The transport of one or more species in a fluid in motion can be described by the diffusion-convection equation.

$$\frac{\partial c}{\partial \mathrm{t}} + (\mathbf{V} \cdot \nabla) c = \mathrm{D}\nabla^2 c \tag{3-8}$$

The diffusion equation, $\partial c/\partial \mathrm{t} = \mathrm{D}\nabla^2 c$, attributed to Fick can only account for the transport of species due solely to diffusion, which can only describe the species transport in a stationary system or a fluid at very low velocity. For a system where the fluid is in motion and convection due to momentum of fluid is present, a convection term, $(\mathbf{V}\bullet\nabla)c$, is introduced. Like the Navier-Stokes equation, the diffusion-convection equation in the form of equation 3-8 is also a non-linear partial differential equation that is difficult to be solved analytically. Therefore, computational fluid dynamics is needed when analysing the species transport in static micromixers.

3.1.4 SECONDARY FLOW AND SEPARATION OF BOUNDARY LAYERS

When a secondary flow pattern is set up in a channel, the main flow along the axis of the channel is superimposed with another flow pattern that is perpendicular to the main flow. Secondary flow results in the lateral motion of fluid across the width and depth of the channel. There are a number of ways in which secondary flow can be created. But for liquid flow in microchannels, the secondary flow is set up when the liquid flows in a curve path. This occurs when the liquid flows in a curved channel, around a sharp bend or corner and around obstructions in which rapid change in flow direction is involved. When liquid flows in a curve path, the liquid at the centre of the microchannel that is travelling much faster than the liquid near the top and bottom walls experiences a higher centrifugal force. The imbalance creates a lateral flow field where the liquid in the centre tends to flow away from the centre of curvature of the path while the liquid at the top and bottom walls tends to flow towards the centre of curvature to replace the liquid at the centre. This is illustrated in *fig. 3-2*. Secondary flow can be set up in laminar flow and is one of the ways to induce lateral movement of different species across the channel to improve mixing performance in the microscale.

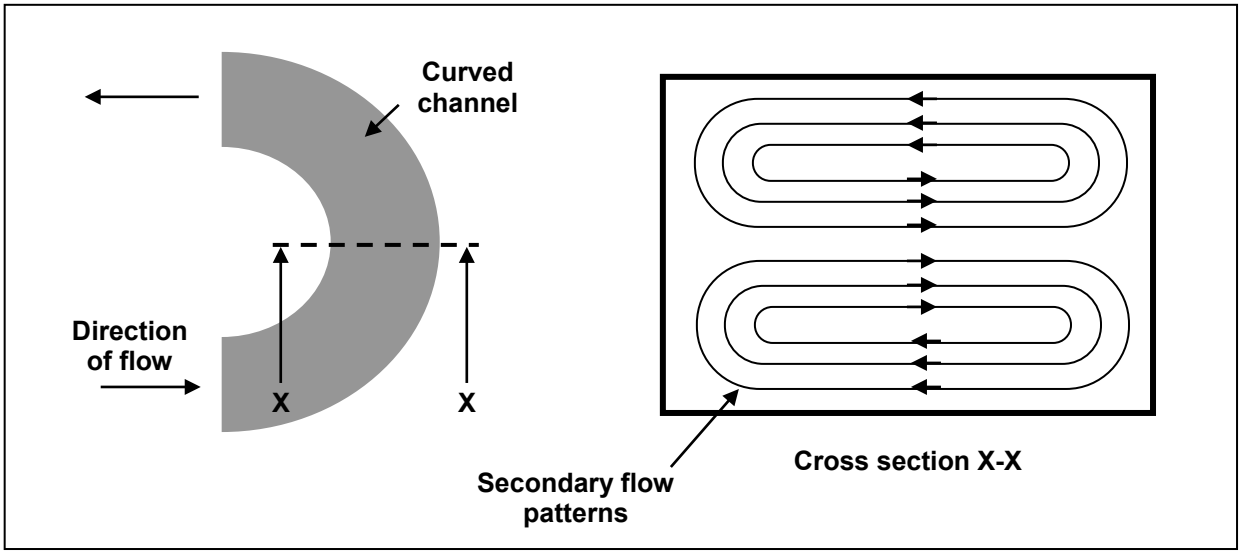

Fig. 3-2 *The setting up of secondary flow pattern in a curved channel due to different magnitudes of centrifugal forces acting on the liquid across the depth of the channel.*

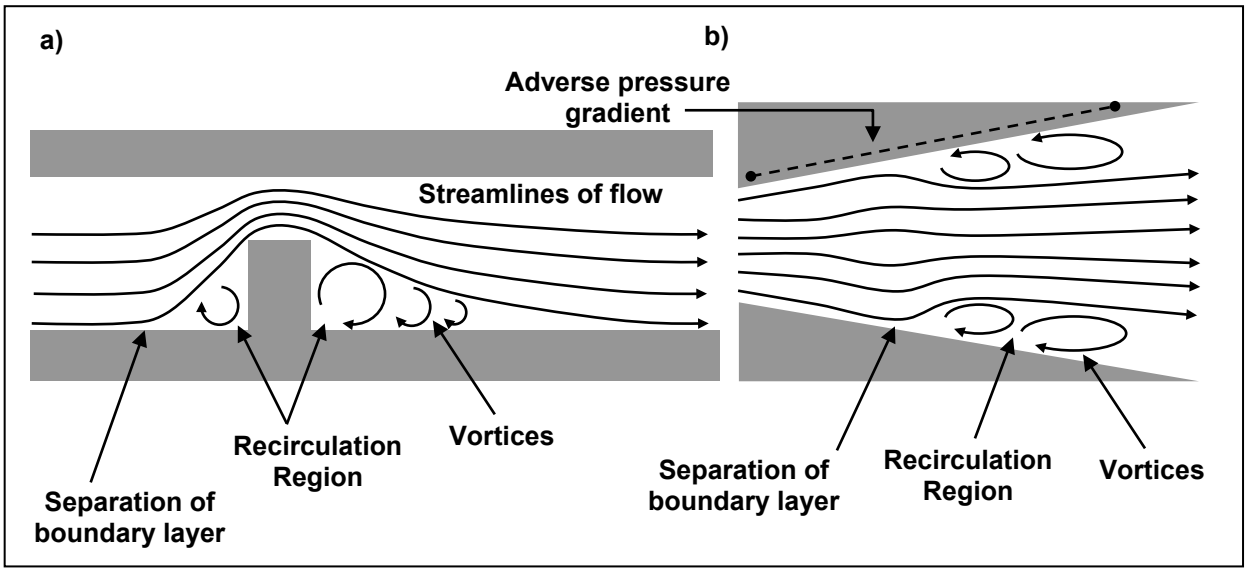

Fig. 3-3 *The separation of boundary layers caused by (a) sudden contraction and expansion or obstruction in the flow path and (b) adverse pressure gradient in a diverging flow.*

When a liquid flowing in a microchannel encounters an abrupt change in the geometry of the flow path or an adverse pressure gradient at the liquid-solid boundary, separation of boundary layers occurs in the flow, provided that the liquid is not under creep flow. In the first case where there is a sudden change in geometry, such as a sudden expansion or contraction in the channel, the liquid is forced to conform to the change in channel geometry but this is limited by the inertia of the flowing liquid that prevents the liquid from assuming the boundary of the channel, separation of liquid boundary layers therefore ensues as illustrated in *fig. 3-3a*. In the second case where there is an adverse pressure gradient along the channel wall, such as that occurring in a diverging channel shown in *fig. 3-3b*, the localised higher pressure region around the wall downstream prevents the liquid flow from assuming the boundary of the diverging channel, thus resulting in the separation of boundary layer. As the liquid flow no longer assumes the boundary of the channel when separation of boundary layer occurs, a region of recirculation of liquid is created between the two boundaries. Vortices are formed in this recirculation region and lateral transport of liquid is more profound resulting in a better potential for mixing.

3.2 MIXING MECHANISMS

According to Gray (1986), the term *mixing* is applied to operations which tend to reduce non-uniformities or gradients in composition, temperature or properties of material in bulk. Many types of mixing are possible and depending on the phases of the materials to be mixed, one mixing method may be more suitable than the other. There are three basic processes involved during a mixing of fluids, namely stretching and folding, diffusion and break-up (Ottino, 1989). Considering initially a blob in a liquid, stretching and folding processes shears and folds the blob into thin filaments with many folds depending on the flow field in the liquid. Diffusion process blurs the boundary of the blob in the liquid and at the same time spreads the concentration of the blob material to its surroundings. Break-up process breaks the blob up into many tiny fragments. Stretching and folding in a mixing process are usually acting together and are due to the flow field in the liquid. Some flow fields are better at causing stretching and folding that the others. For example, a laminar flow field with non-intersecting streamlines in a microchannel is effective in stretching but not folding. A turbulent flow on the other hand contains many vortices that shears and folds the liquid in all directions and in a chaotic manner resulting in a better mixing performance. Diffusion process is a naturally occurring process due to the incessant motion of molecules in the liquids. Molecules of one material tend to move from regions of high concentration to regions of lower concentration. Therefore, two miscible liquids placed in contact will first experience blurring of their boundaries and become mixed after a certain time due to diffusion. Diffusion is however a very slow process, especially in macro-systems, as the mean free path of liquid molecules is in the order of nanometres. Diffusion is also slow when macro-molecules are involved in the mixing. The break-up process is due to the interfacial tension of the material in the liquid. Break-up process is especially obvious when mixing less miscible liquids. The boundaries

between the two liquids are more distinct and extreme stretching of the liquid material causes it to break up creating smaller fragments.

All these three processes result in an increase in the contact area between two liquids and a reduction in the diffusion distance that the liquid molecules need to travel to achieve uniform concentration. As a result, the speed of mixing increases. In practical mixing, the three basic processes of mixing described can be easily achieved together in the macro-scale but is more difficult in the microscale. This is mainly due to the difficulties in achieving turbulence in the microscale. Mixing can be carried out in a stirred tank or through a static mixer in the macro-scale using various designs of impellers and mixing elements to create wide scale vortices and break-up of liquid that rapidly create a homogeneous mixture. Vortices, which are inherent to turbulent flow, can stretch and fold as well as break up a liquid from a blob into many filaments like many entangled ribbons. This coupled with the naturally occurring diffusion process smoothes out the concentration non-uniformities between the filaments to form a homogeneous mixture. In the microscale, turbulent flow is often not possible. So, dedicated effort is needed to create each basic process in a micromixer. Most of the micromixers employed just the diffusion process which is not sufficiently fast to meet the aims of this study. But a few others have also employed stretching and folding as well as break-up processes in their micromixers. *Table 3-1* classifies the passive micromixers described in Chapter 2 into three categories depending on the main basic processes employed by the micromixers in achieving mixing. The analysis on mixing mechanism in this study is centred upon that between two miscible liquids as the micromixers investigated are aimed at the rapid mixing for reaction kinetics studies between antibiotics and enzymes.

Basic mixing processes	Investigators
Diffusion	Elwenspoek *et al.* (1994), Schwesinger *et al.* (1996), Knight *et al.* (1998), Koch *et al.* (1998; 1999a), Erbacher *et al.* (1999), Veenstra *et al.* (1999), Voldman *et al.* (2000), Hinsmann *et al.* (2001), He *et al.* (2001) and Hessel *et al.* (2003)
Stretching and folding	Liu *et al.* (2000), Beebe *et al.* (2001), Mengeaud *et al.* (2002), Yi and Bau (2003) and Hoffmann *et al.* (2003)
Break-up	Schwesinger *et al.* (1996) and Park *et al.* (2004)

Table 3-1 *This table classifies the passive micromixers investigated by other investigators described in Chapter 2 into three categories depending on the basic mixing process employed.*

3.3 CLOSURE

This chapter describes the fundamental theories that will be encountered in this study. A very useful dimensionless parameter – the Reynolds number is introduced, which will be heavily used to characterize the mixing in this study and make possible the comparison between the results obtained and similar existing work. The governing equations for liquid flow and species transport are also introduced, which are then related to liquid flow and mixing in the microscale. The governing equations will be numerically solved with the use of a computational fluid dynamics program when liquid flow and mixing in the proposed micromixer design are analyzed in the next chapter. Separation of boundary layers and secondary flow are two mechanisms intended to be used for generating vortices, and thus more rapid mixing, in the micromixers investigated in this study. The mixing mechanism is

also described, which is made up of three basic processes, namely stretching and folding, diffusion and break-up processes. The stretching and folding processes achieved by the formation of vortices in the micromixer, coupled with the naturally occurring diffusion process, are believed to be the recipe for a rapid mixing micromixer.

MICROMIXER DESIGN AND COMPUTER SIMULATIONS

4.1 THE CHOICE OF MICROMIXER TYPE

The various types of micromixers that have been investigated in the literature are described in Chapter 2. Passive micromixers are more attractive as their fabrication procedures are simpler and in some cases have been shown to be able to achieve faster mixing than active micromixers. Among the passive micromixers, static micromixers are more attractive as they create stretching and folding processes in addition to the naturally occurring diffusion process in achieving complete mixing, which is in contrast to diffusion micromixers that depend only on diffusion process. A static micromixer is therefore seen as a more effective mixing device than a diffusion micromixer. With the reasons mentioned above, the micromixers investigated in this study are static micromixers.

Two designs of static micromixers were investigated. The first design investigated was a micro T-mixer, which was a scale down of its macro-sized counterparts commonly used in chemical engineering applications. The second design was a cross-shaped micromixer that attempted to actively create vortices to enhance its mixing performance by the incorporation of some static mixing elements. The design, fabrication, testing and experimental results of mixing in micro T-mixers will be described in the next section onwards while the investigation work carried out on cross-shaped micromixers will be described in Chapter 8.

4.2 MIXING CONCEPTS

The design of the micromixers investigated in this study is based on the insight on the mixing mechanism described in the previous chapter. Among the three basic processes in mixing, emphasis is given to the stretching and folding processes. This is because diffusion is a naturally occurring process that is present in any case while the break-up process usually involves complicated microchannel structures (Park *et al.*, 2004) and results in the mixing of liquids at different residence times during recombinations. Stretching and folding processes are achieved by creating vortices in the flow of the two liquids in the micromixer as described in the previous chapter. As the presence of vortices is crucial in setting up stretching and folding processes in the microscale, the mixing concepts employed in this study strive to create vortices by various means in a predominantly laminar flow in microchannels.

Turbulent flow in microchannels is not feasible due to the small channel size and the high applied pressure involved. The Reynolds number of flow in microchannels is generally in the laminar regime. Attempt to force a liquid to flow in the turbulent regime by increasing the applied pressure is limited by the mechanical failure of the bonding or material that forms the microchannel. Blom *et al.* (2001) carried out pressure tests on microchannels of different sizes created by anodic bonding between silicon substrate and glass cover lid. It was found that the anodic bond started to fail when the pressure in the microchannels exceeded 9 bar. This pressure was also dependent on the width of the microchannels tested with the wider microchannels failing at a lower applied pressure. It is however possible that by clever use of channel geometry and flow field in liquid, vortices can be generated in laminar flow at a moderate Reynolds number of a few hundreds. The vortices can be generated through secondary flow and separation of boundary layers, which can be attained where there are some discontinuities in the flow conduit such as the presence of a sharp bend, or a junction in

the micromixers. As described in the previous chapter, vortices are effective means in achieving stretching and folding processes in the liquid, which in turn bring about better mixing performance.

The mixing concepts described here are applied in the design of the micro T-mixer and cross-shaped micromixer in this study. It is intended that vortices are created as a result of secondary flow and separation of boundary layers set up when the two liquids collide at the junction in these micromixers or when the liquids flow past some static mixing elements. The lateral flow field and flow recirculation that lead to the generation of vortices can be used to improve the mixing performance in a micromixer where mixing by turbulence is not feasible. Nevertheless, these occurrences are limited to the vicinity of the discontinuities. The amount of vortices generated and their prevalence are very much dependent on the Reynolds number of the flow. As the flow is still in the laminar regime, the vortices decay as they leave the discontinuity and the flow reverts back to laminar flow.

4.3 THE DESIGN OF A MICRO T-MIXER

Two different designs of static micromixers are investigated in this study. The first static micromixer investigated, which is described in this section, is a micro T-mixer. It is similar to those investigated by Hoffmann *et al.* (2003). This study is however carried out independently to that performed by Hoffmann *et al.* The cross section of the microchannels in the micro T-mixers investigated in this study is rectangular, unlike the micromixers fabricated by Hoffmann *et al.* which have trapezoidal cross sections. The upper limit of Reynolds number investigated in this study is also higher while the dimensions of the micro T-mixers fabricated are smaller. The choice to investigate the mixing in a micro T-mixer is made because micro T-mixer is the most fundamental design of a static micromixer. It is also found that a detail mixing characterization in a micro T-mixer has not yet been fully

explored. This is probably due to the general perception that liquid flows in a laminar fashion in microfluidic channels due to the small channel size. At low flow rates, mixing of two streams flowing side by side in a microchannel is effected purely by diffusion. This is unlike their larger counterparts, which uses turbulent flow as a means of rapidly mixing the two different streams that come together.

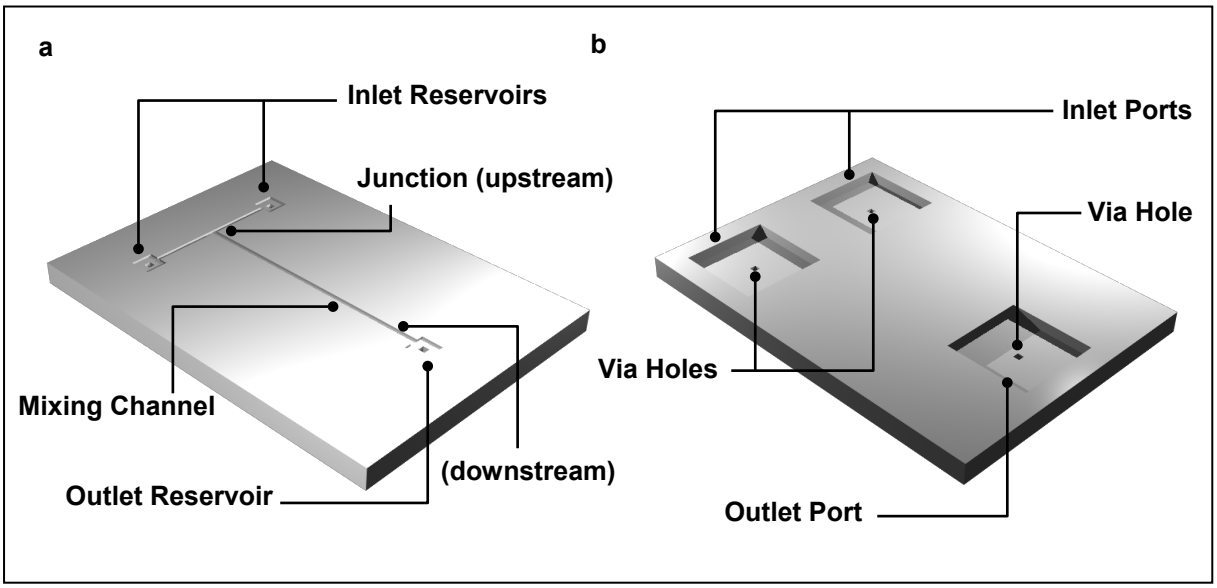

Fig. 4-1 *The front face of the micro T-mixer investigated in this study is shown in (a). It consists of a micro T-mixer connected to inlet and outlet reservoirs at the end of the T. Each reservoir has a via hole located at the centre to allow liquids in and out of the micromixer. The back face of the micro T-mixer is shown in (b). Square inlet and outlet ports are etched to facilitate the entry and exit of liquids into and out of the test chip.*

Fig 4-1 shows the essential features of the micro T-mixer investigated in this study. The micro T-mixer is made out of silicon substrate bonded to a glass cover lid. It consists of two inlet channels to the left and right, and a mixing channel at the centre of the chip. Square reservoirs are connected to the ends of the channels and the centre of the each reservoir contains a via hole connecting the micro T-mixer to the inlet and outlet ports at the backside of the chip. Since an array of micro T-mixers can be produced in batches on a single wafer, micro T-mixers of different channel widths were incorporated in an array. The width of the mixing channel was also designed to be double the width of the side inlet channels. This was to ensure no acceleration or deceleration of flow occurring in the mixing channel. Mixing

channel widths of 20, 40, 60, 100 and 200 μm were incorporated into the design of the micro T-mixers in the array. The depths of the micro T-mixers can vary depending on the etch depth, thus microchannels of different sizes and aspect ratios can be produced on a wafer. The overall dimensions of the micro T-mixer are shown in *fig. 4-2*.

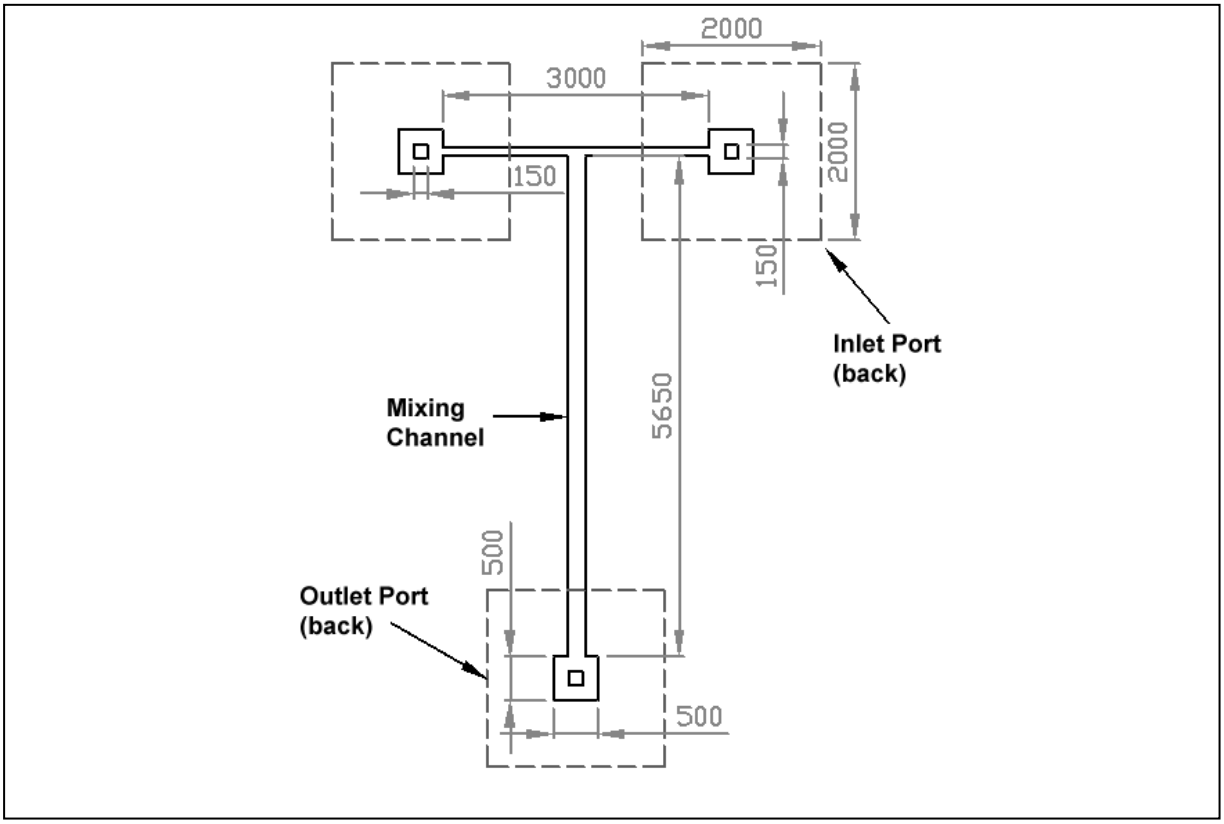

Fig. 4-2 *The diagram shows the dimensions of the micro T-mixer investigated in this study. The dimensions are in microns. Features in dash lines are on the different side of the wafer to those in continuous lines. The width of the mixing channel is twice the width of inlet channels. Mixing channel widths of 20, 40, 60, 100 and 200 μm have been produced in this study. The micro T-mixers are etched to a various depths less than 100 μm.*

The micromixers were designed in such a way that the two liquids to be mixed can be fed into the micromixer from the bottom of the chip while the mixing process can be observed under a microscope from above. The mixing channel was made sufficiently long so that the progress of mixing as a result of the collision of two streams of liquid at the junction can be observed. The inlet channels were made sufficiently long so that a fully developed flow was achieved before reaching the junction. Inlet and outlet ports are square recesses of 2x2 mm^2 for facilitating the connection of the feed tubing to the test chip.

4.4 DESIGN CALCULATIONS

Basic design calculations were carried out to find out the pressure drop in the micro T-mixers at different flow rates. The design calculations considered the macro properties of the flow in the micromixers such as pressure drop and volume flow rate while the micro properties of the flow such as the flow field at the junction and the species concentration distribution in the micro T-mixer were left to be simulated by computer. In this way, the dimensions of the micromixers designed were quickly validated, ensuring that the proposed micromixer designs were able to meet the specified flow rate requirements at a manageable applied pressure. In the calculations, equation 3-7 was extensively used to find out the relationship between applied pressure at the inlets and the flow rate in the micromixers. However, equation 3-7 can only relate the flow rate to pressure drop for flow in a straight microchannel. The micro T-mixer investigated contained a number of microchannels connected together so equation 3-7 was only applied to each of the straight sections of microchannels. The presence of a junction essentially caused an extra pressure drop in the micro T-mixer apart from the pressure drop along the microchannels. This extra pressure drop was accounted for by introducing a pressure loss term, which was characterized by the loss coefficient, K_J. There were also pressure drops caused by the sudden contraction and expansion of the flow conduit at the entrance to the inlet channels and the exit of the mixing channel respectively. The higher the loss coefficient, the greater is the pressure loss across the geometrical structure. In general, the value of loss coefficients is dependent on the flow velocity and the type of geometrical structure that causes the pressure loss. Loss coefficients are defined by the following equation (White, 1999).

$$K = \frac{\Delta p_{loss}}{\frac{1}{2}\rho \bar{u}^2} \tag{4-1}$$

The loss coefficients for sudden contraction, K_C, and expansion, K_E, can also be more conveniently expressed by the following two equations respectively (White, 1999).

$$K_C = 0.42\left(1 - \frac{A_2}{A_1}\right) \tag{4-2}$$

$$K_E = \left(1 - \frac{A_1}{A_2}\right)^2 \tag{4-3}$$

A_1 and A_2 are the cross sectional areas before and after the expansion or contraction. The pressure losses due to sudden contraction and expansion calculated from the loss coefficients given in equations 4-2 and 4-3 were based on the mean flow velocity in the inlet channels and mixing channel respectively.

Loss coefficients are widely used in macro-scale fluid flow in pipes calculations and most valves and fitting manufacturers provide information on the loss coefficient of their valves and fitting. Although loss coefficient values are widely available for macro-scale pipe fittings, no such data is available for bends and junctions in the microscale. An estimate was therefore made based on the existing data for equivalent macro-scale tee fittings. A value of 1 was chosen as the loss coefficient at the junction, K_J, based on the loss coefficient values given by some fitting manufacturers for a tee fitting (Munson *et al.*, 1998; White, 1999). With equation 3-7 and pressure loss calculations due to the junction and at inlets and outlet, the total pressure drop between the liquid in the inlet reservoirs and that in the outlet reservoir were calculated for flow at different Reynolds numbers.

An example of the design calculation procedure is described here. Consider a micro T-mixer with a mixing channel of 100 μm wide and 50 μm deep and a continuous flow of liquid through the micro T-mixer from its inlets to its outlet at a Reynolds number of 500 in the mixing channel, the mean velocity of flow, $\overline{u}$, can be calculated from equation 3-1 to be 7.54 m/s. The density and viscosity of the liquid used in the calculation is 998 kg/m^3 and

0.001003 Ns/m^2 respectively, which correspond to the properties of water at 20°C. The characteristic length used is the hydraulic diameter of the mixing channel, which is 66.67 μm calculated from equation 3-2. The corresponding volume flow rate in the inlet channels and mixing channel can be calculated from the continuity equation, $Q = A\overline{u}$. The volume flow rate in the mixing channel is 37.69 × 10^{-9} m^3/s while the flow rate in the inlet channels is half of that in the mixing channel. The pressure loss at the junction of the micro T-mixer, Δp_J, is calculated with equation 4-1 with a value of 1 for K, which yields a value of 28.35 kPa. The pressure loss due to the entry of the liquid into the inlet channels, Δp_C, can also be calculated with equation 4-1 with the value of K computed from equation 4-2. A_1 and A_2 in equation 4-2 are the cross-sectional areas of the liquid reservoirs and the inlet channels respectively. In this case, A_1 and A_2 are 25 × 10^{-9} m^2 and 2.5 × 10^{-9} m^2 respectively. This gives a value 0.378 for K_C. The pressure loss due to the exit of the liquid from mixing channel into the liquid reservoir, Δp_E, can be calculated with equation 4-1 in the similar way described above but using equation 4-3 to compute the value of K. As the cross sectional area of the mixing channel is twice of that of the inlet channel, A_1 and A_2 are 5.0 × 10^{-9} m^2 and 25 × 10^{-9} m^2 respectively. So A_1/A_2 in equation 4-3 is 0.2 and the resulting value for K_E is 0.64. The pressure losses at the inlets and outlet thus calculated are 10.72 kPa and 18.14 kPa respectively. There is also pressure drop along the inlet and mixing channels, which can be calculated by equation 3-7. The two inlet channels experience the same pressure drop as they meet at the junction and are connected to the same pressure source. The friction constant for the inlet channels can be found in *Table A-1* in Appendix A. The cross-section of the inlet channel has an aspect ratio of 1, its friction factor is therefore 56.91. Substituting the values of flow rate, cross sectional area, hydraulic diameter and length of the inlet channel, friction constant and viscosity of the liquid, the pressure drop along the inlet channel is calculated to be 129 kPa. Similar calculations can be performed for the mixing channel to obtain a

pressure drop of 299 kPa. Summing the pressure drop along the channels, at the junction, at the inlet and outlet, the total pressure drop in the micro T-mixer when the Reynolds number of flow in the mixing channel is 500 is 485 kPa. *Table 4-1* summarizes the total pressure drop at different Reynolds numbers of flow in the mixing channel. The summary given in *table 4-1* is based on a micro T-mixer with a mixing channel of 100 μm wide and 50 μm deep and with the other dimensions as shown in *fig. 4-2*.

Reynolds number	Mean velocity (m/s)	Volume flow rate ($\times 10^{-9}$ m^3/s)	Δp_J (kPa)	Δp_C (kPa)	Δp_E (kPa)	Δp_{total} (kPa)
100	1.51	7.54	1.13	0.43	0.73	87.87
200	3.02	15.08	4.54	1.72	2.90	180.32
300	4.52	22.61	10.21	3.86	6.53	277.35
400	6.03	30.15	18.14	6.86	11.61	378.96
500	7.54	37.69	28.35	10.72	18.14	485.14
600	9.05	45.23	40.83	15.43	26.13	595.90

Table 4-1 *The table summarizes the total pressure drop, Δp_{total}, between the inlet reservoir and the outlet reservoir for different Reynolds numbers in the mixing channel. Δp_J, Δp_C and Δp_E are the respective pressure drop due to the losses at the junction, the sudden contraction at the inlets and sudden expansion at the outlet.*

Mixing channel width (μm)	Mean velocity (m/s)	Volume flow rate ($\times 10^{-9}$ m^3/s)	Δp_J (kPa)	Δp_C (kPa)	Δp_E (kPa)	Δp_{total} (kPa)
200	6.28	62.81	19.69	6.62	7.09	302.32
100	7.54	37.69	28.35	10.72	18.14	485.14
60	9.21	27.64	42.35	16.72	32.80	893.92
40	11.31	22.61	63.79	25.72	53.99	1759.15
20	17.59	17.59	154.35	63.53	142.25	7999.09

Table 4-2 *The table shows the total pressure drop, Δp_{total}, between the inlet reservoir and the outlet reservoir for micro T-mixers with different widths of mixing channel and inlet channel at a Reynolds number of 500 in the mixing channel. The depth of the micro T-mixer is 50 μm in all cases.*

From *table 4-1*, it can be seen that the volume flow rates through the micro T-mixer at Reynolds numbers above 100 is greater than 1 μl/s, which satisfy the require specification on volume flow rate. The total applied pressure required to achieve a certain Reynolds

number of flow increases rapidly from less than 1 bar for a Reynolds number of 100 to about 6 bar for a Reynolds number of 600. This limits the Reynolds number of flow that can be achieved in micro T-mixers with narrow microchannels as they require a very high applied pressure. This is reflected in *table 4-2* where the pressure drop in the micro T-mixers with different cross sectional dimensions of the inlet and mixing channels are shown for a flow at a Reynolds number of 500 in the mixing channel. With the information about the volume flow rate and pressure drop obtained from the design calculations, the achievable flow rate in a micro T-mixer with a particular channel dimension was known, which allowed the suitability of the channel dimensions to be determined.

4.5 COMPUTER SIMULATIONS

Computer simulations were performed to look into the micro properties of the flow in the micro T-mixer, particularly the velocity flow field and the extent of mixing in the micromixer. Computer simulations were performed with the use of a computational fluid dynamics (CFD) simulation program and in the simulation of mixing in a micro T-mixer, Fluent 6 was used. There are many advantages of performing CFD simulations as it can be used to predict the behaviour of fluid flow in almost any system, from the flow of air in the Earth's atmosphere to the flow of liquid in microfluidics. Some examples of applications of CFD simulations can be found in Shaw (1992). To a novice user however, there are also many pitfalls that can be associated with the use of CFD simulations especially when a CFD program is used as a black box to generate simulation results from some input boundary conditions without first acquiring a good understanding in the basic theory of fluid flow. Therefore, precautions have to be taken when carrying out computer simulations to ensure that the simulation results are reflective of the fundamental fluid flow theories. Simplifying assumptions can be made to the fundamental theories so that analytical calculations for a

flow problem, such as the design calculations carried out in the previous section, can be performed. The macro properties of flow deduced from the micro properties obtained in computer simulations can be compared to those obtained from analytical calculations to determine the validity of the simulation results. An accurate simulation should therefore show similarities between the flow properties predicted both numerically and analytically.

4.6 SIMULATION PROCEDURES

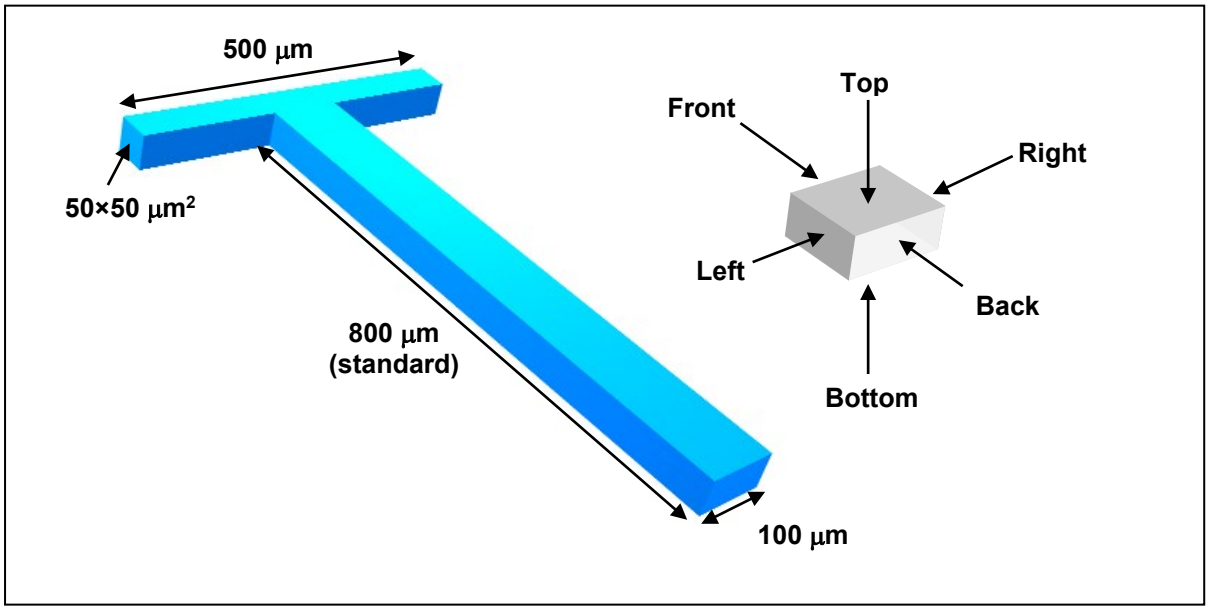

Fig. 4-3 *The diagram shows the dimensions of the 3D solid model used in the computer simulation of mixing. It also illustrates the names used to identify the individual faces of the model.*

3D solid models of the micro T-mixer were built and named in Gambit – the preprocessor for Fluent 6. The dimensions of the solid models are illustrated in *fig. 4-3*. Although micro T-mixers with different widths of mixing channel were designed on a single wafer, the micro T-mixer with 100 μm wide and 50 μm deep mixing channel was simulated. Only the flow field in the microchannels around the junction of the micro T-mixer was simulated as it was the flow field there that was the main area of interest. The flow field in the straight section downstream of the mixing channel and the upstream section of the inlet channels was considered to be laminar. Such a compact but efficient model allowed a finer mesh to be used

while keeping the simulations manageable. The solid model was made up of 656 250 cubic brick elements of 2 μm each.

Two species ⟨a⟩ and ⟨b⟩, having the properties of water at 20 ºC, were simulated to mix in the micro T-mixer. Species ⟨a⟩ was specified to enter the micro T-mixer from the inlet on the left while species ⟨b⟩ was specified to enter from the inlet on the right. Three different scenarios (I – III) were simulated, which corresponded to the flow in the micro T-mixer at different Reynolds numbers. They are summarized together with the corresponding mean velocities specified at the inlets in *table 4-3*. The simulations allowed the effects on mixing performance due to the vortices generated by the separation of boundary layers and secondary flow at the junction to be evaluated.

Scenario	Reynolds number	Mean flow velocity (m/s)
I	121	1.824
II	300	4.522
III	489	7.372

Table 4-3 *The table summarizes the three scenarios of mixing (I to III) in a micro T-mixer simulated for liquid flow at different Reynolds numbers in the mixing channel. The mean flow velocities shown are specified at the inlets of the micro T-mixer.*

For all the scenarios, symmetrical boundary conditions were specified on both the inlets of the micro T-mixer. This was achieved by specifying equal but opposite flow velocity vectors at the two inlets and equal density and viscosity for the two liquids to be mixed. The direction of the liquid velocity at the inlets was normal to the inlet faces. A zero gauge pressure was specified at the outlet face of the model. In all simulations, the SIMPLEC algorithm for pressure-velocity coupling and second order upwind for the computation of Navier-Stokes and diffusion-convection equations were employed. Steady laminar flow model was selected to simulate the flow of liquid in the micro T-mixer with no slip boundary

condition set at the walls of the microchannels. The accuracy of the CFD simulation results obtained was confirmed by plotting the residual values for the continuity, velocity components and mass fraction against iteration steps to ensure that the results have converged.

4.7 CHARACTERIZING THE EXTENT OF MIXING IN SIMULATIONS

Two dimensionless parameters, the intensity of segregation and variation coefficient, were used on the simulation results to characterize the extent of mixing in the micro T-mixer. This allowed the simulation results obtained for various boundary conditions to be compared. They were functions of the standard deviation of the species concentration at a specific distance from the point of introduction of the species. The intensity of segregation and variation coefficient were computed using equation 4-4 and 4-6 respectively.

$$I_s = \frac{\sigma_0^{\,2}}{\sigma_i^{\,2}} \tag{4-4}$$

σ_0 and σ_i are the standard deviations of concentration of a species at the outlet and inlet of the micromixer respectively. The standard deviation of concentration of a species at the outlet was computed from the concentration values at each node on the outlet surface of the 3D model. The standard deviation of concentration at the inlets when no mixing has occurred is given by equation 4-5.

$$\sigma_i = \left[\bar{x}_{va}(1-\bar{x}_{va})\right]^{1/2} \tag{4-5}$$

$\bar{x}_{va}$ is the average volume fraction of species ⟨a⟩ at the inlets, which can be computed by the ratio of volume flow rate of species ⟨a⟩ to the total volume flow rate of the two species at the inlets. Since it was the extent of mixing that was of greater interest in this study, the intensity of mixing, I_m, which was defined by $1–I_s$ was also computed. The variation coefficient was computed by

$$\frac{\sigma_0}{\overline{x}_{va}} = \left\{ I_s \left[\left(\frac{1}{\overline{x}_{va}} \right) - 1 \right] \right\}^{1/2} \tag{4-6}$$

The intensity of segregation and variation coefficient have a value of zero for a perfectly homogeneous mixture while the corresponding value of the intensity of mixing is unity. For a completely segregated mixture, the intensity of segregation has a value of one while the intensity of mixing has a value of zero. The corresponding value of variation coefficient on the other hand depends very much on the average volume fraction of the species considered at the inlets. However, it is sufficient to have up to a certain degree of mixing, not necessarily a perfectly homogeneous mixture, for many applications. A variation coefficient of below 0.05 is considered sufficient as a criterion for complete mixing in most applications (Fluitec Documentation). Further descriptions of these parameters are provided by Gray (1986). Mass fraction data at the outlet of the micromixer was extracted from the simulation results to compute the values of the parameters described above. By comparing the intensity of mixing and variation coefficient values at the outlet of the micro T-mixer for different Reynolds numbers, the improvement of mixing caused by the generation of vortices due to separation of boundary layers and secondary flow at the junction was determined.

4.8 SIMULATION RESULTS AND DISCUSSION

The simulation results for the three scenarios are shown in *fig. 4-4* in the form of mass fraction plots for species ⟨a⟩ at a residence time of 177 μs after the two liquids collide at the junction. This residence time was derived from the time of travel of the two liquids in the mixing channel of 800 μm length in scenario II. Comparison of the extent of mixing was carried out for liquids at the same residence time instead of the same distance from the junction in the mixing channel. This is because the two liquids at the outlet face for example would have been in contact for different durations for flows at different Reynolds numbers.

The standard 3D micro T-mixer model had a mixing channel length of 800 µm. A micro T-mixer model with a longer mixing channel length of 1304 µm was therefore constructed for the simulation of mixing in scenario III while the mass fraction plot for scenario I was extracted at a distance of 322 µm from the junction.

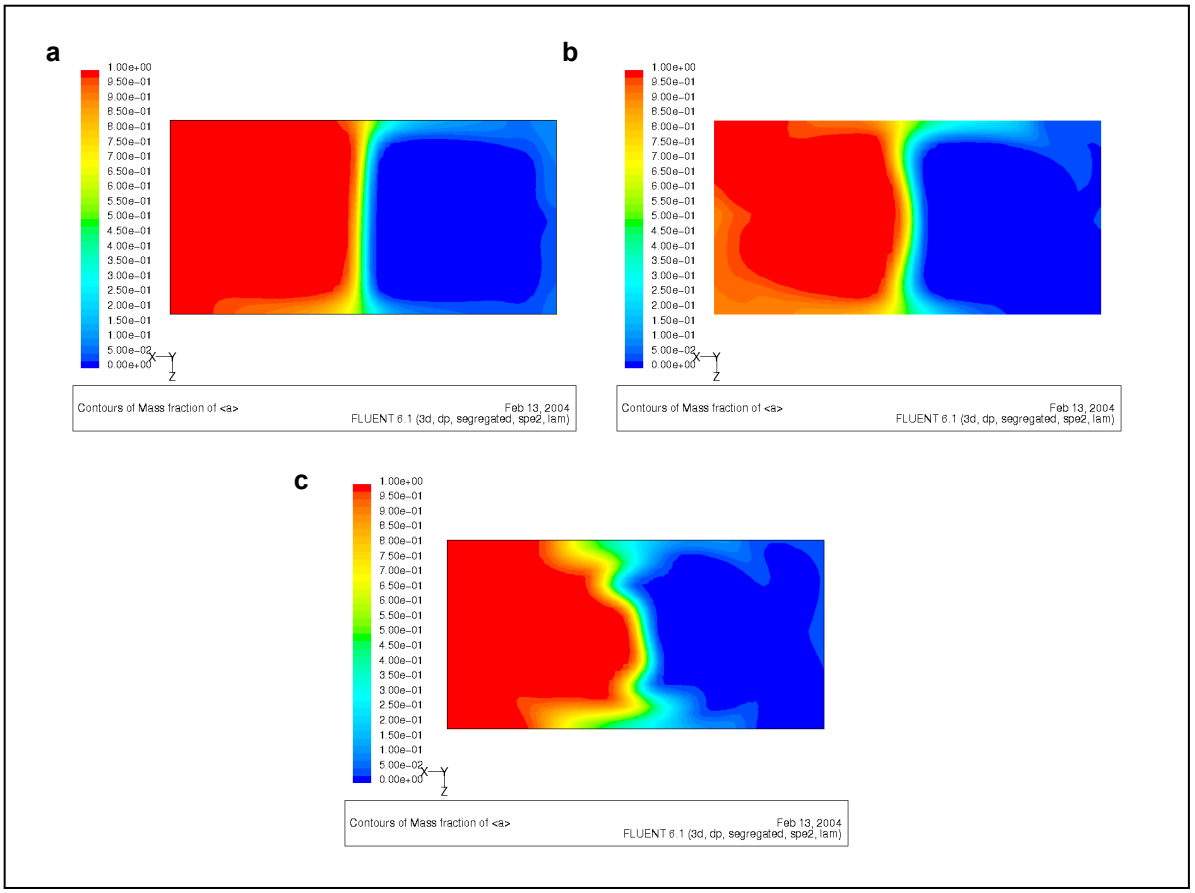

Fig. 4-4 *The three contour plots show the mass fraction distribution of species ⟨a⟩ at a residence time of 177 µs after the two liquids collide at the junction for three different Reynolds numbers in the mixing channel, with a) at 121, b) at 300 and c) at 489. It can be seen that mixing performance improves with increasing Reynolds number of flow.*

Scenario	Intensity of mixing	Variation coefficient	Volume flow rate ($\times 10^{-9}$ m^3/s)
I	0.1003	0.9485	8.95
II	0.1390	0.9279	22.24
III	0.1677	0.9123	36.21

Table 4-4 *The table shows the intensity of mixing and variation coefficient values calculated from the mass fraction data obtained from the computer simulations. The volume flow rates in the micro T-mixer deduced from the simulation results are also shown.*

It can be seen from *fig. 4-4* that the extent of mixing improves with increasing Reynolds number of flow in the mixing channel. At a Reynolds number of 121, the viscous effect in the flow is dominant compared to the inertia effect, resulting in the two liquids being segregated on the two halves of the cross-section. At a higher Reynolds number of 300, the effect from the inertia of the flow increases. The interface of the two liquids is no longer straight but slightly curved. At an even higher Reynolds number of 489, folds are formed in the interface, resulting in a larger area of contact between the two liquids and thus an improved mixing performance. The intensity of mixing and variation coefficient values for the three scenarios are shown in *table 4-4*. Large areas of the two liquids in the cross section are still unmixed as identified by the large red and blue areas in the mass fraction contour plots and the small intensity of mixing and variation coefficient values. The volume flow rates deduced from the simulation results were confirmed by the corresponding values from design calculations.

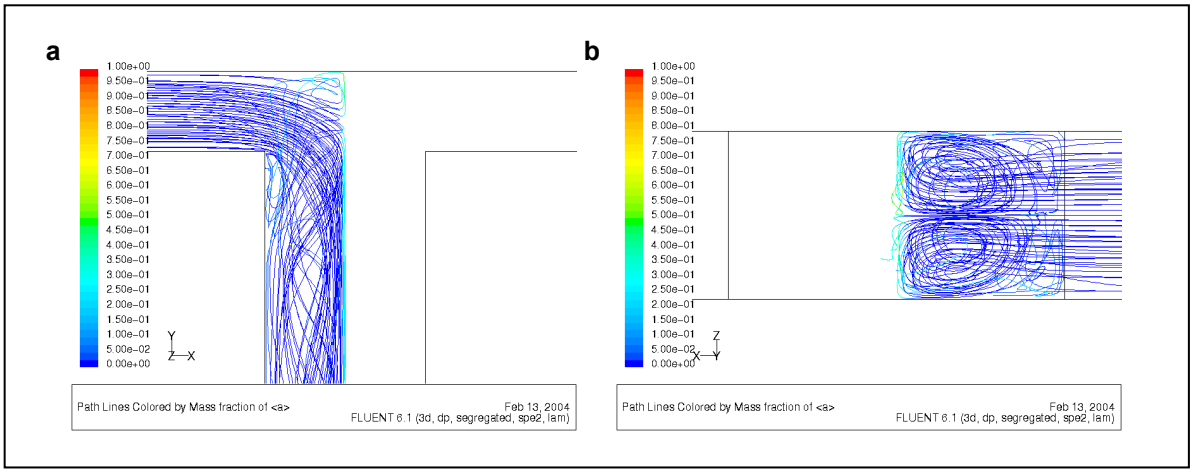

Fig. 4-5 *The fluid trajectory plots of species ⟨b⟩ in the micro T-mixer seen from the top (a) and front (b) faces for scenario III.*

It can also be observed from the mass fraction contour plots that the extent of mixing is better at the top and bottom surfaces in the cross-section. This is the effect from secondary flow in the micro T-mixer where the secondary flow pattern perpendicular to the direction of the flow as shown in *fig. 3-2* sweeps the better mixed liquids at the interface to the walls of

the mixing channel through the top and bottom surfaces of the channel. This is further supported by the fluid trajectory plots for scenario III shown in *fig. 4-5*. The fluid trajectory plot in *fig. 4-5a* shows that the liquid entering the micromixer from one side is mostly confined to the same side in the mixing channel. The fluid trajectory plot in *fig. 4-5b* shows the secondary flow patterns set up in the mixing channel resulting in a better mixing at the top and bottom surfaces of the mixing channel.

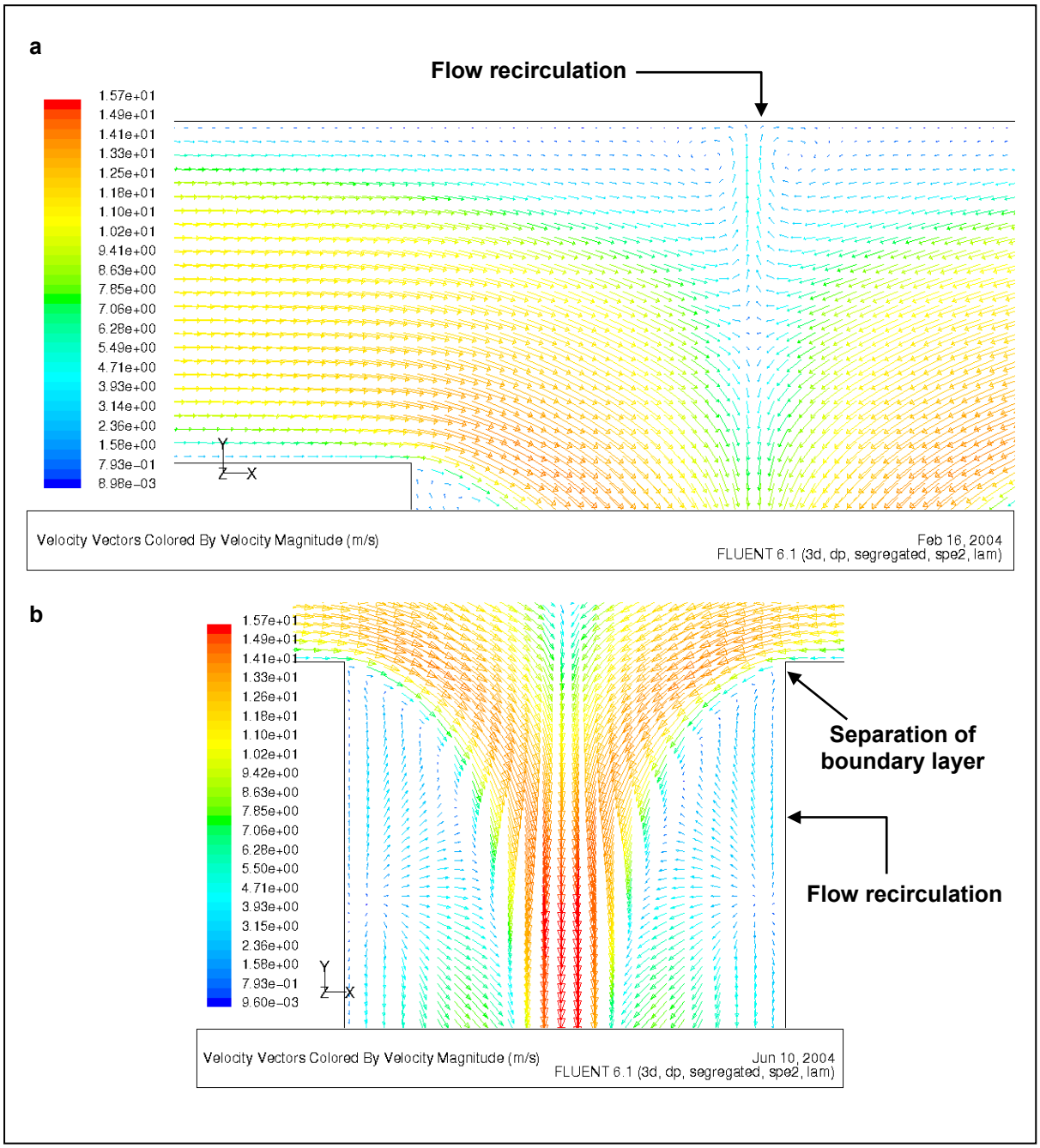

Fig. 4-6 *The velocity vector plots at mid-depth of the micro T-mixer show the separation of boundary layer and flow recirculation at the upper region of the junction (a) and after the sharp corners (b).*

The separation of boundary layers in micro T-mixer is evident from the velocity vector plots shown in *fig. 4-6*, which occur at the sharp corners at the junction and also in the upper region of the junction where to two liquids collide. A recirculation region can also be observed from the velocity vector plots downstream of a separated boundary layer that has the potential of causing improved mixing performance in the micro T-mixer.

4.9 CLOSURE

The micromixers that are being investigated in this study are static micromixers. Based on the understanding of the mixing mechanism, the concept adopted for achieving rapid mixing in the microscale is by the generation of vortices. The generation of vortices is the result of secondary flow in the microchannel and the separation of boundary layers caused by an abrupt change in the boundaries of the flow conduit. The designs of the micro T-mixer and the cross-shaped micromixer to be described later apply these mixing concepts to achieve mixing. The characterization of mixing performance in a micro T-mixer is prompted by the lack of such work in the literature. The study of such a fundamental micromixer sets a foundation for further improvement through modifications in the future. Basic design calculations were performed to estimate the rate of production of mixture in a micro T-mixer with the chosen cross-sectional dimensions and the pressure drop across the micromixer. This ensures that the cross-sectional dimensions of the micro T-mixer adopted in the design are suitable for achieving the flow rate specification with a reasonable applied pressure.

Computer simulations were also carried out to look into the micro properties of flow and mixing in a micro T-mixer. The volume flow rates deduced from the computer simulations were confirmed by the design calculations. The simulation results show improved mixing with increasing Reynolds number of flow in the mixing channel. However, the intensity of mixing and variation coefficient values at a specific residence time after the

two liquids collide show that a large fraction of the two liquids remained unmixed. The relatively better extent of mixing at the top and bottom surfaces in the cross-section of the mixing channel is explained by the secondary flow set up in the channel. The separation of boundary layers and flow recirculation are also evident from the velocity vector plots obtained from the simulation results.

EXPERIMENTATION: FABRICATION

5.1 FABRICATION PROCEDURES – AN OVERVIEW

The micro T-mixers investigated in this study were fabricated using a 4-inch double sided polished silicon wafer with a thickness of 425 μm. The patterns of the square via holes, micro T-mixers and inlet and outlet ports were first made on three separate mask plates. These patterns were then transferred onto the silicon wafer through UV photolithography. The patterns were etched by a deep reactive ion etching (DRIE) process in a dry etcher manufactured by Surface Technology Systems (STS). The front face of the etched wafer was anodically bonded to a 4-inch, 500 μm thick Pyrex glass wafer. Closed conduits of the micro T-mixer were formed from open trenches after the anodic bonding step. The bonded wafer assembly was then diced into individual chips using a diamond tip wafer cutter. The back side of the individual chip was then bonded to a clear polystyrene plate of 3 cm^2 using Loctite® adhesive. Before the chip was bonded to the polystyrene plate, through holes of 1.58 mm in diameter were drilled through the plate for facilitating the connection of liquid feed tubing to the chip. Poly-ether-ether-ketone (PEEK™) tubing was then connected to the through holes in the polystyrene plate with Loctite® adhesive, completing the fabrication process with the chip ready to be used for mixing characterization work. *Fig. 5-1* shows the images in the various stages of the fabrication process of the micro T-mixer. *Fig. 5-1a* shows the wafer assembly after anodic bonding was carried out, *fig. 5-1b* shows the individual chip

that was produced after it was bonded with a polystyrene plate while *fig. 5-1c* shows the completed chip ready for use with PEEK™ tubing already connected to it. Each of the fabrication processes will be described in details in the following sections.

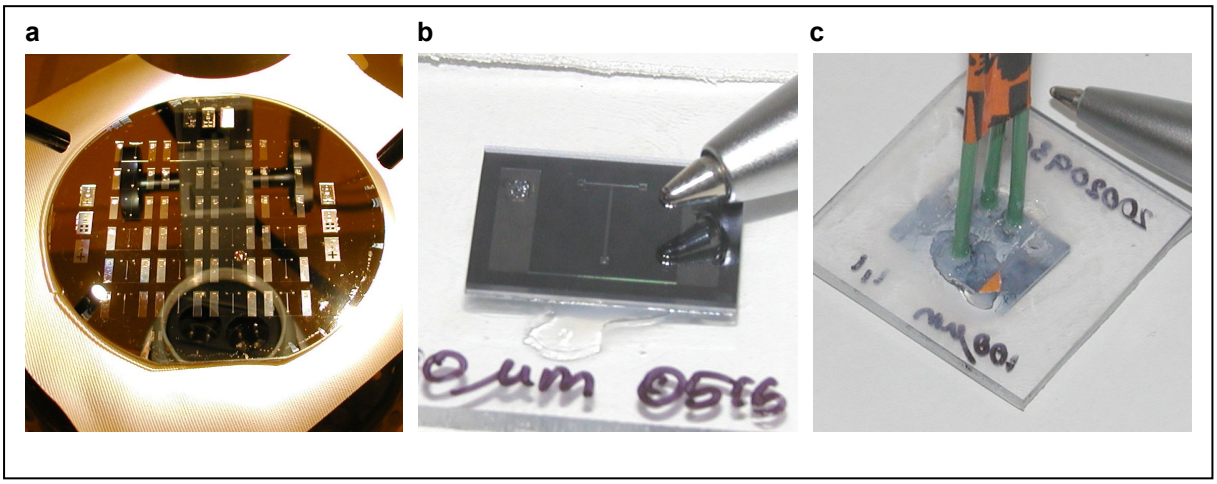

Fig. 5-1 *The images show the various stages in the fabrication of the micro T-mixers. a) shows the silicon-glass wafer assembly after anodic bonding was performed. b) shows the front face of the individual chip after bonding with the polystyrene plate. The two large reservoirs on both sides of the micro T-mixers are for a separate study not described here. c) shows the chip completed with feed tubing ready to be used for mixing characterization work.*

5.2 MASK DESIGN

The first step in the fabrication process of a micro T-mixer is to put the design into a layout drawing in a number of layers depending on the number of processing steps. A mask is a quartz plate with the patterns of the features to be transferred to a silicon wafer made transparent or opaque to light, depending on whether a light field or a dark field mask is used. For a chrome mask, the opaque area on the glass plate is a layer of chrome. The features on the mask are written by an electron beam mask writer based on the layout drawing supplied to the mask writer. A light field mask has the features to be transferred in chrome while a dark field mask is the inverse of the former.

In the fabrication of the micro T-mixer, the L-Edit – Layout Editor Version 8.03 in MEMS Pro V2™ by Tanner Research, Inc. was used to generate the GDSII layout drawing files of the micro T-mixer compatible with most mask writers. The masks were produced

from the GDSII files by the Central Microstructure Facility in Rutherford Appleton Laboratory, Oxford. Dark field masks were used in the photolithography process together with a positive photoresist. Three mask layers were required in the fabrication of the micro T-mixers. One of the masks contained the patterns of the square via holes. The patterns of the micro T-mixers and those of the inlet and outlet ports were each on a separate mask as shown in *fig 5-2*. An array of 24 micromixers as shown in *fig. 5-1a* was designed on the masks allowing the micromixers to be fabricated in batches on 4-inch wafers. The micromixers in the array had different channel widths in order to maximize the variation of test piece produced within each batch.

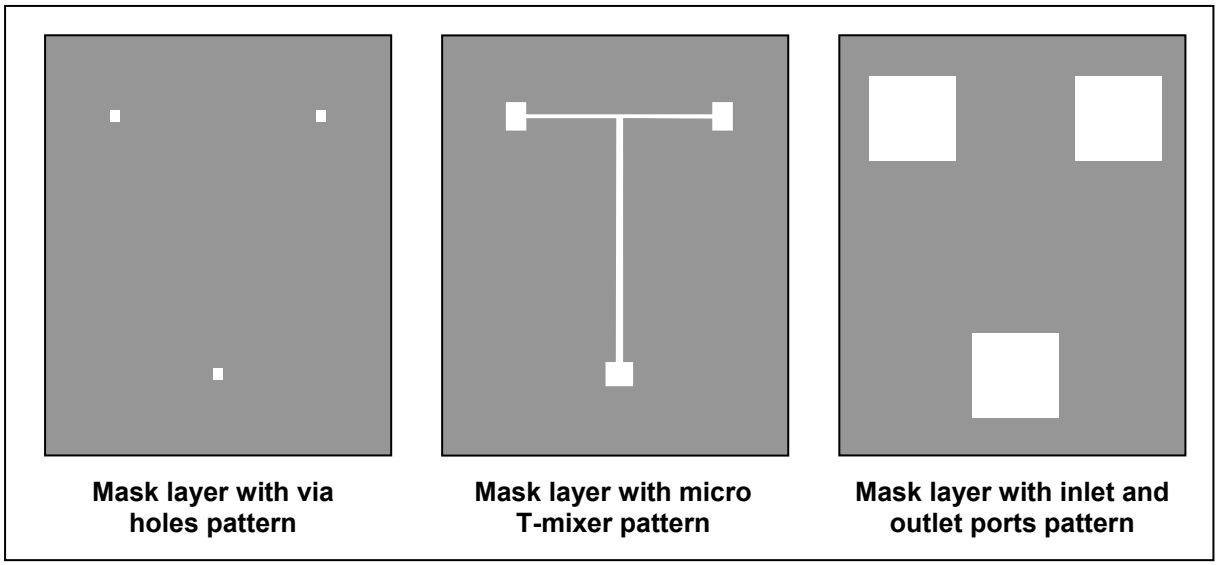

Fig. 5-2 *The diagram shows the patterns on the three mask layers used in the photolithography process.*

In order to align each mask to the etched patterns on the silicon wafer, alignment markers as shown in *fig. 5-3* were designed on the masks. It was very important to be able to align the patterns on the mask to the etched patterns on the wafer accurately so that the new features transferred onto the silicon wafer were on the designated locations. The alignment markers consisted of a number of '+' and square patterns in different sizes in rectangular windows. The rectangular windows allowed the '+' or the square patterns on the wafer to be easily found while the '+' or square patterns on the mask layer aligned with those on the

wafer. The '+' and square patterns were conjugate of each other to allow even small misalignments to be detected easily.

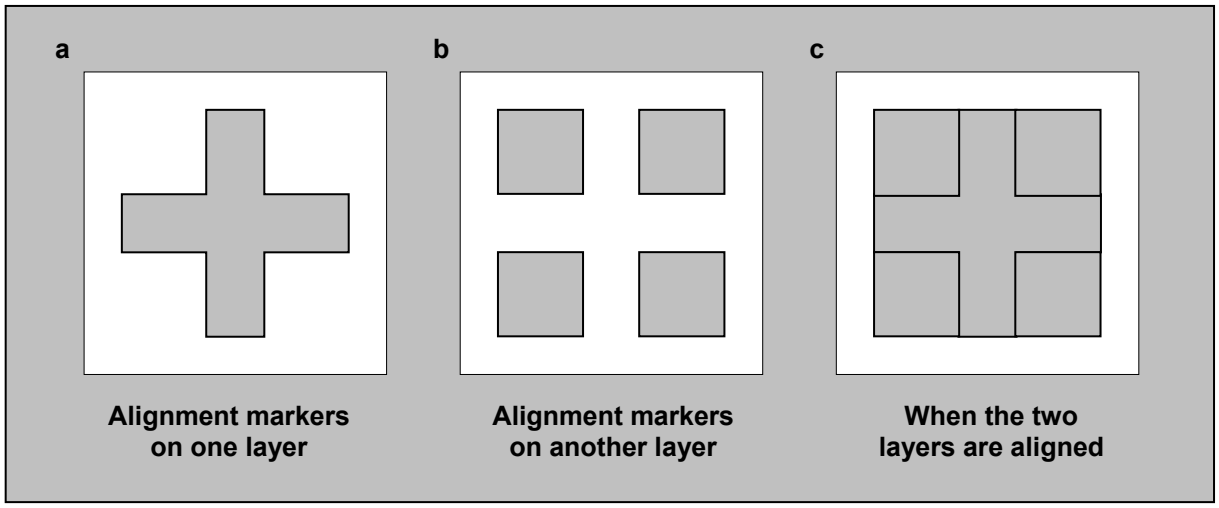

Fig. 5-3 *The diagrams illustrate how '+' and squares patterns in a window are used as alignment markers to align the features on a mask to the features already on the silicon wafer.*

5.3 PHOTOLITHOGRAPHY

Photolithography process involves using light and a mask layer to transfer the patterns on the mask layer to the surface of a silicon wafer coated with a layer of photoresist. Photoresist is a photo sensitive material that either cross-links or disintegrates when exposed to light of a particular wavelength. A positive photoresist disintegrates while a negative photoresist cross-links when exposed to light. In the photolithography process for producing the micro T-mixer, slightly different process parameters were used when different features were transferred to the silicon wafer. This is because different features with different depths to be etched require photoresist coatings of different thicknesses. The features of via holes were first transferred to the silicon wafer. This was then followed by the features of the micro T-mixer and finally the features of inlet and outlet ports on the back side of the wafer. In all cases, AZ 5214E photoresist produced by Clariant was used in the positive mode and it was spin coated on the silicon wafer. Exposure was carried out with UV radiation. The silicon

wafer with latent image was developed in AZ 726 MIF tetra-methyl ammonium hydroxide (TMAH) developer to remove the disintegrated photoresist and to expose the underlying silicon substrate. After rinsing the developed silicon wafer with de-ionized water to remove any excess developer, the wafer was etched by DRIE process described later. The photoresist left on the etched wafer was removed by undergoing a 20-minute oxygen plasma etching. The photolithographic process described above was repeated for the subsequent layers of features.

Due to the different depths required for the different features, the silicon wafer was etched for different durations in a dry etcher. As the photoresist layer was gradually depleted in the etcher, a thick photoresist layer was required when deep features were etched. For the features of square via holes and inlet and outlet ports, a thick layer of photoresist was required. The thickness and quality of the coating is however a function of the spin speeds. 2000 rpm is the minimum spin speed which an acceptable quality of coating can be produced. According to the data sheet for AZ 5214E photoresist provided by Clariant, the characteristic thickness of the coating spun at 2000 rpm is 1.98 μm. This was however not sufficiently thick for the etch duration intended. This problem was overcome by spinning multiple layers of photoresist on the wafer according to the following recipe. The first layer of photoresist was spun on the wafer at 2000 rpm for 20 seconds, preceded and followed by slower spins of 600 rpm for 5 seconds. The wafer was then baked for 20 seconds at a temperature of 110 °C. The wafer was let to cool down before the procedure was repeated to apply the second coating to the wafer. A 50-second bake at the same temperature was performed for the last layer of coating applied. Up to three coatings can be applied in this way to produce a thick layer of photoresist for prolonged etching. The flatness of the photoresist coating deteriorates with more than three coatings. The contact between the wafer and the mask plate during exposure will be affected when this happens. Besides, too thick a

photoresist layer presents problems in the exposure and development of the photoresist coating. Two layers of coating were applied for the via hole and the inlet and outlet port patterns while just one coating was sufficient for the micro T-mixer patterns.

The UV exposures for the via hole and micro T-mixer patterns were carried out on a Canon PLA-501FA mask aligner with an illumination power of 12.6mW/cm^2. But when transferring the patterns of the inlet and outlet port to the back side of the wafer, the patterns had to be aligned to the patterns already etched on the front side. A double sided mask aligner was therefore required to perform a front-to-back aligning and this was performed on a Karl Suss MA45 double sided mask aligner. When two coatings were applied, a 20-second exposure time was performed; otherwise a 12-second exposure time was used for a single layer of coating.

5.4 Deep Reactive Ion Etching

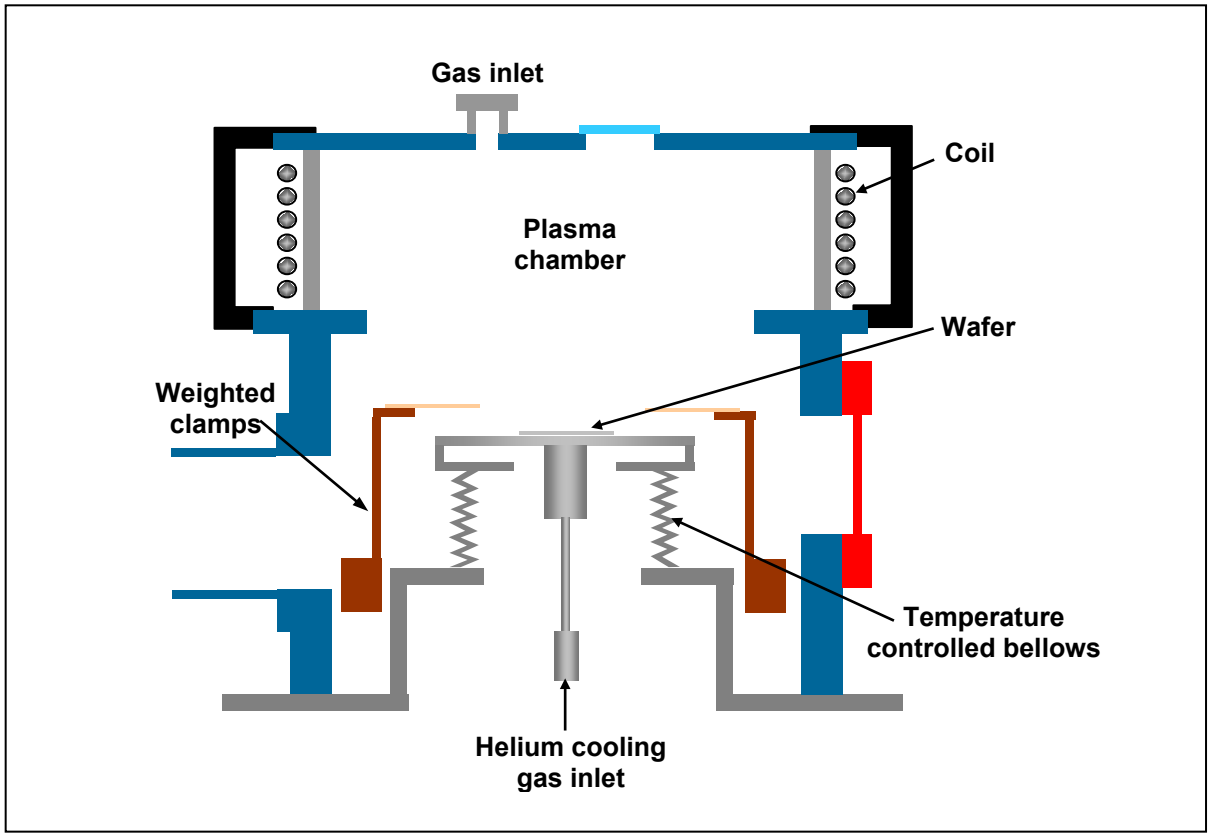

Fig. 5-4 *The schematic diagram shows an STS ICP system that was used to etch the features in the micro T-mixer.*

Deep reactive ion etching (DRIE) enables features to be etched deep into a silicon substrate from less than 10 μm to over 500 μm while maintaining the anisotropy of the etch. The result is the production of features with high aspect ratio and almost vertical sidewalls. The etching by DRIE process is not limited by the crystallographic planes of the silicon, therefore offering flexibility in the design of microstructures. As it is a dry etching process, it also eliminates the problem of stiction associated with wet etching. Some examples of application made possible by DRIE are described by Clerc *et al.* (1998). In this study, the DRIE process is effected in an inductively coupled plasma (ICP) etcher manufactured by STS using a silicon dry etch technique invented by Lärmer and Schilp (1992). The ICP etcher utilises the Advanced Silicon Etch (ASE^{TM}) process created from this technique that employs a sidewall passivation to attain anisotropy in the etched features. A schematic diagram of the STS ICP system is shown in *fig. 5-4*. Unlike conventional plasma tools, ICP systems are able to produce high plasma densities at low pressures. A high plasma density improves etch rate while a low pressure reduces ion scattering and thus improving the control of the etch profiles. Other benefits of an ICP system are the more efficient transport of species into deep trenches that reduces micro-loading characterized by the formation of silicon 'grass' and the better confinement of the plasma that results in the reduction of losses. The details of an ICP system can be found in McAuley (2001).

In a conventional reactive ion etching (RIE) system, no separate etch and passivation steps are present. The etch precursor gases supplied to the process chamber are dissociated into a plasma of ions and radicals where the bombardment of ions onto the surface of the substrate and the reaction between the radicals and the substrate molecules result in the etching of the substrate. But in the ASE^{TM} process, the sidewall passivation step is separated from the etch step by using sequentially alternating etch and deposition steps to achieve anisotropy even at high aspect ratios. The etch and passivation gases used are SF_6 and C_4F_8

respectively. During the passivation step, the C_4F_8 precursor gas is dissociated to produce CF_x^+ ion and $CF_x\cdot$ radical species. The latter form a polymeric passivation layer on the silicon surfaces. The process is isotropic and is illustrated in *fig. 5-5a*. The passivation step is followed by the etch step and the passivation gas in the plasma chamber is replaced by the etch gas. The passivation layer on horizontal surface is removed by the bombardment of SF_x^+ ions created by the dissociation of the SF_6 precursor gas as shown in *fig. 5-5b*. The passivation layer on the vertical surface is less bombarded and so is not removed. The passivation layer protects the sidewall from subsequent etch steps, therefore maintaining the anisotropy of the etching. The radicals that are created together with the ions etch the exposed silicon surfaces after the horizontal passivating layer is removed. The passivation and etch steps are then repeated in the same manner to produce features with vertical sidewalls. As etching in the vertical direction and passivation of sidewalls can be controlled separately, the parameters can be adjusted independently to achieve the best anisotropy.

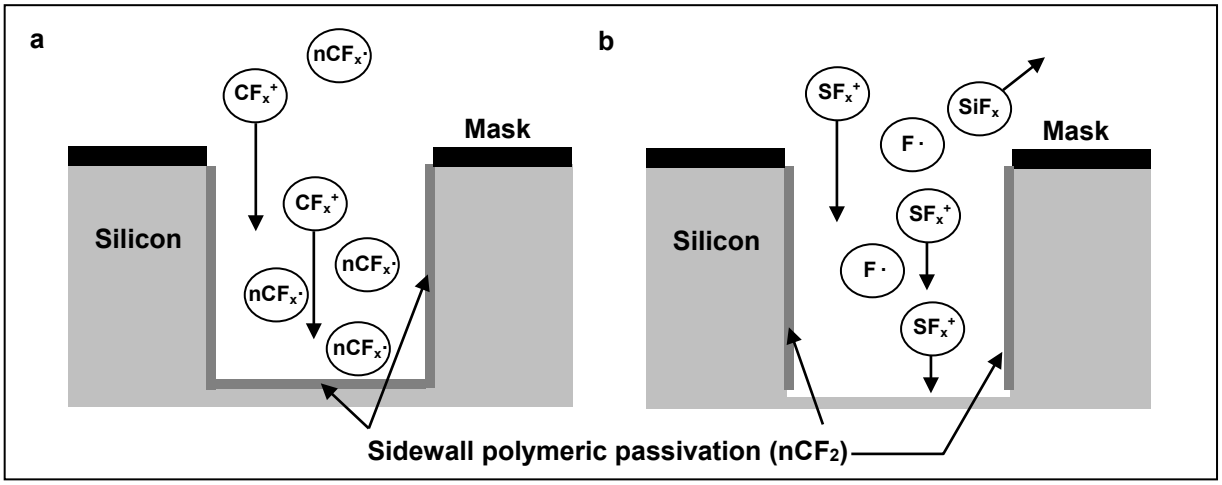

Fig. 5-5

a) Polymeric passivation layer formed by the dissociated C_4F_8 precursor gas during the passivation step.

b) Passivation layer at bottom of channel is removed by the bombardment of ions and the exposed silicon substrate is then etched by radicals during the etch step.

In etching the features of the micro T-mixer, a coil power of 600W was used in both etch and passivation steps. An additional platen power of 12 W was applied during etch step. The coil power is used to dissociate the etch and passivation precursor gases into their

respective ions and radicals for etching and deposition of the passivation layer. Increasing the platen power improves the directivity of the ions and therefore increases the etch rate and at the same time also increases the mask sputter rate. The volumetric flow rates of the SF_6 and O_2 etch gases during etch step were 130 sccm and 13 sccm respectively while the flow rate of the C_4F_8 passivation gas during passivation step was 100 sccm.[1] The pressures in the plasma chamber during etch and passivation steps were maintained at 30 mTorr and 20 mTorr respectively. The etch and passivation cycle times were 13 seconds with a ratio of 8:5 for the etch and passivation times. The effects of changing these etching parameters on etch rate, etch selectivity and etch profile can be found in a parametric study of DRIE using an ICP source carried out by Jansen *et al.* (2001). The micrographs in *fig. 5-6* show the cross sections of the trenches etched using the above process conditions. Trenches with vertical sidewalls were produced, which when bonded with a glass lid formed closed microchannels with rectangular cross-section.

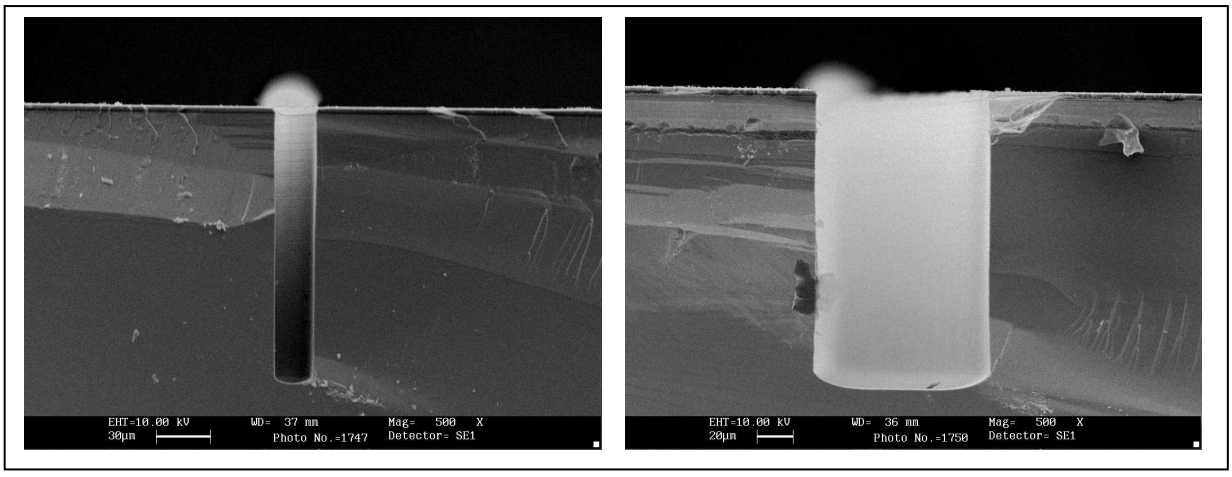

Fig. 5-6 *The micrographs of the cross-sections of microchannels in different widths on the same wafer. On the left is a microchannel with a width of 20 µm and a depth of 154 µm. On the right is a microchannel of 100 µm wide and 180 µm deep.*

The etch depth is dependent on the duration of the etching. An etch duration of 100 minutes was used to etch the via holes to a depth of more than 250 µm. Two depths of 50 µm

[1] *A Standard Cubic Centimetre per Minute (sccm) is defined as a mass flowrate of a cubic centimetre of gas per minute at a pressure of 1 atmosphere and a temperature of 273 K.*

and 82 μm for the micro T-mixer channels were produced with etch durations of 20 and 40 minutes respectively. The etch duration used to etch the inlet and outlet ports at the back side of the wafer was 100 minutes, resulting in the features coinciding with the via hole features on the front side of the wafer. The relationship between etch depth and etch duration is a function of feature size and loading for the same process conditions set on the etcher. Loading is the percentage of exposed area on the wafer to be etched. It is therefore common that under the same process conditions, the etch rate for a large reservoir is faster than that for a narrow trench and the etch depth achieved by a wafer with a low loading is higher than that achieved by a wafer with a high loading for the same etch duration. The phenomenon of aspect ratio dependent etch rate has been investigated and described by Kiihamäki and Franssila (1999), Kiihamäki (2000) and Kiihamäki *et al.* (2000) while the loading effects on etch rate have been described by Karttunen *et al.* (2000).

5.5 THROUGH WAFER ETCHING

Through wafer etching is required in the production of the micro T-mixers in this study. It allows the liquids to be fed from the back side of the chip while the mixing process in the micro T-mixer can be observed from the front under an optical microscope. However, a through wafer etch can not be carried out directly in an STS ICP etcher described in the previous section. This is because the back side of the wafer is cooled by a circulating helium cooling gas when the etching process is proceeding. As soon as the wafer is etched through, the process conditions in the plasma chamber are significantly affected due to the leakage of the helium cooling gas into the plasma chamber. In order to overcome this problem, a handle wafer is used where the handle wafer and the wafer to be etched through are bonded together by photoresist. This prevents the helium cooling gas from leaking into the plasma chamber when the wafer is etched through.

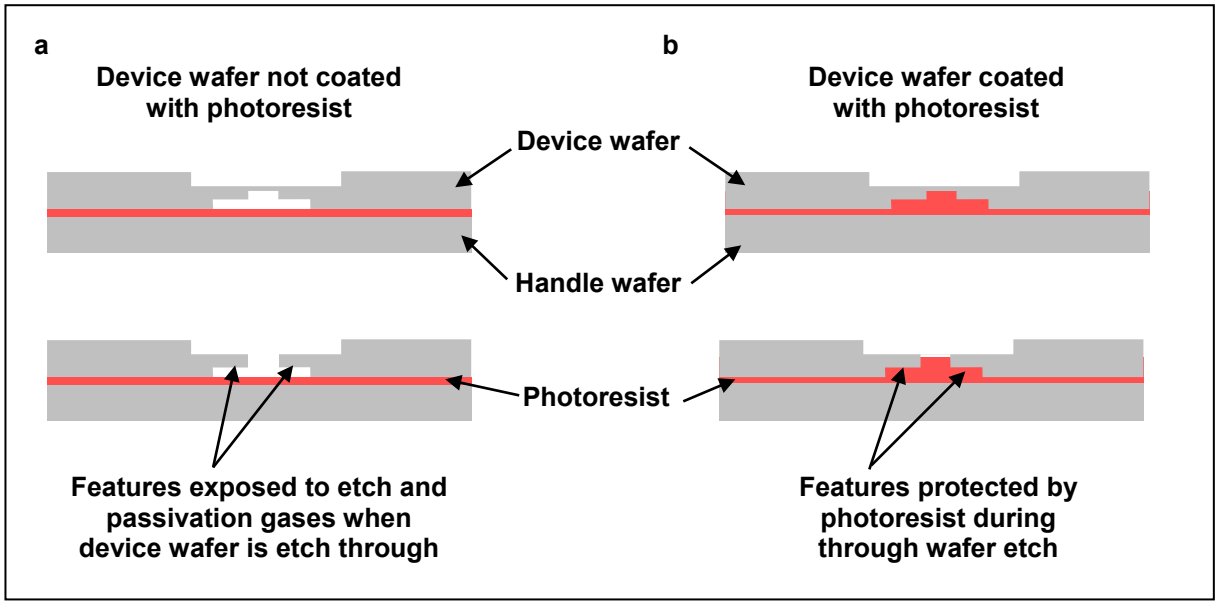

Fig. 5-7 *When the device wafer is not coated with a layer of photoresist (a), the features on the front side of the device wafer is exposed and damaged by the etch and passivation gas when the wafer is etched through. When a layer of photoresist is coated (b), the features are protected from damage caused by the etch and passivation gases.*

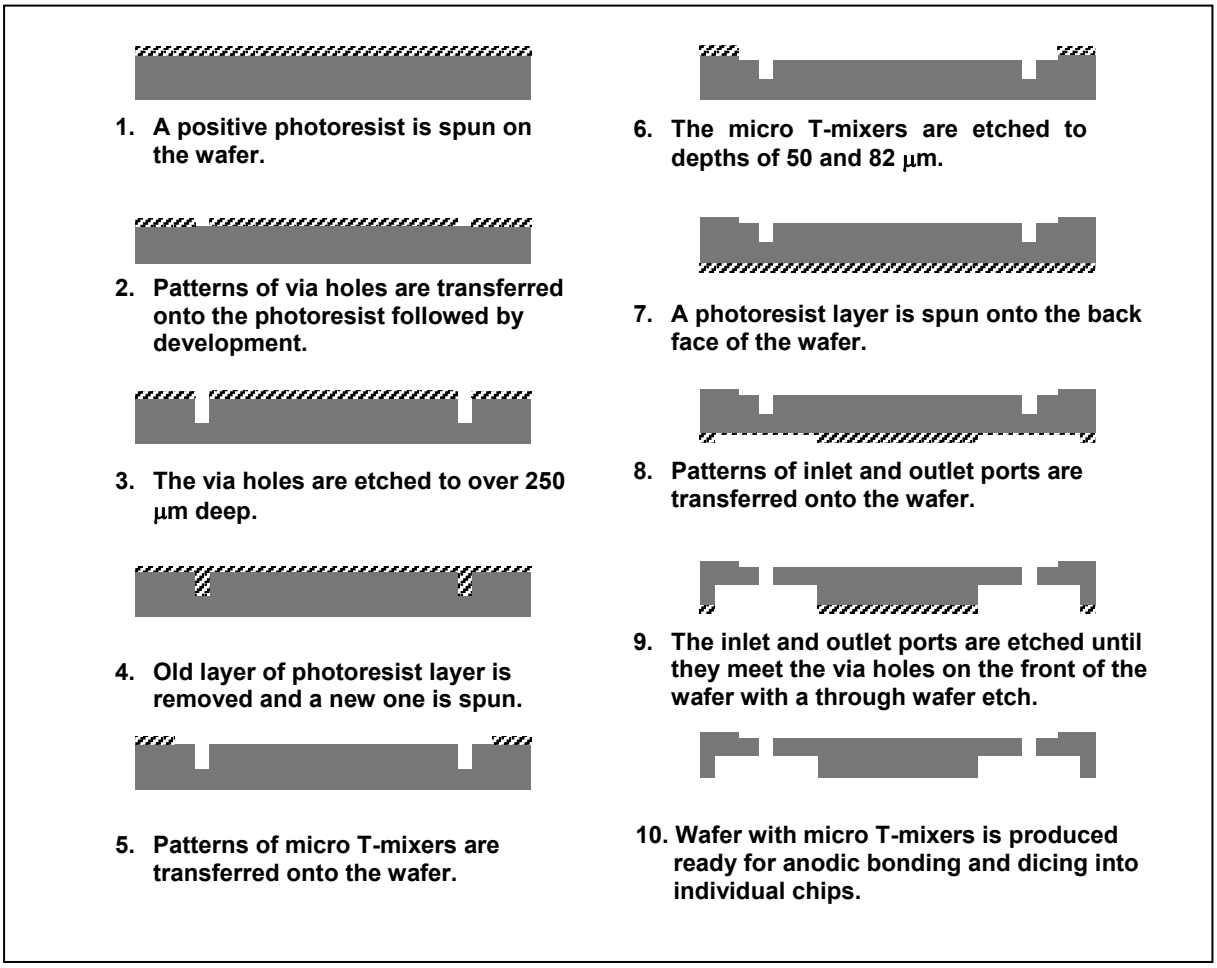

Fig. 5-8 *The diagrams show the sequence of photolithography and etching processes involved in the production of the micro T-mixers.*

The following procedures were followed when a through wafer etch was carried out. The handle wafer was baked at 150 °C for 30 minute to ensure a dry surface for optimum photoresist adhesion. A layer of Clariant AZ 5214E photoresist was spin-coated onto both the handle and device wafers at 2000 rpm for 20 seconds. The two wafers were then pressed together firmly after aligning the wafer flats together. A photoresist layer was coated on both sides to prevent the etched features on the front face from being exposed and damaged by the etch and passivation gases when the device wafer was etched through from the back. By spin-coating a layer of photoresist on the front side of the device wafer before bonding, the features were coated and thus were being protected by the photoresist as shown in *fig. 5-7*.

The bonded wafers were then placed on a cool hotplate and weights were placed on the wafers. This was to prevent the wafers from separating before placing the weights due to the evolution of solvent gas from the photoresist coating at high temperature. The hotplate was then switched on and the wafers were baked at 110 °C for 90 minutes. The wafers prepared were then ready for through wafer etch in an STS ICP etcher. When the through wafer etch was completed, the wafers were separated by immersion in a concentrated nitric acid solution at 50 °C for a few hours. The process steps that have been described so far can be summarized in a flow diagram as shown in *fig. 5-8*.

5.6 ANODIC BONDING

Anodic bonding is a very useful tool for packaging MEMS sensors. It allows silicon and glass substrates to be bonded together without the need for adhesive. It has been widely used in the production of pressure sensors (Tohyama *et al.*, 1996) and accelerometers (Xiao *et al.*, 1999) and it has also been proven to be an enabling technology for microfluidic devices (Li *et al.*, 2004). In pressure sensors and accelerometers, cavities in the silicon have to be hermetically sealed to ensure high performance. The use of adhesive is not desirable due to

the evolution of gas from the adhesive to the sealed cavity with time, thus affecting the performance and accuracy of the devices. Anodic bonding on the other hand electrostatically bonds silicon and glass together on the molecular level, therefore eliminating the possibility of the loss of vacuum in the sealed cavities. In microfluidic devices, anodic bonding enables a glass lid to be bonded onto a silicon wafer with etched trenches and cavities to form closed microchannels and reservoirs. The use of anodic bonding in microfluidic devices eliminates the possibility of contamination by the adhesive. Pyrex glass is particularly suited for anodic bonding with silicon due to its material composition. There are many types of Pyrex glass available depending on the trace elements present in the glass that result in the glass having certain special properties. For example, Pyrex 7070 has high resistivity that makes it suitable for applications where a good dielectric stability is required. But for normal applications where special properties are not required, Pyrex 7740 is the most common and reliable for anodic bonding with silicon. The evaluation of anodic bonding between various glass types and silicon was carried out by Rogers and Kowal (1995).

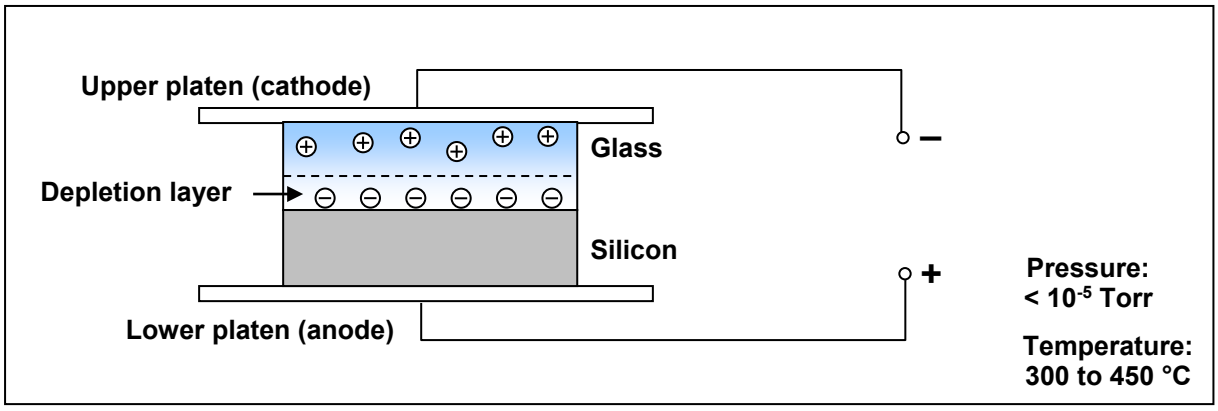

Fig. 5-9 *The diagram illustrates the silicon to glass anodic bonding process. The high temperature and electric potential applied result in the formation of a depletion layer in the glass wafer that strongly attracts the silicon wafer.*

After a through wafer etch was performed onto the wafer and the wafer separated from its handle wafer, the wafer was anodically bonded to a Pyrex 7740 glass wafer produced by Corning. In the anodic bonding process, the glass and silicon wafers to be anodically bonded were placed on the upper and lower platens respectively in the process

chamber of an anodic bonder. During the anodic bonding process, the process chamber was pumped down to a vacuum of less than 1×10^{-5} Torr. Any solvent molecule that might have been adsorbed onto the silicon surface was therefore removed. The wafers were then heated up to a temperature of 400 °C before the two wafers were aligned and pressed together by raising the lower platen. For normal anodic bonding process, temperatures between 300 and 450 °C are commonly used. The upper and lower platens were connected to a potential difference enabling an electric field to be applied across the wafer assembly. The upper platen acts as the cathode while the lower platen acts as the anode. To effect the anodic bonding process, a potential difference of up to 1 kV was applied across the wafers in contact. The progress of the bonding was determined by observing the spreading of the coloured interference fringes. These interference fringes disappeared leaving a darker background colour when the anodic bonding process was completed.

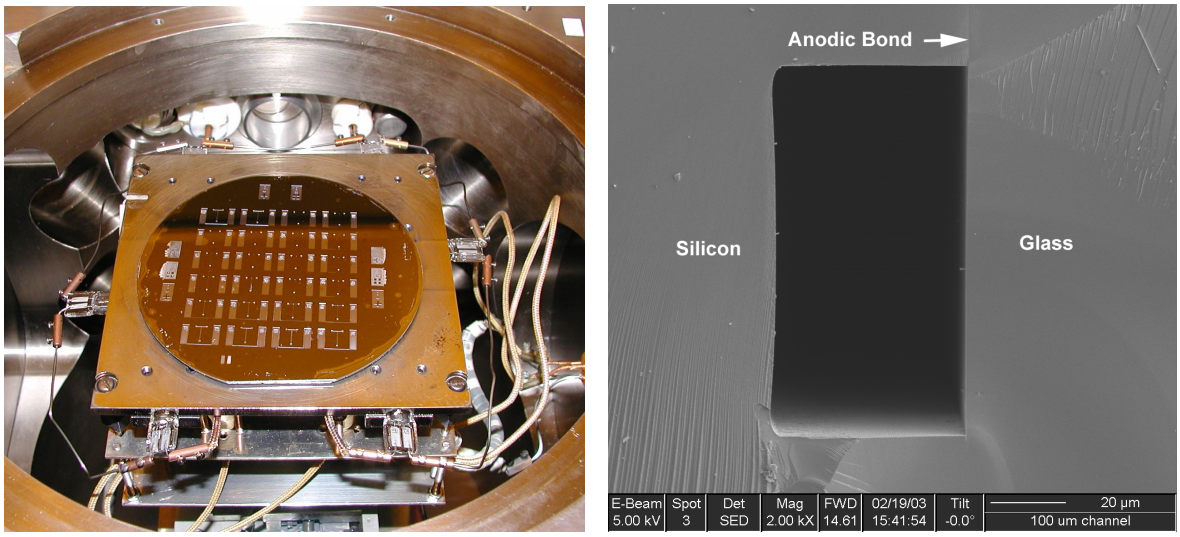

Fig. 5-10 *The photograph on the left shows the glass-silicon wafer assembly after anodic bonding is carried out. The micrograph on the right shows the cross-section of one of the microchannels formed by anodic bonding.*

The strong bond that is formed during the anodic bonding process can be attributed to the electrostatic attraction between the two wafers. When the two wafers were heated to a

high temperature, the positive sodium ions in the glass wafer become mobile. These mobile sodium ions are repelled by the silicon wafer acting as an anode away from the glass-silicon interface when an electric potential is applied across the wafers as shown in *fig. 5-9*. A depletion layer consisting of oxygen anions with high electric field strength is formed in the glass wafer as a result, therefore strongly attracting the silicon wafer. The high attraction between the wafers brings oxygen anions closer to the silicon to form chemical bonds with silicon. This results in a high strength achieved by anodic bonds. *Fig. 5-10* shows the silicon-glass wafer assembly after anodic bonding process is performed and the cross-section of one of the microchannels formed by the anodic bonding process.

5.7 WAFER DICING AND INTERCONNECTION

After the silicon device wafer was bonded to the Pyrex glass wafer, the wafer assembly was diced into 24 individual chips. This was carried out on a wafer cutter machine with a diamond saw. The individual chip measured 15 mm by 11 mm. The silicon device layer that was bonded to the Pyrex glass layer on its front was bonded to a clear polystyrene plate on its back. This produced an assembly where the silicon device layer was sandwiched between Pyrex glass and polystyrene plate. The polystyrene plate measured 3 cm by 3 cm with three through holes drilled to facilitate the connection of feed tubing before it was bonded to the silicon-glass chip. The locations of the through holes were in alignment with the inlet and outlet ports on the chip. Loctite® adhesive was used to bond the polystyrene plate onto the silicon-glass chip. A polystyrene plate was used instead of a Pyrex glass plate because of the difficulties encountered in making through holes in Pyrex glass wafers with the available equipment. As a polystyrene plate was used, anodic bonding was not possible. Adhesive was used in the bonding instead. After a sandwiched micro T-mixer chip was produced as shown in *fig. 5-1b*, feed tubing was connected to the through holes on the polystyrene plate and

secured with adhesive as shown in *fig. 5-1c*. The PEEK™ feed tubing used was obtained from Upchurch Scientific. The micro T-mixer chip produced was then ready to be used in mixing characterization work.

5.8 CLOSURE

The detailed fabrication process of the micro T-mixer used in this study has been described in this chapter. The various process parameters used in each processing step are summarized here in *table 5-1*.

Process step	Process parameter
Spin coating	Photoresist: Clariant AZ 5214E Spin: 600 rpm for 5s, 2000 rpm for 20s and 600 rpm for 5s Intermediate bake: 110°C for 20s Final bake: 110°C for 50s Number of photoresist coatings: Patterns with via holes: 2 Patterns with micro T-mixer: 1 Patterns with inlet and outlet ports: 2
Photolithography	Radiation: UV light Exposure time: 12 seconds exposure – one-layer photoresist coating. 20 seconds exposure – two-layer photoresist coating.
Development	Developer: Clariant AZ 726 MIF (TMAH) Developing time: 30 to 60 seconds
DRIE	Etch gas: SF_6; Passivation gas: C_4F_8 Etch Durations: Via holes – 100 mins. Micro T-mixers – 20 and 40 mins. Inlet and outlet ports – ca. 100 mins.
Anodic bonding	Material: 500 μm thick Pyrex 7740 glass wafer Pressure: $< 10^{-5}$ Torr Temperature: 400°C Potential difference: 1 kV

Table 5-1 Summary of the process parameters used in the fabrication of the micro T-mixers investigated in this study.

EXPERIMENTATION: TESTING

6.1 EXPERIMENTATION SYSTEM

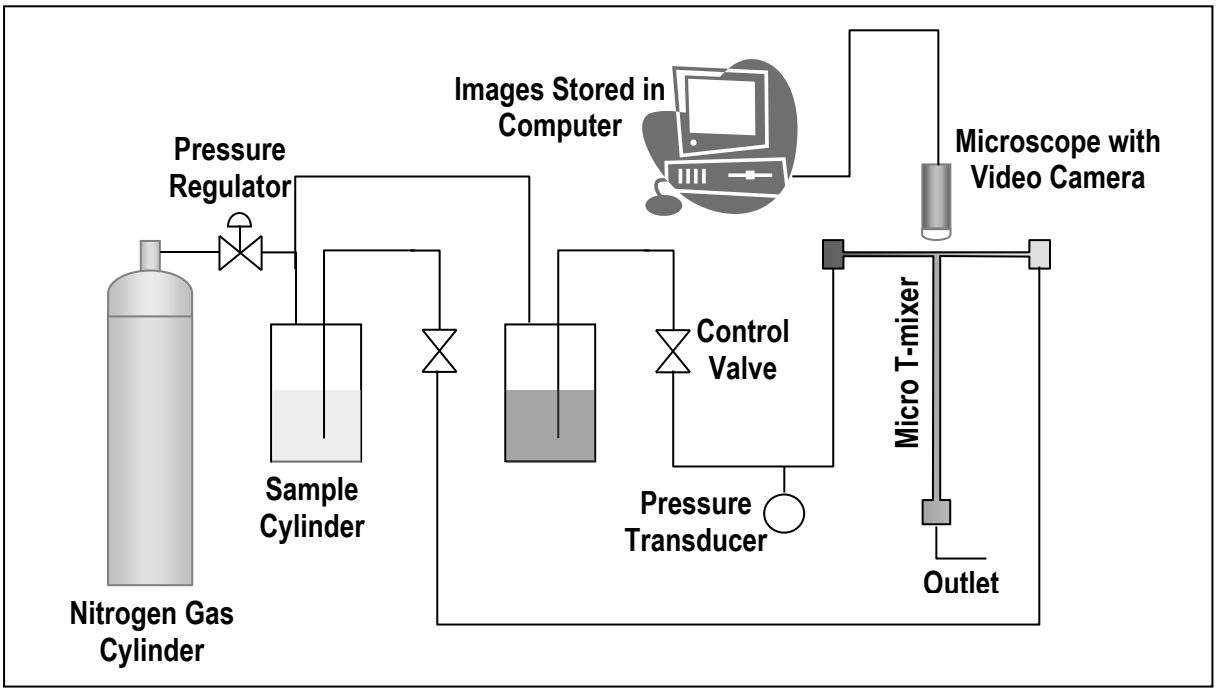

Fig. 6-1 *The schematic diagram shows the experimentation system for the mixing characterization work.*

The micro T-mixer chips fabricated with the processes described in the previous chapter were used in the mixing characterization work. The schematic diagram of the experimentation system is illustrated in *fig. 6-1*. The two liquids to be mixed were separately contained in two stainless steel sample cylinders from Swagelok®. The sample cylinders had a volume capacity of 150 ml and were able to withstand an internal pressure of 124 bar. The inlets of the micro T-mixer were each connected to the outlet of the sample cylinders by

PEEK™ tubing. PEEK™ valves, also obtained from Upchurch Scientific, were used to control the liquid entry into the micro T-mixer. The pressure of the liquid just before entering the micro T-mixer was measured by a GE Druck PTX 500 pressure transducer. The inlets of the stainless steel sample cylinders were connected together by a tee-piece that in turn was connected to a nitrogen gas cylinder, which provided the pressure required to cause liquid flow in the micro T-mixers.

Before the mixing experiments were carried out, the stainless steel sample cylinders were filled with the liquids to be mixed. The liquids were pre-filtered by passing them through a filter with 0.2 μm pore size before they were stored in the cylinders. This was to ensure no blockage in the micro T-mixer due to particulates that may be present in the liquids. Two sets of liquids were used in the mixing characterization work. The first set was a commercial blue colour dye solution and colourless de-ionized water. The commercial blue dye was diluted with de-ionized water to a ratio of 1:9. The mixing experiments were then repeated by using two chemical solutions that produced a distinct colour change when they were mixed. Since the liquids used were aqueous solutions, the density and viscosity of the liquids were assumed to be that of water at 21.5 ºC, the temperature at which the experiments were carried out.

During mixing experiments, pressure from the nitrogen gas cylinder was applied to the liquids in the stainless steel sample cylinders. The applied pressure was controlled by a regulator at the outlet of the gas cylinder. The pressure at the inlet to the micro T-mixer was measured by a pressure transducer, which had been calibrated using a dead weight tester. The mixing process was observed under a Leica Ergolux 200 optical microscope fitted with a Sony SSC-DC50A colour video camera. Images were captured at various applied pressures and at various locations along the mixing channels. At every applied pressure, the flow rate of the mixture in the micro T-mixer was measured by timing the volume of the mixture

collected at the outlet. With the assumption that the depths of microchannels with the same width on the same wafer were the same, the depths of microchannels were obtained by measuring the depth of a microchannel of another micro T-mixer chip from the same wafer. The measurements were acquired in a Focused Ion Beam (FIB) Strata^{TM} DB235 produced by FEI Company. By knowing the cross sectional dimensions of the microchannels, mean flow velocity and Reynolds number of the mixture in the micro T-mixer were calculated. The dimensions of the four sizes of micro T-mixers investigated and described in this study, namely micro T-mixers A, B, C and D, are summarized in *table 6-1* and *fig.4.2*.

Micro T-mixer	A	B	C	D
Mixing channel width (μm)	200	200	100	60
Depth (μm)	82	51	51	51
Hydraulic diameter (μm)	116	81	67	55

Table 6-1 *The table shows the cross sectional dimensions of the mixing channels in the four sizes of micro T-mixer investigated in this study. The hydraulic diameters of the microchannels range from 55 μm to 116 μm. The widths of the inlet channels are designed to be half of that of the mixing channel.*

6.2 CHARACTERIZING THE EXTENT OF MIXING IN EXPERIMENTS

The colour images captured were converted into greyscale images that gave only the luminance of the image in 256 levels. This was done because it was more effective to analyse the combined effect of red, green and blue elements in a pixel on an image than to analyse the three colour elements separately. The images were then analysed by using the image processing techniques similar to that described by Koch *et al.* (1999b). A computer program was written in Visual Basic to analyse the red, green and blue (RGB) levels of the pixels along a line drawn across the mixing channel of the micro T-mixer. The RGB values of a pixel in a greyscale image are essentially the same, which is the luminance level of that pixel. This enabled the progress of mixing along the mixing channel and the uniformity of

concentration across the channel to be quantified and compared, according to the combined effect of RGB values in the images.

In order to determine the point of complete mixing, a reference luminance level that is observed when the mixture is completely mixed was first determined. This was obtained by feeding a premixed solution into the micro T-mixers, capturing and subsequently processing the images as already described. The uniformity of the luminance levels across the outlet of the mixing channel at a particular applied pressure was compared with the reference luminance levels at the same locations. Due to the light source of the optical microscope and small differences in the sensitivity of light sensors in the camera, some noise was present in the luminance level data. There are also reproducible structures in the luminance level data that produce high peaks and deep troughs on the luminance level curve across the mixing channel as shown in *fig. 6-2a*. These reproducible structures are caused by imperfections in the etching that resulted in the presence of dark colour features on the bottom of the channel as shown in *fig. 7-3*. The presence of noise and the reproducible structures made the comparison between different sets of data difficult. In order to remove these relatively high frequency noise and reproducible structures, Fourier analysis was performed on the data by using the Fourier analysis capability in Microsoft Excel to reveal the low frequency concentration changes across the mixing channel as shown in *fig. 6-2b*. The deviation of the resultant luminance curve from its mean, δ, across the mixing channel gives an idea of the extent of mixing at the outlet (*fig. 6-2c*). A luminance level curve having large deviations from its mean means incomplete mixing while a small deviation indicates uniform concentration of blue dye at the outlet. But due to low frequency noise, the reference luminance curve is never a horizontal straight line as shown by the curves in *fig. 6-2d*. The low frequency noise may be due to the bottom surface of the channel that is not perfectly flat. To establish how close a luminance deviation curve has to be to the reference luminance

deviation curve for it to be considered fully mixed, normalized deviation values, $\widetilde{\delta}_{p,i}$, were calculated from equation 6-1.

$$\widetilde{\delta}_{p,i} = \frac{\delta_{p,i} - \delta_{ref,i}}{2\sigma_{ref}} \tag{6-1}$$

where $\delta_{p,i}$ is the deviation from mean at the i^{th} pixel with applied pressure p, $\delta_{ref,i}$ is the deviation from mean at the i^{th} pixel on the reference image and σ_{ref} is the standard deviation of the difference in luminance levels between the original reference luminance curve and the smoothened reference luminance curve after Fourier analysis is performed on it. The $\delta_{p,i}-\delta_{ref,i}$ term in equation 6-1 eliminates the low frequency noise with the assumption that the low frequency noise is the same regardless of the extent of mixing and the applied pressure. Complete mixing is considered achieved if across the outlet, the difference between the luminance deviation curve at applied pressure p and the reference deviation curve is within 95% of the variation in the reference luminance levels from its mean. In other words, complete mixing is achieved if $\left|\widetilde{\delta}_{p,i}\right| \le 1$ for all pixels across the mixing channel. The applied pressure when this is achieved is considered the applied pressure required to cause complete mixing. The Reynolds number of flow in the mixing channel and the corresponding mixing time when this occurs can then be calculated. *Fig. 6-2e* and *fig. 6-2f* show how the above criterion is used to determined if complete mixing is achieved. For a poor mixing at the outlet in Case A, the luminance level curve is not within the range of luminance levels bounded by 95 percentile of the reference luminance curve indicated by the dash lines. For a good mixing at the outlet in Case B, the luminance level curve lies within the ranges bounded by the dash lines fulfilling the criterion for complete mixing.

The extent of homogeneity of a mixture determined by the above procedures is limited by the resolution of the images. Any non-uniformity in blue dye concentration within a pixel in the images cannot be resolved due to the finite resolution of light sensors in the camera.

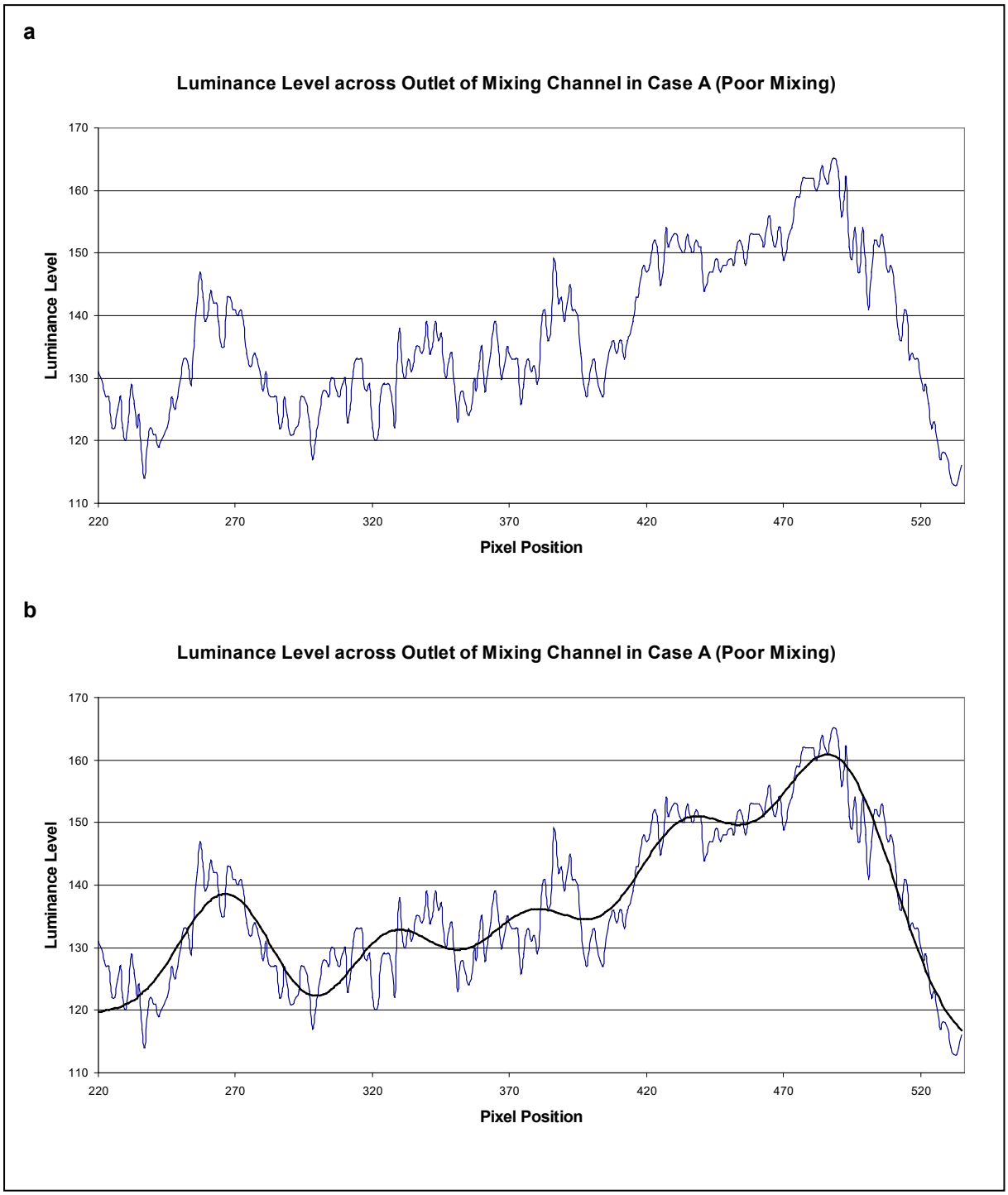

Fig. 6-2 *(a) The luminance level plot of Case A representing poor mixing is extracted from the image captured in the experiment. Note the presence of high frequency noise in the curve. (b) Fourier analysis is performed onto the data in (a) to remove the high frequency noise, producing a smoother luminance level curve (black).*

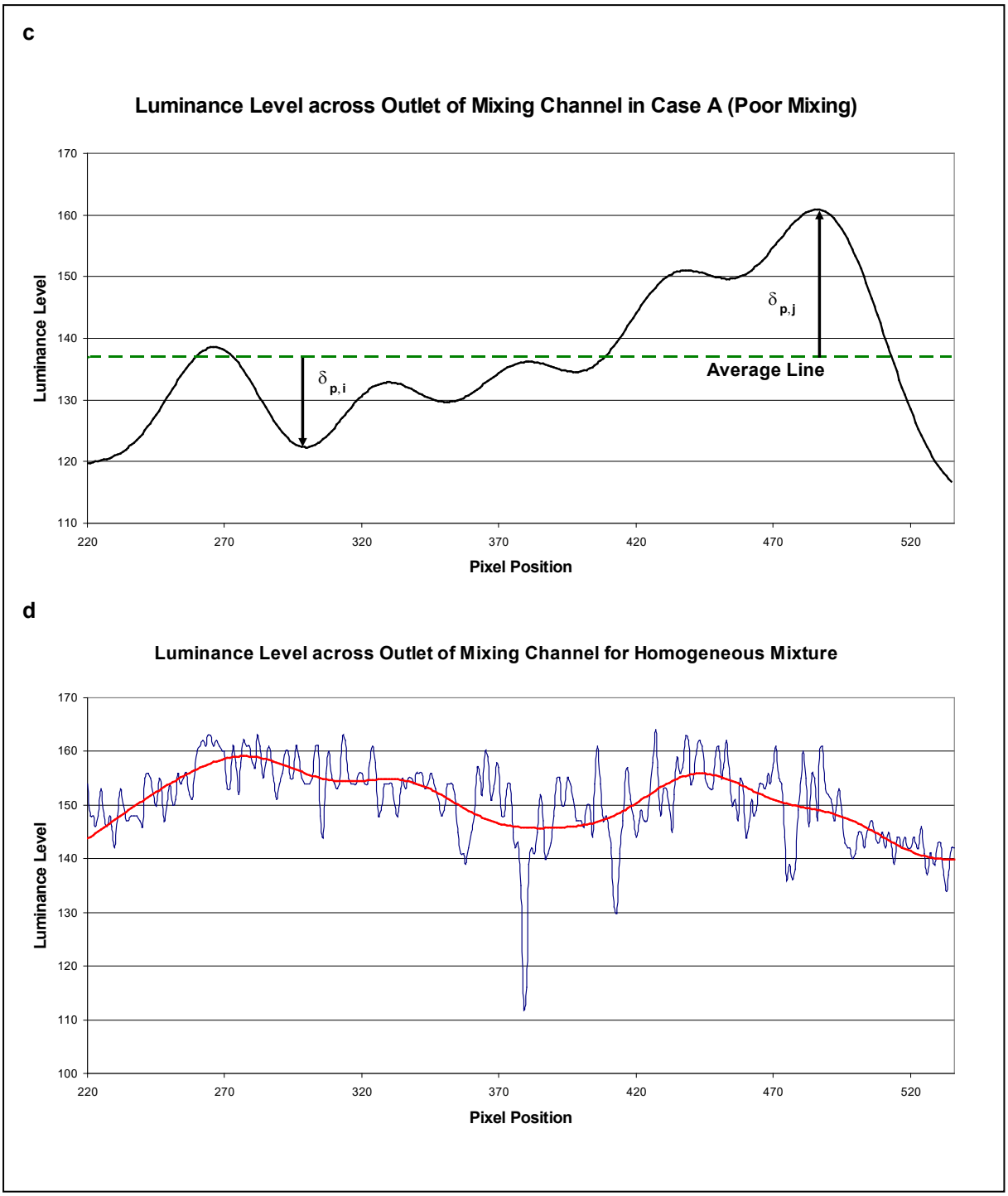

Fig. 6-2 *(c) The deviation at the i^{th} pixel on the smoothened luminance level curve from its mean is denoted by $\delta_{p,i}$. (d) The luminance level curve and the corresponding smoother red curve for a homogeneous mixture in the outlet of the mixing channel.*

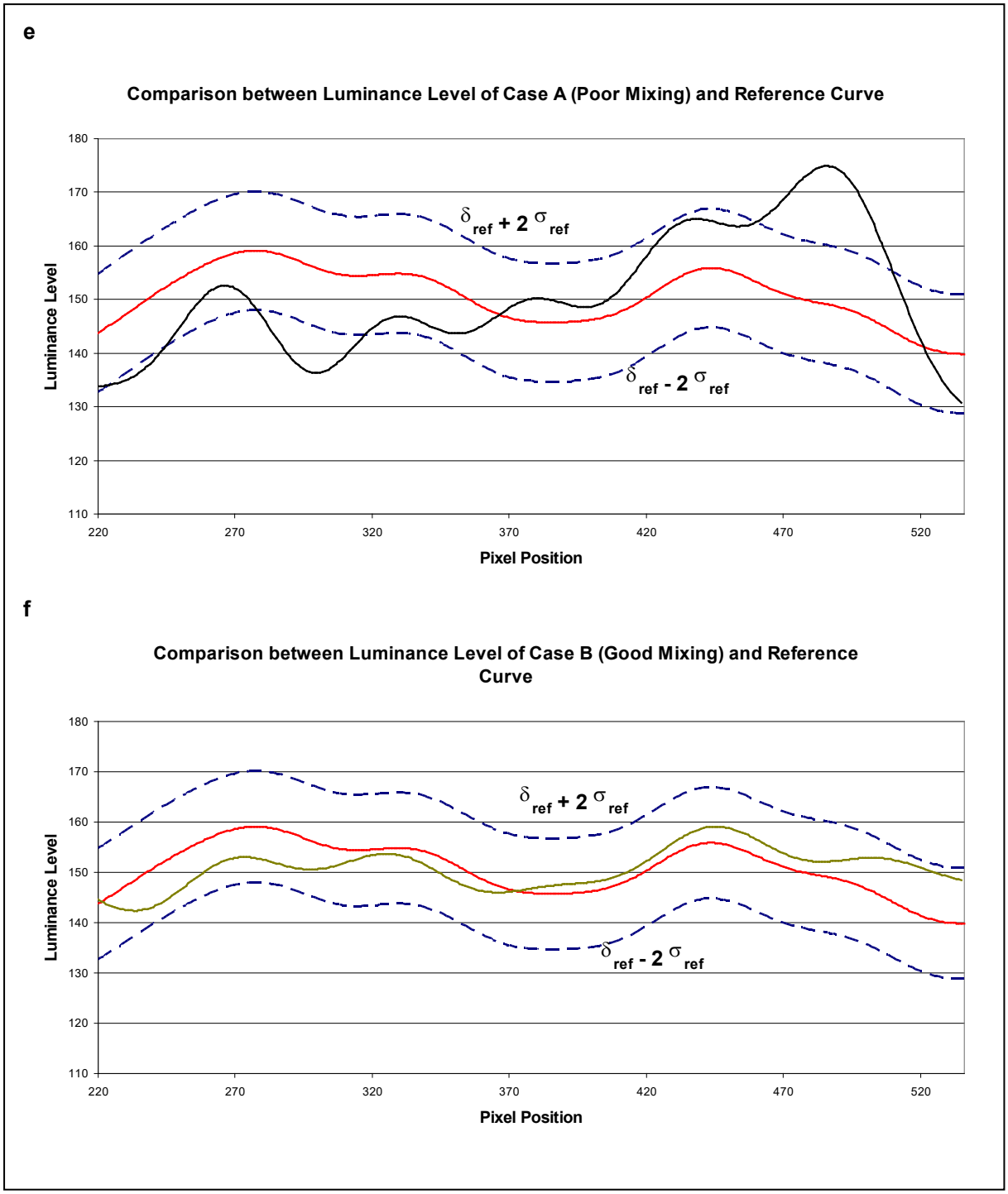

Fig. 6-2 *(e) The smoothened luminance level curve obtained in (b) is compared with the range set by 2 standard deviations of the data for a homogeneous mixture from its mean. (f) When a smoothened luminance level curve is within the range of 2 standard deviations, complete mixing is considered achieved.*

Complete mixing defined above only implies that the mixture is uniform down to a distance equivalent to a pixel. The distance equivalent to a pixel in the images is approximately 0.65 μm. In the worst case scenario if the two liquids were completely segregated within a pixel, the subsequent time which the two liquids needed to completely mix by diffusion would be an order of magnitude shorter than the mixing times of the micro T-mixers investigated. Therefore, this extra diffusion time does not significantly affect the mixing times determined by the method described above.

6.3 MIXING BETWEEN TWO CHEMICAL SOLUTIONS

It was noted by Hardt and Schönfeld (2003) that the extent of mixing in a micromixer characterized using a dye in an aqueous solution could have been amplified if the layers of unmixed liquids were stratified horizontally but not oriented vertically in the flow. The light beam that was transmitted to measure the concentration of blue dye cut across layers of unmixed dye and clear liquid, giving an impression of good mixing due to the averaging effect from the stratified layers. Although it was not intended that the dye and clear liquid formed horizontal stratified layer when they collided at the junction of the micro T-mixer, it was nevertheless possible that horizontal lamella of unmixed liquid were formed in the mixing channel resulting in an illusion of good mixing. The formation of these horizontally stratified layers could be a result of asymmetrical flow patterns caused by different flow velocities at the inlets.

In order to find out whether the results of mixing obtained from the use of blue dye and colourless liquid were susceptible to artefacts described above, the mixing experiments were repeated by using two chemical solutions that gave a distinct colour change when they were completely mixed as suggested by Hessel *et al.* (2003). The chemical reaction used to characterize complete mixing in the micro T-mixer was the hydrolysis of dichloroacetyl

phenol red (DCAPR) by sodium hydroxide (NaOH) solution. The method of preparation of DCAPR and the measurement of its second order reaction rate are described in Appendix B. Before DCAPR was used in the mixing experiments, it was dissolved in an organic solvent such as acetonitrile in a slightly acidic buffer to form a pale yellow colour solution. DCAPR solution has a short hydrolysis time of about 100 μs with 0.1 M of NaOH solution and is therefore suitable for rapid mixing experiments performed here. The experimental procedures for mixing with blue dye and colourless liquid were adopted in the mixing experiments with DCAPR solution. When the two solutions were completely mixed, a dark red colour solution, which appeared as pink in the micro T-mixer, owing to the short path length, was observed. Similar to the case with blue dye, an already hydrolysed DCAPR solution was fed into the micro T-mixer and its image captured. This image was used as a reference for comparing with other images captured during mixing experiments to determine if complete mixing was achieved.

6.4 ATOMIC FORCE MICROSCOPY ON ETCHED SILICON SURFACES

The surfaces of etched channels were characterized by an Atomic Force Microscope (Burleigh ARIS-3300 Personal AFM) to investigate if the liquid flow in microchannels can be affected by the surface roughness of the channel walls. The surface roughness of the channel walls can be determined by an atomic force microscope (AFM), which measures the attractive Van der Waals forces between the sample surface and the tip of a tiny cantilever beam brought very close to the surface to be measured as shown in *fig. 6-3*. When the tip of the cantilever beam is dragged over an area above a sample, the cantilever beam is deflected an amount proportional to the attractive force, which is reflective of the surface topography of the sample. The amount of cantilever deflection is detected by the change in direction of

the beam of laser reflected by the tip of the cantilever. This allows the surface topography of the area to be computed from the deflection of the laser beam.

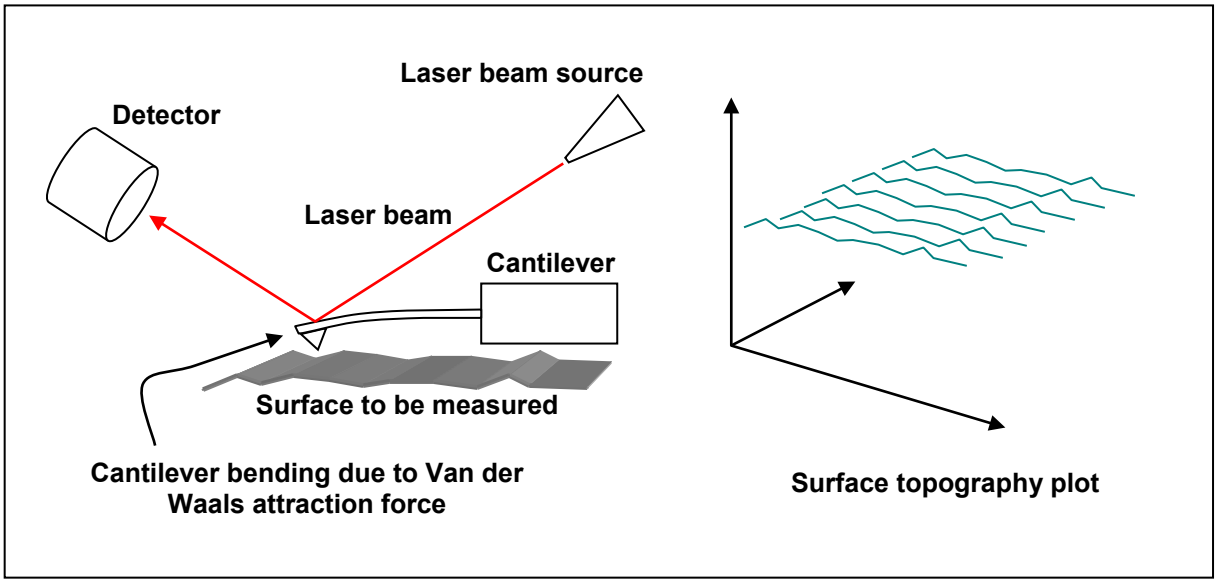

Fig. 6-3 *The deflection of the cantilever caused by the attractive Van der Waals forces is detected by the change in direction of the laser beam reflected by the tip of the cantilever. This set up a relationship between the surface topography and the change in laser beam deflection, enabling the surface topography of the sample to be plotted as shown on the right.*

In order for the cantilever beam of an AFM to approach the vertical sidewalls of a microchannel from above, silicon chips containing microchannels of different widths were cleaved along the microchannel and the samples were mounted in a way that the sidewall was facing upwards. The microchannels measured had a greater depth of more than 100 μm although the microchannels in the micro T-mixers were generally less than 100 μm in depth. This was to enable the change in surface roughness of the vertical sidewall to be investigated. With the AFM in non-contact mode, where the tip of the cantilever did not touch the surface during measurements, the surface topographies at different depth of the vertical sidewall for microchannels of different widths were measured and their results collected and analyzed.

6.5 CLOSURE

The experimentation system set up to perform mixing characterization work and the procedures followed to collect the essential mixing performance data have been described in detail in this chapter. The methods and procedures for characterizing the extent of mixing and determining the point of complete mixing in the micro T-mixers have also been described. Besides using blue dye and colourless de-ionized water as the two liquids for mixing, DCAPR and NaOH solutions that produce a distinct colour change when mixed have also been used to verify the results obtained by mixing blue dye and de-ionized water. Surface roughness measurements have also been carried out on etched silicon surfaces by atomic force microscopy to find out if the liquid flow in microchannel is affected by surface roughness of the channel sidewall. All the results from the experiments will be described in the next chapter.

RESULTS

7.1 MIXING PERFORMANCE OF MICRO T-MIXERS

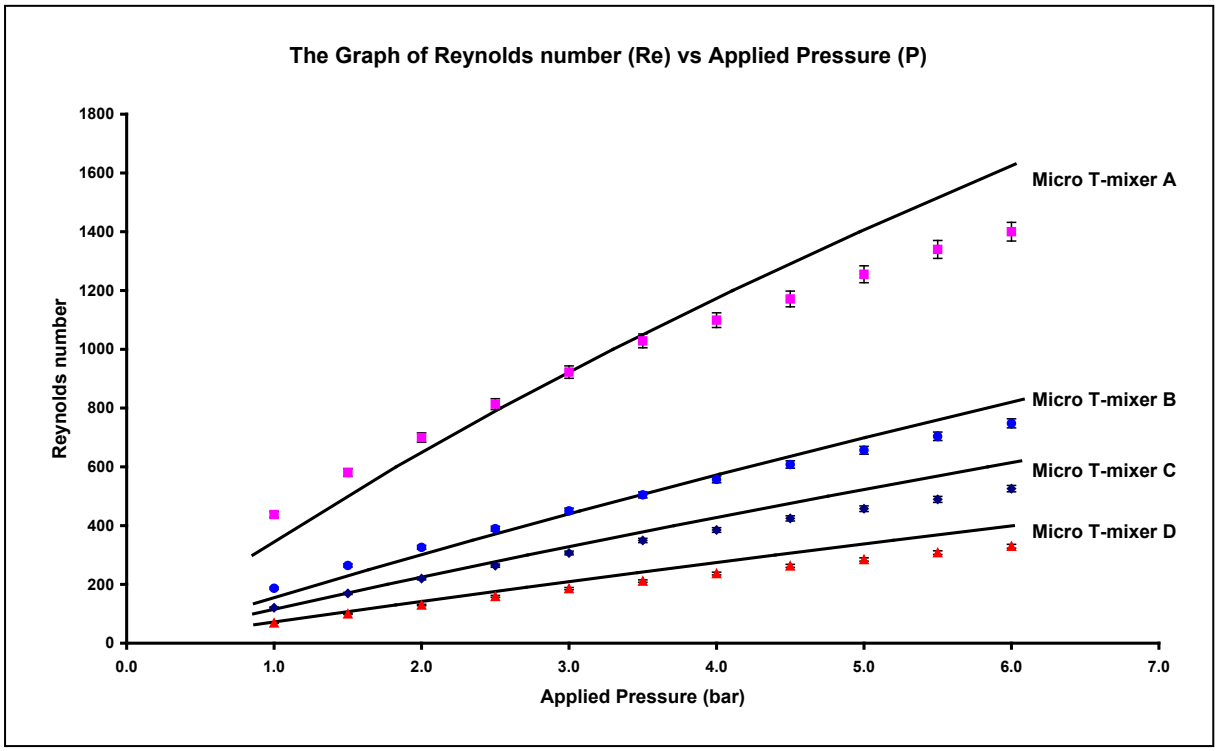

Fig. 7-1 *The graph of Reynolds number of flow in the mixing channel against the applied pressure at the inlets for four sizes of micro T-mixer A, B, C and D investigated in this study. The points are obtained experimentally while the solid lines are the corresponding theoretical curves computed by the method described in Section 4.4.*

In the mixing experiments performed with the fabricated micro T-mixer chips, an applied pressure of up to 6 bar has been used. Leakage due to failure of the bonding between silicon substrate and the polystyrene plate usually occurred at above 6 bar. No failure in the anodic bond between silicon substrate and Pyrex glass plate has been observed under the range of pressures applied. The relationship between the applied pressure and the Reynolds number in

the mixing channel of the micro T-mixer was obtained by measuring the volume flow rate at different applied pressures. *Fig. 7-1* shows a graph of Reynolds number in the mixing channel against the applied pressure at the inlets for the four sizes of micro T-mixers A, B, C and D investigated in this study. The corresponding theoretical curves computed by using the method described in Section 4.4 are also plotted onto the same graph. A Reynolds number of up to 1400 has been achieved in those micro T-mixers having wider channels while a value of only up to a few hundreds has been obtained for those having narrower channels.

In the mixing experiments with micro T-mixers using blue dye and colourless liquid, images were captured at the junction and downstream of the mixing channel at various applied pressures. The same was performed in the mixing experiments using DCAPR solution. *Fig. 7-2* shows a set of images observed at the junction of micro T-mixer B while *fig. 7-3* shows another set of images illustrating the progress of mixing at downstream of the same mixing channel with increasing applied pressure. For mixing experiments using DCAPR solution, the progress of mixing in the mixing channel of micro T-mixer C at different applied pressures is shown in *fig. 7-4*.

It can be seen from the set of images in *fig. 7-2* that at low applied pressure, there was a distinct boundary between the colourless liquid and the blue dye solution when they came together at the junction (*fig. 7-2a-b*). Similar observations can also be observed when DCAPR solution was used in the mixing experiments. A distinct interface between DCAPR and NaOH solutions can be clearly seen. No formation of pink colour solution was observed in the mixing channel as shown in *fig. 7-4a-b* indicating no extensive mixing at low applied pressure. This is somewhat expected as the Reynolds number of flow in the microchannel is low at low applied pressure. The mixture flows in a laminar fashion at low Re. Laminar flow does not encourage mixing between the two liquids and mixing occurs mainly by diffusion. There was some cross flow at the junction when the pressure was increased. This can be

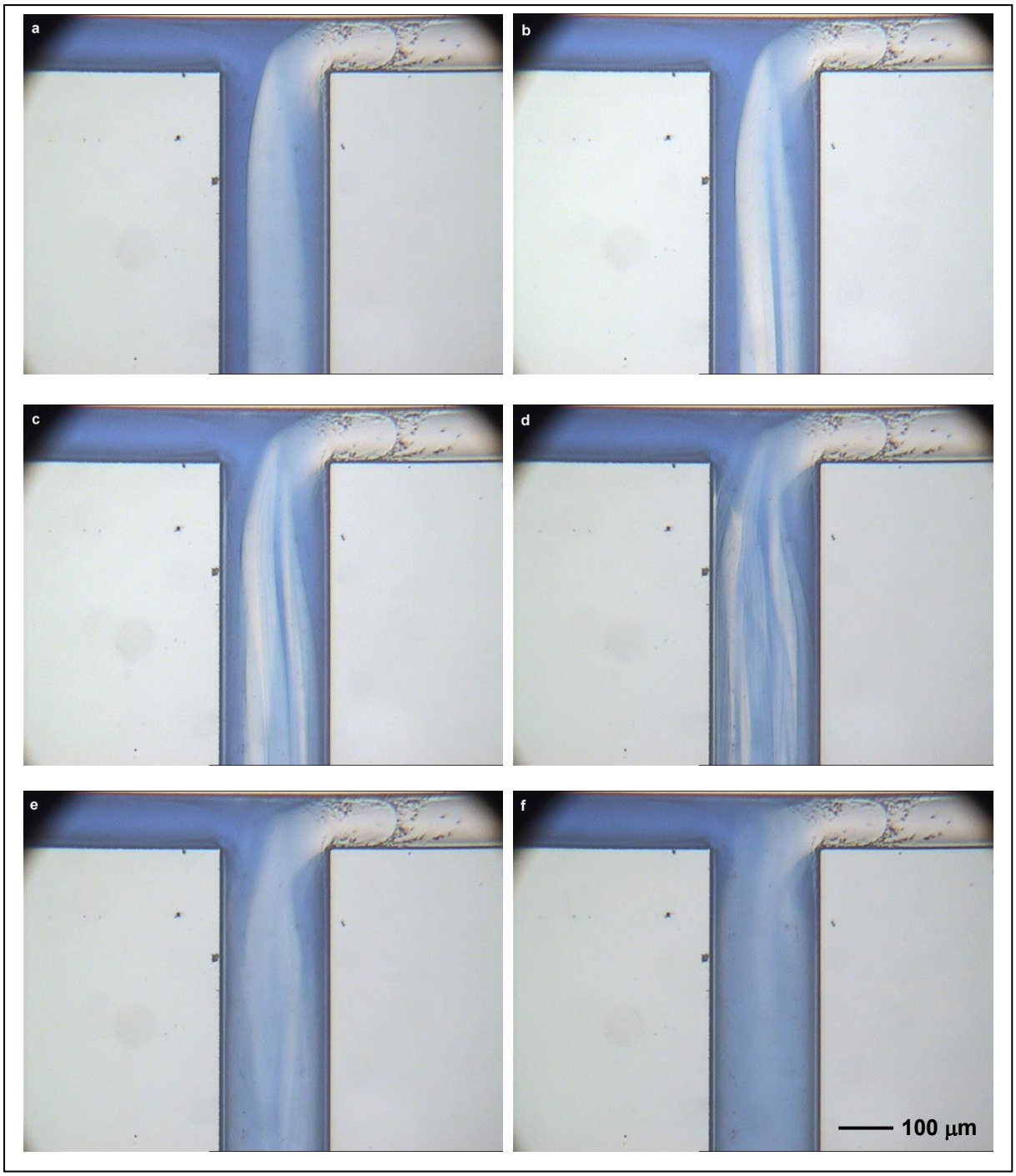

Fig. 7-2 *The observations of the mixing process at the junction of micro T-mixer B at different Reynolds numbers, with their corresponding applied pressures in brackets – (a) 206 (1.12 bar), (b) 311 (1.88 bar), (c) 340 (2.11 bar), (d) 387 (2.48 bar), (e) 422 (2.77 bar) and (f) 585 (4.27 bar).*

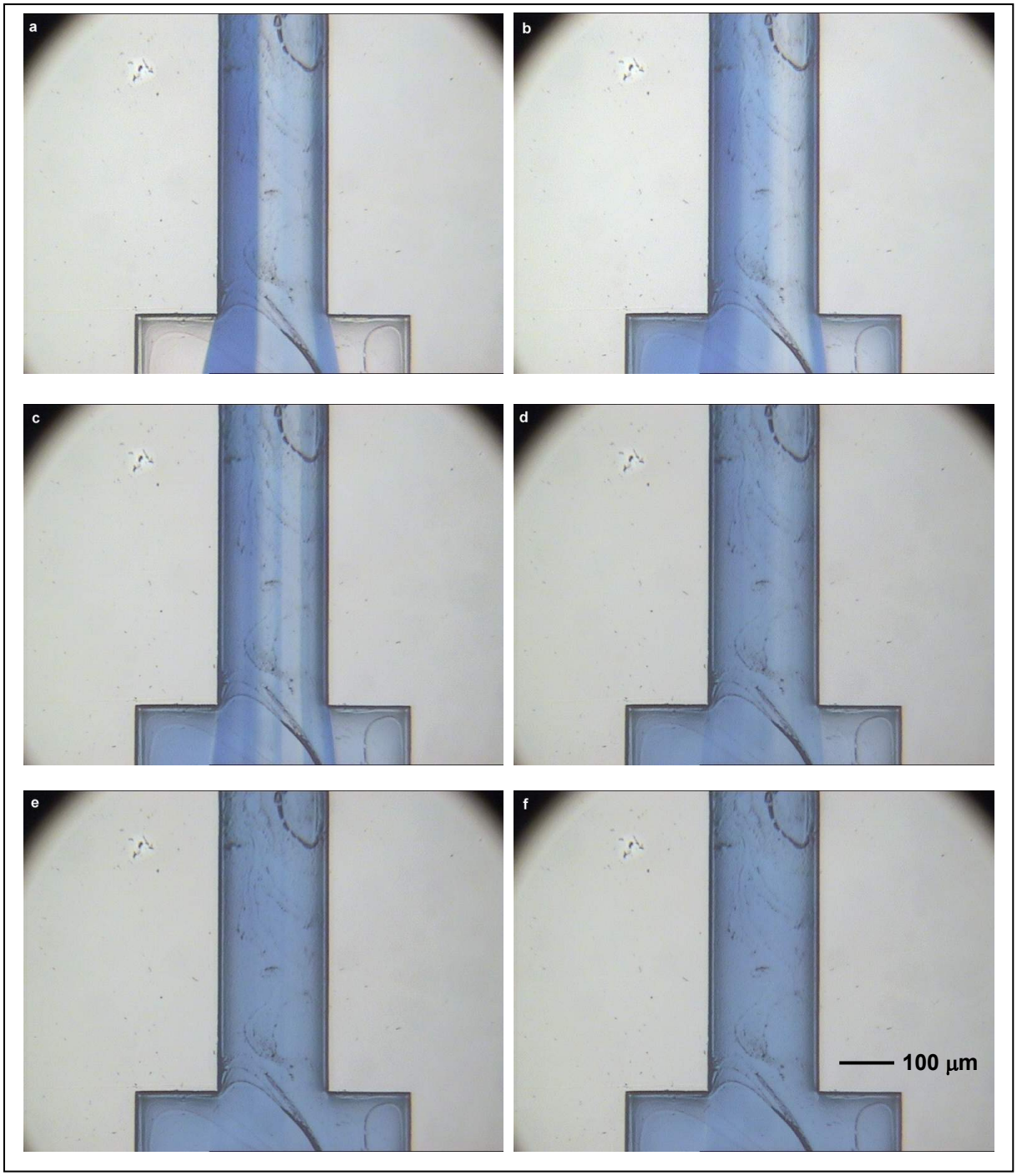

Fig. 7-3 *The observations of the mixing process at the end of the mixing channel of micro T-mixer B at different Reynolds numbers, with their corresponding applied pressures in brackets – (a) 249 (1.40 bar), (b) 331 (2.04 bar), (c) 368 (2.33 bar), (d) 461 (3.10 bar), (e) 535 (3.79 bar) and (f) 615 (4.57 bar).*

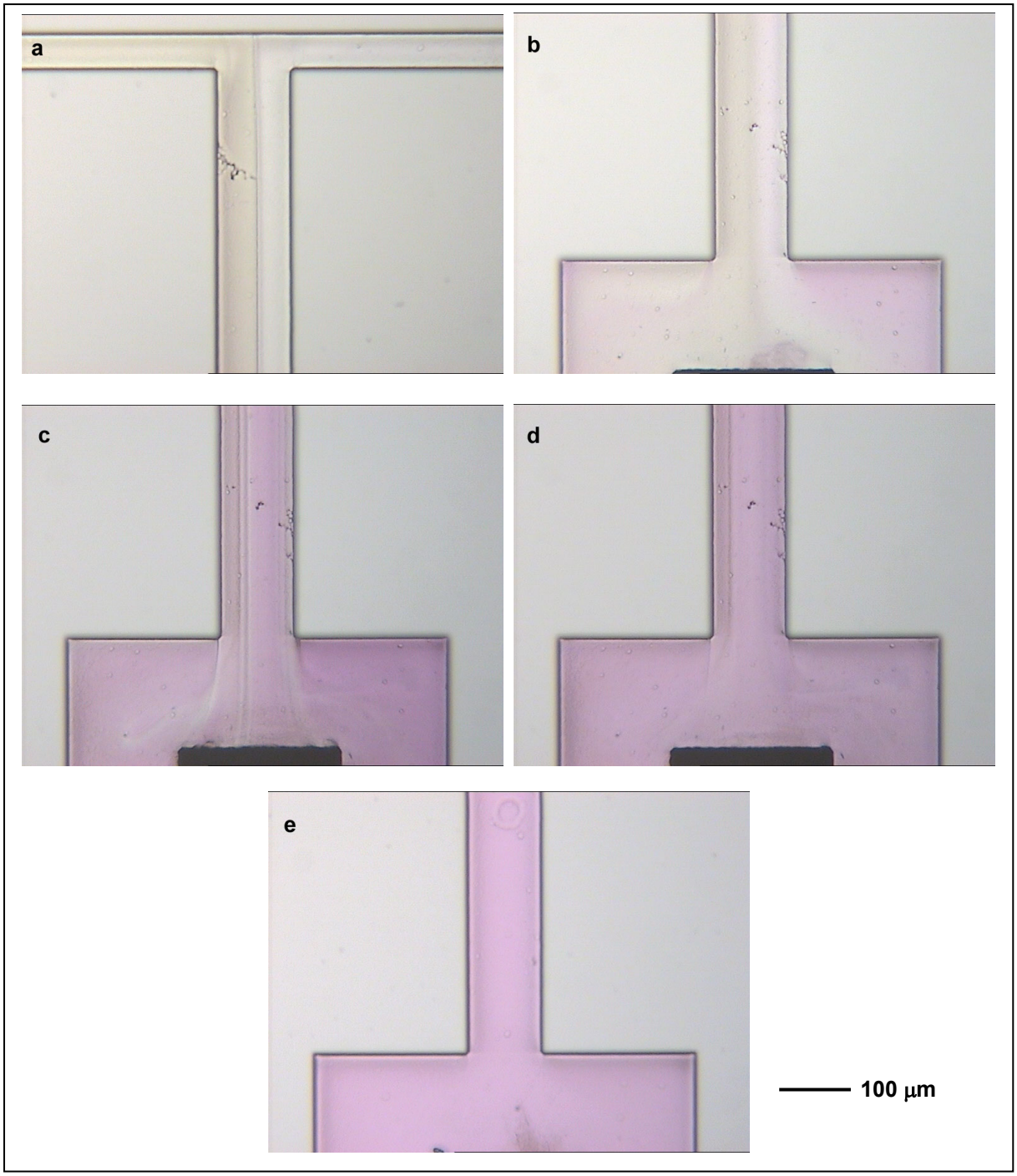

Fig. 7-4 *The optical micrographs above show the observations obtained from micro T-mixer C. Distinct interface between DCAPR and NaOH solutions can be observed in (a) and (b) when the Reynolds number of flow is low. At intermediate Reynolds number of flow, formation of striations of pink solution can be seen at the downstream of the mixing channel in (c). At a Reynolds number of over 400 in the mixing channel, a uniform pink solution is obtained as shown in (d) indicating complete mixing. The images in (b) to (d) are compared with the reference image in (e) containing a premixed solution.*

more clearly seen in the mixing between blue dye and colourless liquid (*fig. 7-2*) than between DCAPR and NaOH solutions (*fig. 7-4a-b*) due to the difference in contrast between the two mixing liquids. The phenomenon of cross flow will be discussed in Chapter 9. This cross flow resulted in some blue dye reaching the opposite sidewall in the mixing channel. When the applied pressure was further increased, the two streams broke up into striations at the junction as shown in *fig. 7-2c-d*. The number of striations increased with increasing applied pressure. These striations of different liquids reduced the diffusion distance of the blue dye, thus resulting in a better mixing downstream of the mixing channels as shown in *fig. 7-3b-d* and *fig. 7-4c*. However, as the mixtures were still flowing in a laminar fashion along the mixing channel, mixing was mainly effected by diffusion across the striations. Although better mixing was achieved when the striation widths were thin, a homogeneous mixture was not obtained at the end of the mixing channel at this stage.

When applied pressure was increased to about 3.8 bar in micro T-mixer B, the striations at the junction disappeared and the result was a much better uniformity of blue dye concentration across the channel. The corresponding Reynolds number when this happened was 535. At 4.3 bar as shown in *fig. 7-2f*, the blue dye across the mixing channel at about 500 μm downstream of the junction was already uniform. No significant improvement in the concentration uniformity was achieved at an applied pressure of more than 4 bar. Nevertheless, volume flow rate and flow velocity of the mixture in the micro T-mixer increased with increasing applied pressure, hence a more rapid mixing can be achieved.

In the mixing experiments with DCAPR solution in micro T-mixer C, when a high pressure of 5.5 bar was applied, a uniform pink colour solution was observed at downstream of the mixing channel as shown in *fig. 7-4d*. The presence of an artefact characterized by a brown line along the left hand side of the mixing channel was caused by the production of a small amount of particles from the reaction between DCAPR and NaOH that resulted in the

deposition of these particles onto the walls of mixing channel with time of use. The formation of a uniform pink colour solution indicated that DCAPR and NaOH solutions were well mixed at downstream of the mixing channel. The intensity of the pink colour solution in *fig. 7-4d* was compared with that in *fig. 7-4e*, which was the image captured with a premixed solution. The similarity in the intensity and uniformity of the pink colour solution between the two images confirmed that the completion of mixing observed through experiments using blue dye and colourless liquid was not an artefact created by the formation of horizontal stratified layers of unmixed liquids in the mixing channel.

Similar observations were also observed in micro T-mixers A and D tested, which can be summarized together with the other micro T-mixers as follows. At low applied pressure when the resulting Reynolds number of flow in the mixing channel was below 150, distinct interface between the two liquids can be seen in the mixing channel. No significant mixing was observed in the entire mixing channel. When the Reynolds number was in the range between 150 and 400, striations of blue dye can be observed in the mixing channel, the number of which increased with increasing Reynolds number. Cross flow may occur at the junction resulting in a larger area of contact between the two liquids. A larger contact area and a shorter diffusion distance between the two liquids resulted in a better mixing observed in the mixing channel. When the Reynolds number was in the range between 400 and 500 in micro T-mixers A, B and C, the striations of blue dye disappeared to give a uniform concentration at the downstream of the mixing channel. Complete mixing of the two liquids occurred in this range of Reynolds number.

The point of complete mixing was determined by applying the procedures detailed in the previous chapter. *Table 7-1* summarizes the Reynolds numbers in the mixing channel when complete mixing is achieved and the corresponding mixing times for the micro T-mixers tested in this study. The mixing time is considered to be the time of travel of the

mixture from the junction to the outlet reservoir at where the luminance level data is collected. Complete mixing was not observed at the outlet of micro T-mixer D in the range of applied pressures investigated in this study. At an applied pressure of 6 bar, striations of blue dye can still be observed at the outlet of micro T-mixer D. The normalized deviation of the luminance levels was greater than 1 at places across the channel. This was expected because the Reynolds number of flow in the mixing channel at 6 bar was only 327, which was still below the range required for complete mixing to be achieved.

Micro T-mixer	Reynolds number in mixing channel	Mixing time (ms)	Applied pressure (bar)
A	442	1.48	1.0
B	467	0.97	3.2
C	489	0.77	5.5
D	-	-	-

Table 7-1 *The table shows the Reynolds numbers and applied pressures when complete mixing is achieved and their corresponding mixing time for the micro T-mixers tested in this study. The mixing time is the time of travel of the mixture from the junction to the outlet reservoir where the mixture is completely mixed upon reaching there. Complete mixing is not achieved in micro T-mixer D for the range of applied pressures used in this study.*

7.2 SURFACE ROUGHNESS OF ETCHED SURFACES

The AFM measurements of etched silicon surfaces revealed the presence of horizontal undulations in the form of waves along the vertical sidewalls of a microchannel. They are more distinct and uniform at the first 30 μm distance from the top of the channel and their uniformity and amplitude progressively deteriorate deeper into the channel as shown in *fig. 7-5*. The depth which the horizontal undulations remain uniform and continuous as shown in *fig. 7-5a* is not a function of the depth of the channel. In other words, the surface features at the bottom of the sidewall shown in *fig. 7-5b* and *fig. 7-5c* may not be observed if the channel considered is much shallower than the 150 μm depth of the microchannels measured in this

study. For example, if a DRIE microchannel is just 20 μm, then the entire depth of the sidewall is populated with the uniform and continuous horizontal undulations.

The formation of the horizontal undulations is a result of the alternating etch and passivation steps in the ASE^{TM} process. During the passivation step, polymeric fluorocarbon passivation layer is deposited onto the silicon surfaces (*fig. 7-6a*). During the subsequent etch step, the horizontal passivation layer is removed by ion bombardment to expose the underlying silicon substrate (*fig. 7-6b-c*). The fluorine radicals from the etch gas then etch the silicon isotropically, undercutting the photoresist mask (*fig. 7-6d*). The alternating passivation and etch steps that follow create peaks and troughs along the depth of the vertical sidewall (*fig. 7-6e-h*).

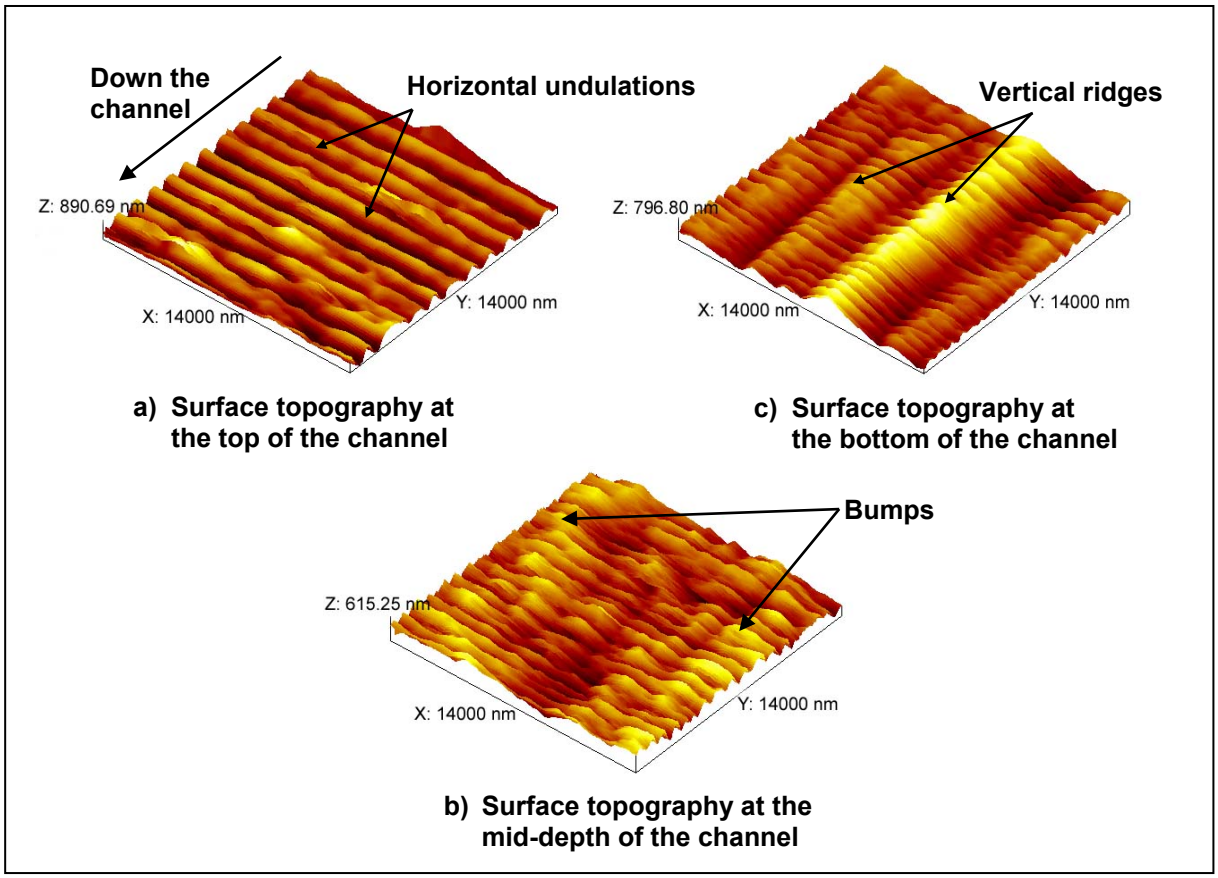

Fig. 7-5 *AFM measurements of the sidewall of a 200 μm wide and 150 μm deep microchannel. The uniformity and continuity of the horizontal undulations deteriorate with increasing depth.*

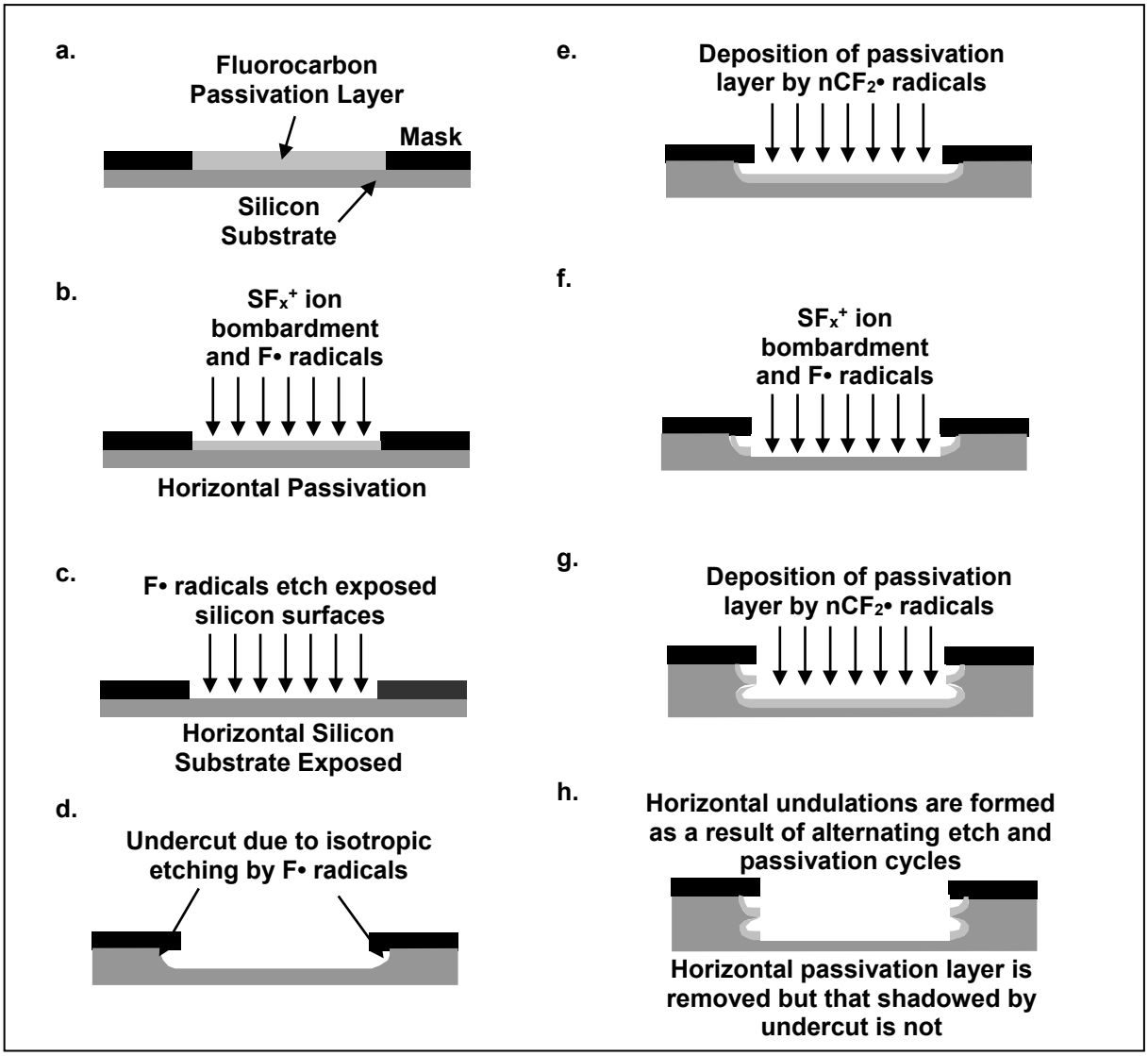

Fig. 7-6 *Step-by-step illustration of the formation of horizontal undulations as a result of alternating etch and passivation cycles.*

The decrease in uniformity and continuity of the horizontal undulations is due to the increasing difficulty of the ion and radical species to reach the bottom of the channel, as the depth of the channel increases during etching. Ions in the plasma that arrive at the bottom of the channel have less energy as the channel is etched deeper into the substrate. The reflection of ions after colliding with the bottom surface of the channel causes ion-shadowing effect that increases the loss of energy of the incoming ions. Surface ion bombardment is necessary to remove the horizontal passivation layer for etching in the vertical direction to proceed. With lower ion energy and less fluorine radicals arriving at the bottom of the channel, rates

of etching and passivation are reduced leading to less distinct horizontal undulations. This also leads to the RIE lag effect where etch rate is higher for larger features but lower for smaller features and explains the change in the frequency of horizontal undulations between the top and bottom of the channel.

At the same time when the uniformity and continuity of the horizontal undulations deteriorate with increasing depth, vertical ridges start to form. The formation of the vertical ridges usually starts at a depth of about 30 μm from the top of the channel and varies slightly for microchannels of different widths. Starting with many irregular bumps along the horizontal undulations at around mid-depth of the 150 μm deep channel as shown in *fig. 7-5b*, ridges in the vertical direction become more distinct at the bottom of the channel and are superimposed with the horizontal undulations as shown in *fig. 7-5c*. At the bottom of the channel, the amplitude of the vertical ridges is greater than that of the horizontal undulations. The distance between the vertical ridges is also very irregular and is generally greater than that between the horizontal undulations. The vertical ridges are much less uniform than the horizontal undulations, as the ridges do not have a regular peak and trough pattern.

As the vertical ridges are irregular, it is believed that they are not the effects of the regular alternating etch and passivation cycles in the ASE^{TM} process. The removal of passivation layer and the etching of exposed silicon surfaces are enhanced by ion bombardment, which is directed vertically towards the silicon wafer. The trajectory of some ions may deviate from the perfectly vertical direction. The implication of this is the grazing and scrubbing of ions on the sidewall of microchannels. The deeper is the location at the sidewall, the more distinct are the vertical ridges as the deviation of ion trajectory from vertical increases with depth. The random nature of the ion bombardment is therefore responsible for the irregular nature of the vertical ridges. However, ridges already formed at the upper part of the sidewall grow larger and deeper towards the bottom of the sidewall.

This is because ion trajectories are unimpeded when the ions travel along the troughs of the vertical ridges already formed, resulting in the ridges being more distinct at the bottom of the channel. It is often observed in DRIE that towards the bottom of a deep etch, quite distinct vertical ridges are formed like that shown in *fig. 7-7* while distinct vertical ridges are not observed for a shallow etch as shown in *fig. 7-8*.

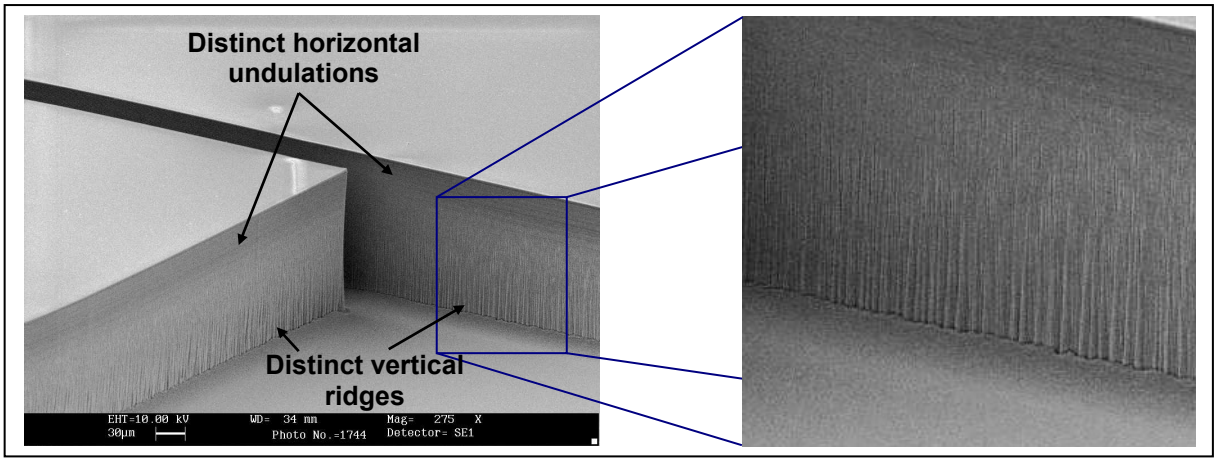

Fig. 7-7 *A close-up of a DRIE structure showing the vertical ridges formed at the bottom of the sidewall are becoming more distinct towards the bottom.*

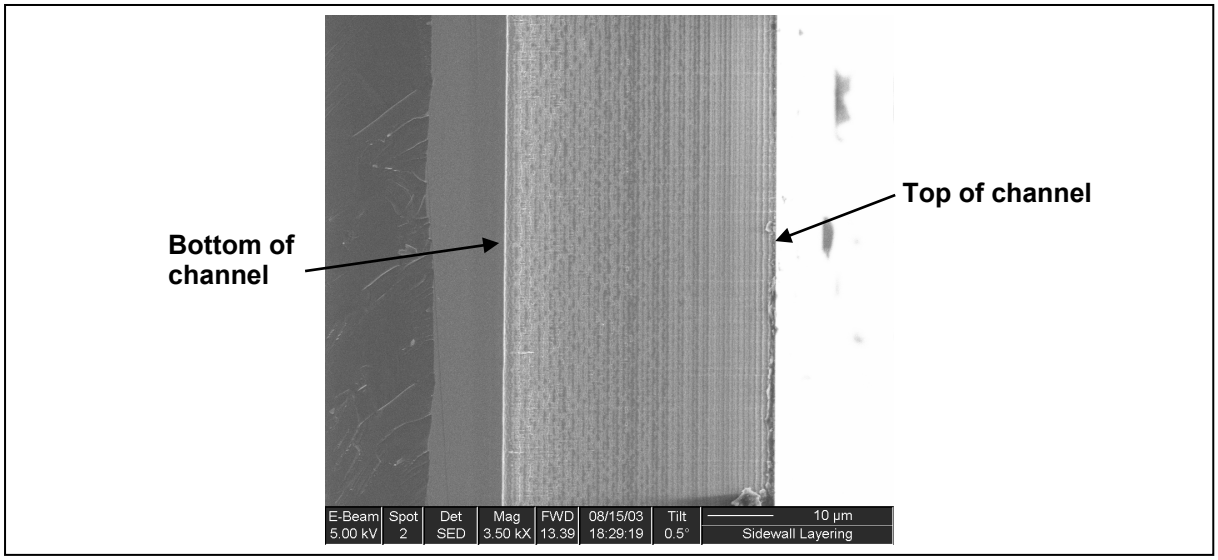

Fig. 7-8 *The SEM micrograph shows the vertical sidewall of a shallow channel of about 40 mm deep. Distinct vertical ridges are not present at the bottom of the channel unlike that shown in fig. 7-7.*

From the data collected by AFM, average surface roughness, R_a, for the measured area defined by equation 7-1 can be calculated.

$$R_a = \frac{1}{N}\sum_{j=1}^{N}\left|\varepsilon_j\right| \tag{7-1}$$

The average roughness values of the sidewall at the top of the channel for microchannels of different widths are tabulated as shown in *table 7-2*. The average roughness values of the sidewall increase with the width of the channel. For a 10 μm wide channel, the average roughness of the channel is about 50 nm. For a 200 μm wide channel, the average roughness is to about 100 nm. In a narrow feature, it is more difficult for the ion and radical species to reach the bottom of the channel than one with a wide feature. In addition, ion shadowing effect is also more severe in a narrow channel. Therefore, the amount of passivation and etching in each etch and passivation cycle is less in a narrow channel compared to a wide channel. Based on the etch and passivation mechanism illustrated in *fig. 7-6*, small amount of passivation and etching results in milder undulations and so a smaller average surface roughness in narrow microchannels.

Microchannel width (μm)	10	20	30	50	100	200
Average roughness, R_a (nm)	49.69	43.83	58.34	75.38	89.87	94.34

Table 7-2 *The table shows the average roughness values at the top of the sidewall for microchannels of different widths.*

7.3 SIMULATIONS WITH ASYMMETRICAL BOUNDARY CONDITIONS

By performing some simple calculations based on the numbers obtained in the experimental results described in the beginning of this chapter, one can see from *table 7-1* that the mixing times achieved in the micro T-mixers are in the order of milliseconds. This is three orders of magnitude faster than the mixing time predicted by Fick's Law (Cussler, 1984) if mixing in the mixing channel is caused solely by diffusion. But since there is some degree of convection in the micro T-mixer, it is possible to explain the improvement of mixing

performance by the creation of secondary flow and the generation of vortices due to the separation of boundary layers around the sharp bends at the junction as described in Chapter 3. However, the published work by Mengeaud *et al.* (2002) and Yi and Bau (2003) carried out to investigate the effects of secondary flow around bends in microchannel on mixing suggested that secondary flow alone cannot fully account for the excellent mixing performance observed. It was shown that significant improvement of mixing performance was achieved only when subsequent bends were located at the point of reattachment of the separated boundary layer and the Reynolds number of flow was greater than 80. As the micro T-mixers investigated in this study only have a straight mixing channel, the enhancement of mixing performance through recirculation induced transverse velocity components could be minimal. The hypothesis that the enhanced mixing performance in the micro T-mixer is due to the surface roughness of the microchannels as proposed by Mala and Li (1999) to have caused an early onset to turbulence is also not valid. The surface topography measurements carried out on the vertical sidewalls of microchannel show that for a 200 μm wide channel, the average surface roughness is only about 100 nm, which implies a relative roughness, ε/d, of 0.0005. According to the Moody diagram, such a channel is considered to be hydraulically smooth at the Reynolds number of flow encountered in the experiments. At a Reynolds number of 489, Scenario I of computer simulations described in Chapter 4 corresponds to the case of micro T-mixer C in the mixing experiments when complete mixing is obtained at the downstream of the mixing channel. However, distinct differences between the experimental observations and the computer simulation results were observed.

To further understand the flow field in the micro T-mixer that resulted in the orders of magnitude enhancement of mixing performance, computer simulations of mixing in a micro T-mixer as described in Chapter 4 were again carried out but with different scenarios. In additional to the three scenarios (I – III) already simulated, five new scenarios (IV – VIII)

were simulated, each with different boundary conditions. They are summarized in *table 7-3* together with those already described in Chapter 4. The 3D solid model used in the simulations is the same as already described and its dimensions correspond to micro T-mixer C used in the mixing experiments. Scenario I to III modelled the standard case at different Reynolds numbers with the liquids entering the micro T-mixer in a direction normal to the boundary face with equal velocity and viscosity on both inlets. Scenarios IV and V modelled the cases when there were small *z* velocity components at the inlets for two different Reynolds numbers in the mixing channel. The *z* velocity components used were relatively small at 1% of their *x* velocity components. Scenario VI modelled the case when asymmetrical velocity magnitudes were applied at the inlets while Scenario VII modelled the case when different viscosities were used for each liquid. The settings for Scenario VIII were the same as Scenario IV except that the *z* velocity components were larger at 10% of their *x* velocity components. The other simulation parameters used remained the same as already described in Chapter 4.

Scenario	Velocity at left inlet (m/s)		Velocity at right inlet (m/s)		Dissimilar viscosities	Re
	x component	z component	x component	z component		
I	1.82	0	-1.82	0	no	121
II	4.52	0	-4.52	0	no	300
III	7.37	0	-7.37	0	no	489
IV	7.37	0.0737	-7.37	-0.0737	no	489
V	1.82	0.0182	-1.82	-0.0182	no	121
VI	7.60	0	-7.14	0	no	489
VII	7.37	0	-7.37	0	yes	489
VIII	7.37	0.737	-7.37	-0.737	no	489

Table 7-3 *The table shows the boundary conditions specified for the eight scenarios simulated. Scenario I to III reflect the standard cases where the boundary conditions are symmetrical. Scenarios IV to VI model the case when the liquid velocities on the two inlets are different, independently in magnitude and direction. Scenario VII models the case when the viscosities of the two liquids are different and Scenario VIII is similar to Scenario IV except that the magnitudes of the z velocity components are larger.*

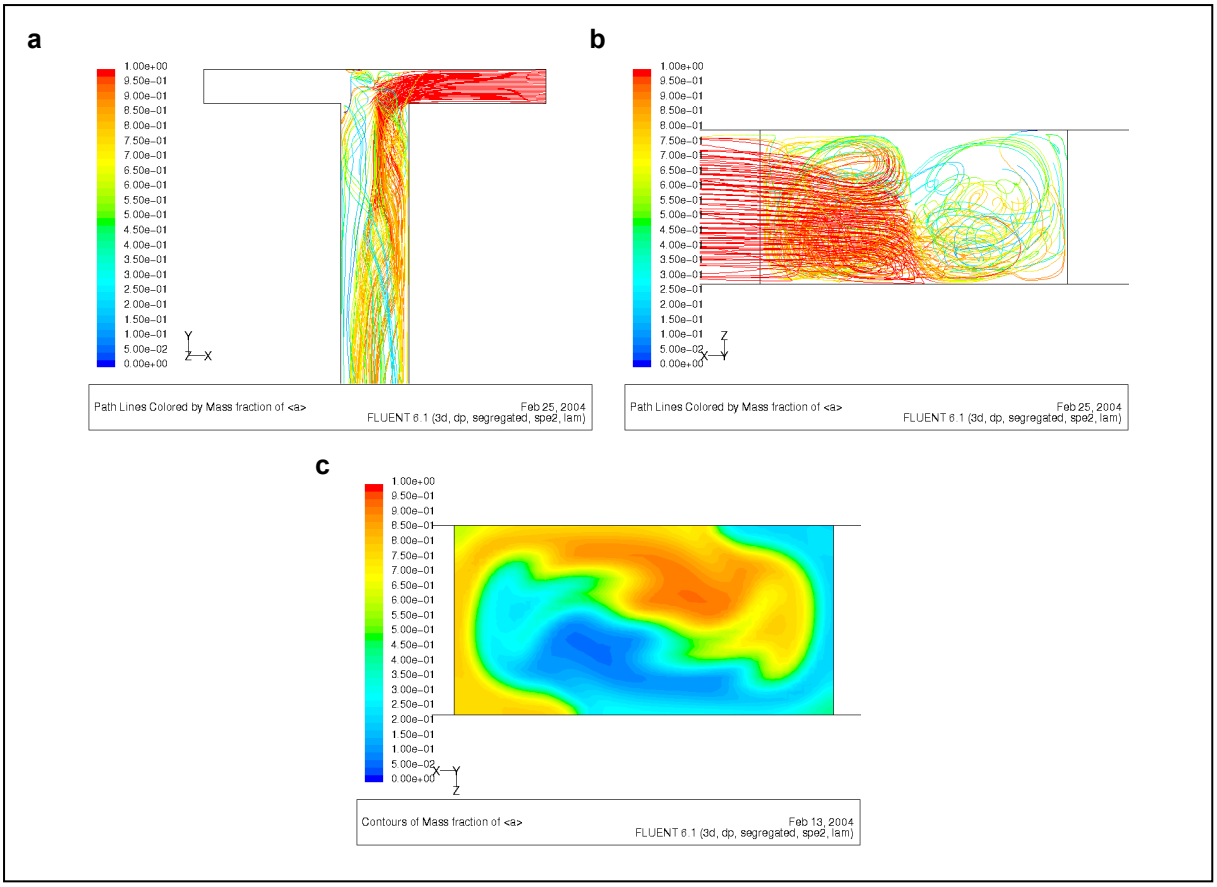

Fig. 7-9 *The diagrams show the simulation results of Scenario IV. (a) and (b) show the top and front view of fluid trajectories of species ⟨a⟩. The presence of z velocity components at the inlets results in extensive crossover of species in the mixing channel. (c) shows the mass fraction contour plot of species ⟨a⟩ at the outlet face. Better mixing is achieved and swirling flow in the mixing channel is evident from the displacements of peak species concentrations.*

The simulation results for the standard cases have already been described in Chapter 4. In Scenario IV and V when *z* velocity components were present in the liquids at the inlets, the liquids entering the micro T-mixer were no longer normal to the boundary but at an angle to the *x-y* plane. The liquid containing species ⟨a⟩ had a *z* velocity component downwards while that containing species ⟨b⟩ had a *z* velocity component upwards. When the Reynolds number of flow was high, as in Scenario IV, the species from the inlets were able to reach beyond the centreline of the mixing channel as shown by the fluid trajectory plots of species ⟨a⟩ in *fig. 7-9a* and *fig. 7-9b*. The symmetry in the flow field as observed in Scenario I did not occur. According to *fig. 7-9b*, the liquid stream with species ⟨a⟩ travelled downwards while

that with species ⟨b⟩ travelled upwards when they collided at the junction, creating a swirling flow along the mixing channel. This transverse motion of species in the mixing channel, coupled with the separation of boundary layer at the bend resulted in a significant enhancement of mixing performance observed at the outlet face, confirmed by the mass fraction plot of species ⟨a⟩ in *fig. 7-9c*. The same cannot be said for Scenario V when the Reynolds number of flow was much lower. The flow field in the junction was symmetrical, as obtained in Scenario I with very poor mixing at the outlet face.

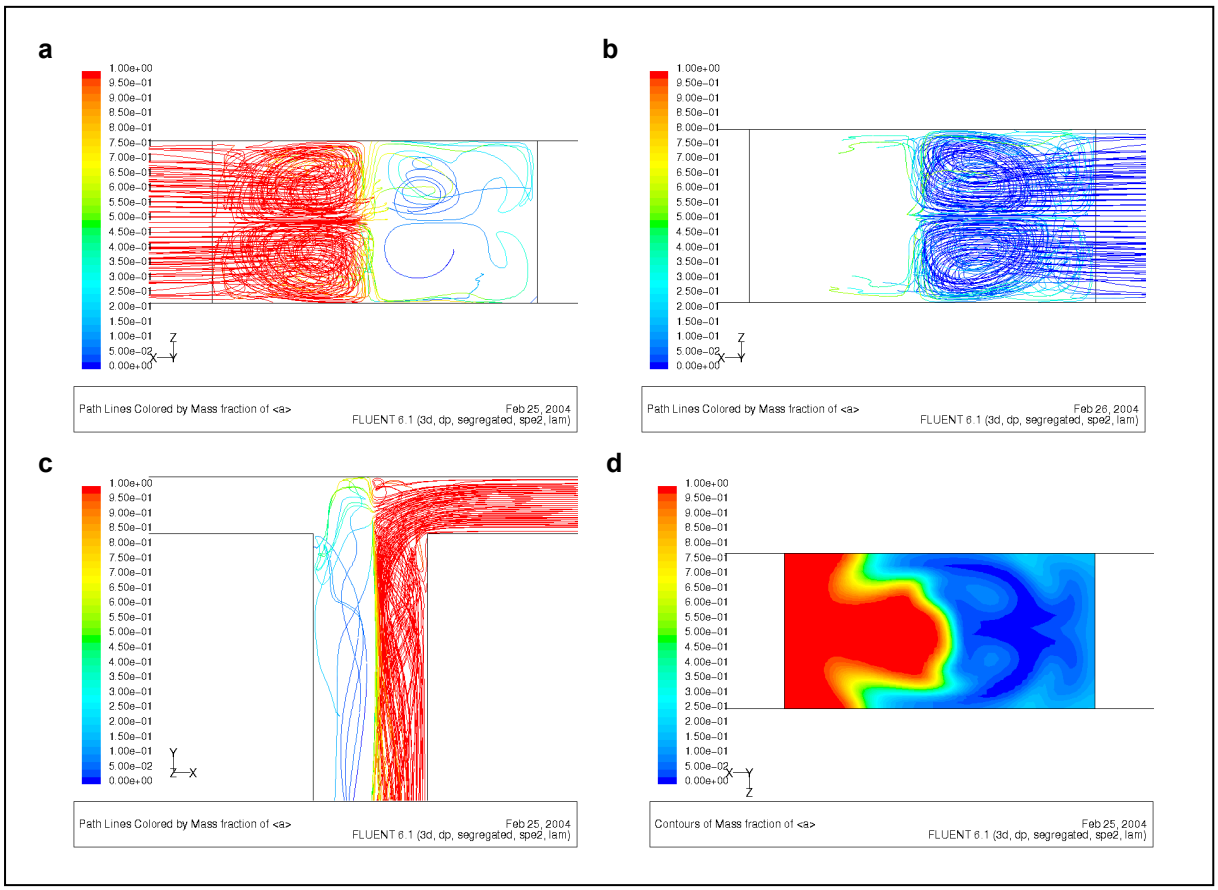

Fig. 7-10 *The diagrams show the simulation results of Scenario VI. (a) shows the fluid trajectories of species ⟨a⟩ while (b) shows the fluid trajectories of species ⟨b⟩. The difference between the velocities at the inlets results in some species ⟨a⟩ crossing the centreline to the other side but that does not occur for species ⟨b⟩ – (c). (d) shows the mass fraction contour plot of species ⟨a⟩ at the outlet face.*

In Scenario VI, the Reynolds number of flow in the mixing channel was maintained at 489 while the flow velocities at the inlets were made different so as to create an asymmetrical flow condition at the inlets. As a result of higher flow velocity on the left inlet

of the micro T-mixer, some species ⟨a⟩ managed to travel to the opposite side of the mixing channel but no species ⟨b⟩ managed to travel beyond the centreline of the mixing channel. This is illustrated by the flow trajectory plots and a mass fraction contour plot in *fig. 7-10*. The viscosity of the liquid with species ⟨b⟩ was assigned to be twice of that with species ⟨a⟩ in Scenario VII. It was aimed to investigate the effect of dissimilar viscosities of the liquids on the mixing performance in a micro T-mixer. It was found that the liquid with species ⟨a⟩, due to its lower viscosity, was able to reach beyond the centreline of the mixing channel through the top and bottom surfaces of the micro T-mixer when it collided with the liquid with species ⟨b⟩ as shown in *fig. 7-11*.

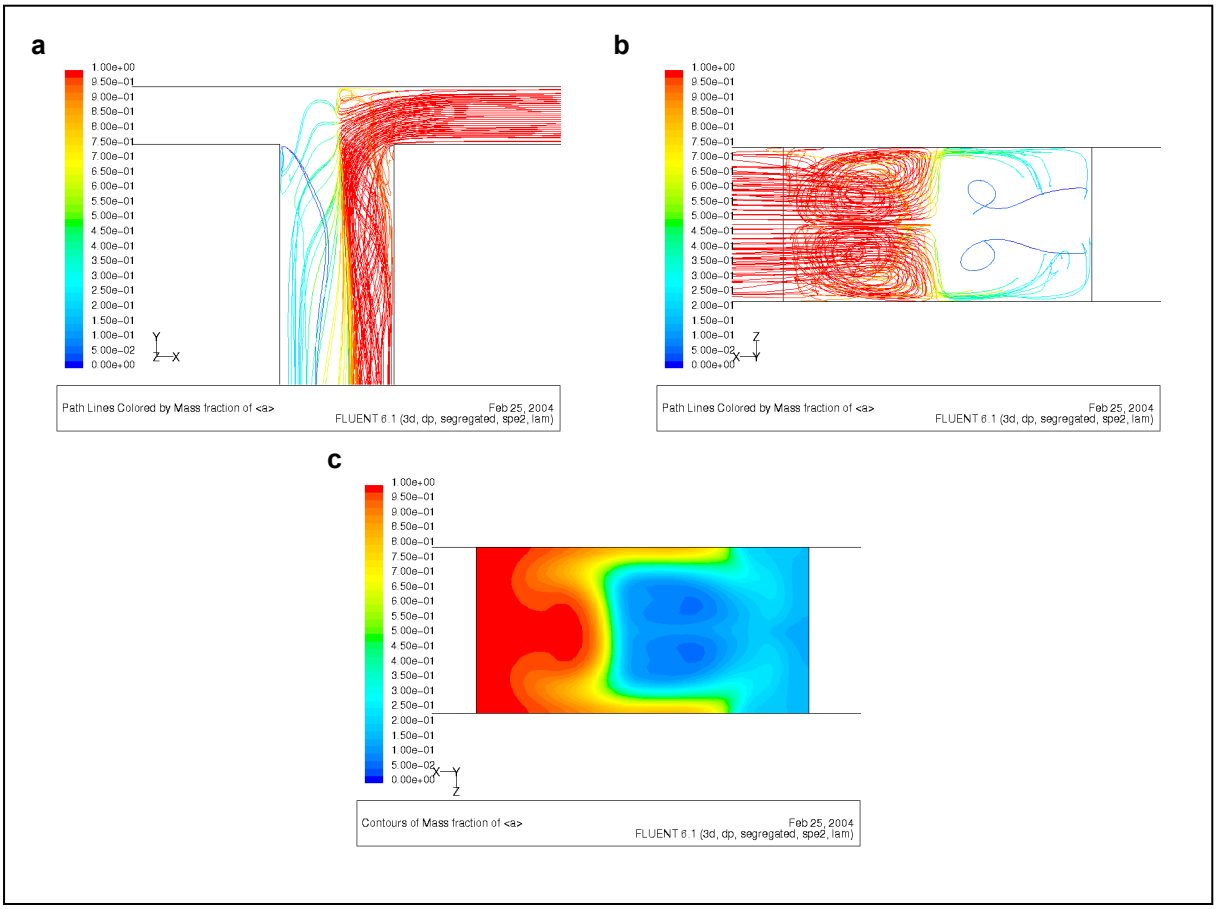

Fig. 7-11 *When the viscosity of the two liquids are different as simulated in Scenario VII, the fluid trajectory plot shows the crossover of the less viscous liquid with species ⟨a⟩ through the top and bottom surfaces of the micro T-mixer.*

Scenario VIII demonstrated the effect of larger z velocity components on the mixing performance of a micro T-mixer. When the z velocity component was at 10% of the x velocity component, the extent of mixing in the outlet face was the best among the scenarios simulated, which can be seen from the mass fraction plot in *fig. 7-12*. The extent of mixing in the outlet face can be characterized by a dimensionless parameter called the intensity of mixing, I_m, as described in Chapter 4. *Table 7-4* summarizes the intensity of mixing values at the outlet face for the six scenarios simulated. It can be seen that Scenario VIII achieved the best mixing performance followed by Scenario IV while the extent of mixing at the outlet in Scenario V is the poorest.

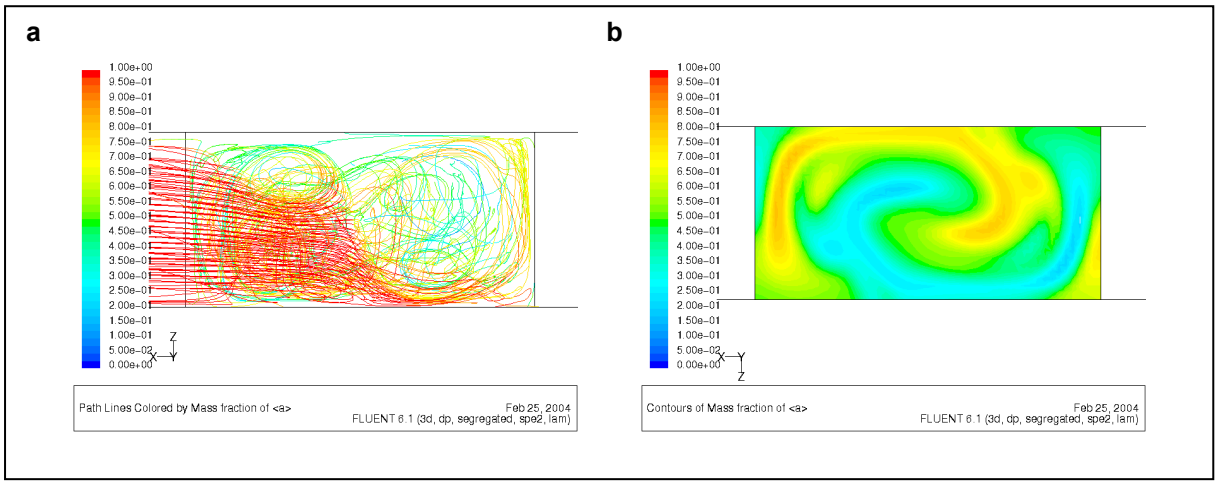

Fig. 7-12 *The fluid trajectory(a) and mass fraction contour plot (b) of species ⟨a⟩ at the outlet face shows a very significant improvement in mixing performance achieved when higher z velocity components are specified in Scenario VIII.*

Scenario	I	II	III	IV	V	VI	VII	VIII
Intensity of mixing	0.1003	0.1390	0.1677	0.7000	0.0874	0.2284	0.4614	0.9044

Table 7-4 *The table shows the intensity of mixing values at the outlet face of the micro T-mixer for the eight scenarios simulated. They are computed from the mass fraction values at each node on the outlet face using the method already described in chapter 4.*

7.4 CLOSURE

The mixing performances in micro T-mixers of different sizes at different applied pressures at the inlets have been described in detail. It was found that complete mixing in micro T-mixers generally occurred when the Reynolds number of flow in the mixing channel was in the range between 400 and 500. This translated to mixing speeds of about 1 millisecond. The rapid mixing achieved in the experiments could not be explained entirely by the separation of boundary layers and the generation of vortices at the junction when comparing the result with those in literature. Surface topographical measurements of the microchannel sidewalls by AFM also did not indicate that the enhanced mixing performance was due to higher surface roughness in the microchannels. Further computer simulations were carried out to gain further insight on the mechanisms of mixing in the micro T-mixers that resulted in the enhanced mixing performance. Apart from mixing under symmetrical boundary conditions already simulated, additional simulations were carried out but with asymmetrical boundary conditions specified at the inlets. The simulation results showed that the introduction of small z velocity components in opposite directions at the two inlets caused swirling flow in the mixing channel, resulting in extensive crossover of the liquids to the other side of the mixing channel. Asymmetrical flow conditions at the inlets such as unequal inlet velocity and viscosity of the two liquids were also shown to result in crossover phenomenon, albeit to a smaller extent. A detailed discussion of all the experimental observations and simulation results, and also the comparison between the results obtained in this study and similar work performed by others will be presented in Chapter 9.

MIXING IN A CROSS-SHAPED MICROMIXER

8.1 THE DESIGN OF A CROSS-SHAPED MICROMIXER

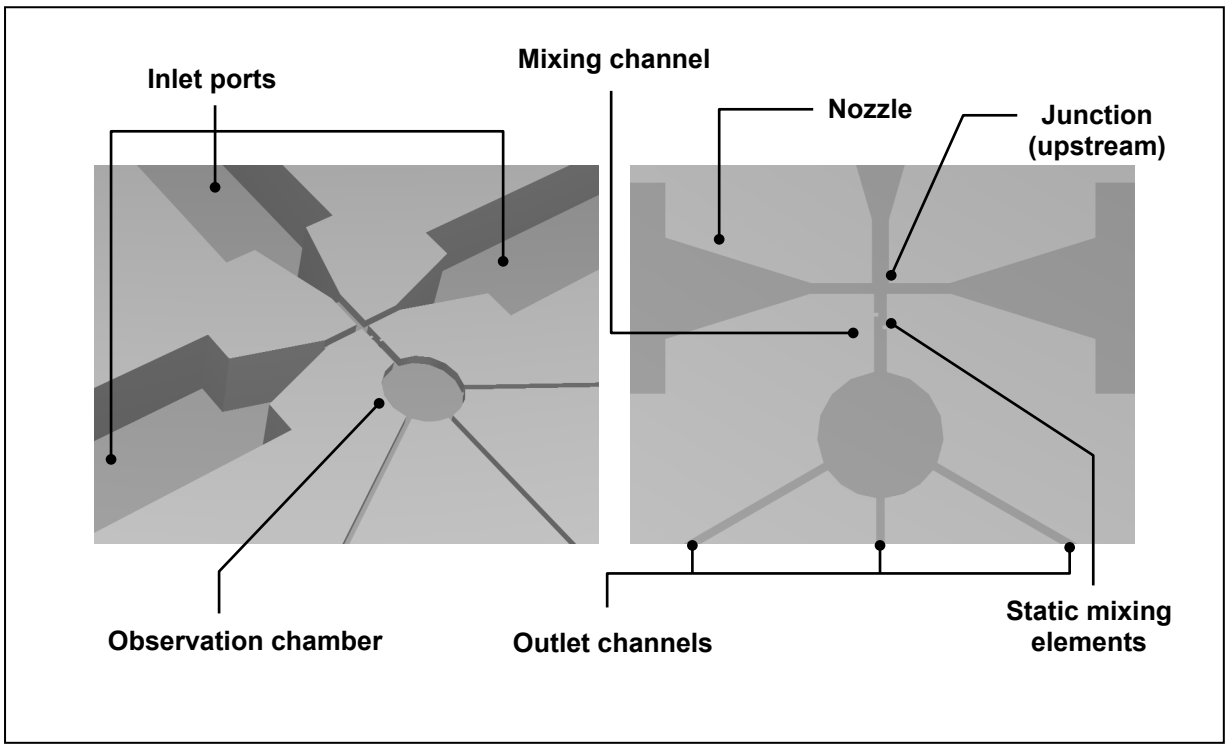

Fig. 8-1 *The diagrams show the close up view of the cross-shaped micromixer model, which consist of a cross-shaped micromixer in the centre connected by three inlet reservoirs and an observation chamber. Static mixing elements are introduced in the mixing channel of the micromixer. Three narrow outlet microchannels are connected at three different locations to the observation chamber.*

The second static micromixer investigated is a cross-shaped micromixer incorporated with static mixing elements. The micromixer has the shape of a cross as illustrated in *fig 8-1* with three inlet channels and a mixing channel. The ends of the inlet channels are connected to rectangular inlet reservoirs while the end of the mixing channel is connected to a circular

observation chamber where the mixture is collected for the intended spectroscopic measurements. The connecting nozzles between the reservoirs and the inlet channels facilitate smooth liquid entry into the micromixer. Three narrow outlet channels are connected to the observation chambers at three different locations. The narrow outlet channels connect the observation chamber to the atmosphere. Similar to the micro T-mixers, the microchannels in the cross-shaped micromixers have rectangular cross sections. The cross-sectional dimensions of the microchannels are in the range of tens of micrometres to ensure sufficiently high rate of mixture production while maintaining sufficiently small amount of each reagent used. The dimensions of the cross-shaped micromixer are illustrated in *fig. 8-2* and *8-4*.

During operation, one of the liquids to be mixed enters the micromixer through the inlet channel in the middle while the other liquid enters through the inlet channels on both sides of the micromixer. The two liquids collide at the junction and the resulting mixture flows in the mixing channel where the two liquids are mixed. Static mixing elements are incorporated at the walls of the mixing channel, and in some occasions at the junction, to enhance the mixing performance of the micromixer by generating secondary flow and separation of boundary layers in the flow. In all cases, the maximum height of the static mixing elements from the wall of the mixing channel is 10 μm. This is to avoid the introduction of static mixing elements in the mixing channel from suppressing the flow in the micromixer to an extent that vortices are difficult to be generated. For the static mixing elements at the junction, they are 5 μm rectangular protrusions in all cases. Similar to the case of designing micro T-mixers, an array of cross-shaped micromixers is designed and batch-fabricated on a single piece of wafer. This allows static mixing elements of different shapes and numbers to be incorporated into the micromixers. Rectangular, trapezoidal, triangular and semicircular static mixing elements are incorporated into the design as shown

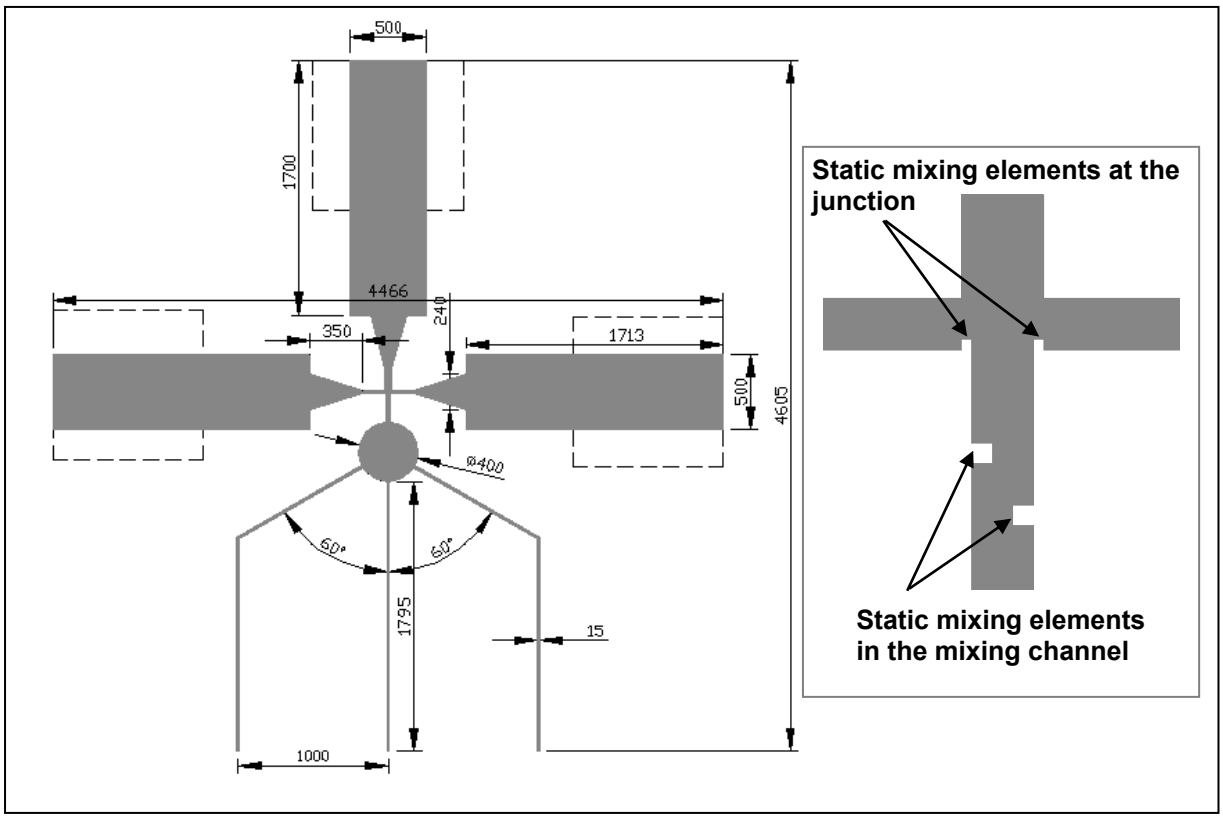

Fig. 8-2 *The dimensions of the cross-shaped micromixer (in micrometres) investigated in this study. Dash lines indicate features on the back face of the chip. The inset shows the static mixing elements at the junction that are introduced in some of the micromixer designs besides those in the mixing channel.*

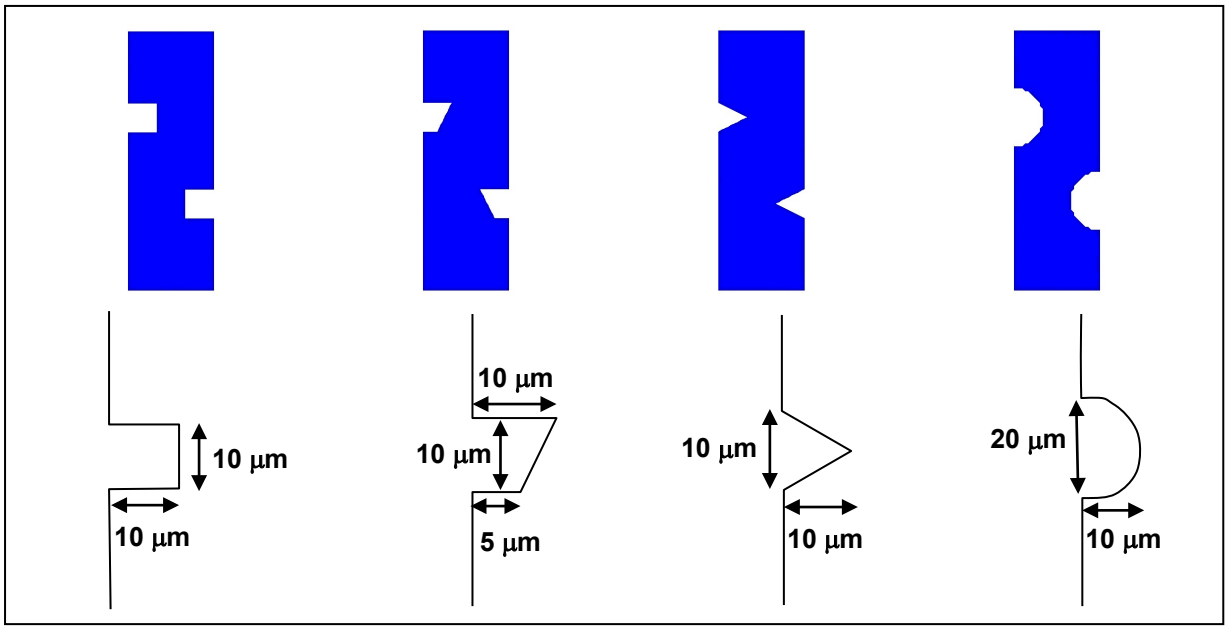

Fig. 8-3 *The four different shapes of static mixing elements introduced in the mixing channel namely rectangular, trapezoidal, triangular and semicircular are illustrated above together with their dimensions.*

in *fig. 8-3*. Besides, micromixers with and without static mixing elements at the junction and different numbers of static mixing elements are also designed within the array of micromixers.

The cross-shaped micromixer is intended to be used as a stopped-flow device where the two liquids to be mixed come together in the micromixer, collide and mix in the mixing channel and are collected in the observation chamber before the flow stops altogether. A stopped-flow device uses very little reagent for each analysis, making it more desirable than a continuous flow device when expensive reagents are involved. Incorporating microvalves in the micromixer that close when the observation chamber is filled will make the design much more complicated. Besides, the main aim of this study is to achieve rapid mixing in the micromixer. Therefore, a simpler alternative is sought. The three narrow outlet channels connected to the observation chamber are just 15 μm wide, making them the narrowest part of the micromixer. The purpose of the narrow channels is to allow easy escape of air from the micromixer but restrict the flow of liquid. As the viscosity of air is much lower than that of liquid, the flow of air through the narrow channel is much easier than the flow of liquid. Admittedly, the narrow outlet microchannels cannot stop the flow of liquid altogether, but it can make the micromixer behave more like a stopped-flow micromixer without unduly increasing the complexity of the design.

In theory, the mixing performance of a cross-shaped micromixer is better than a micro T-mixer because in a cross-shaped micromixer, a larger contact area between the two liquids is possible with one liquid sandwiched between the other liquid. In the mixing of two liquids, the speed of mixing are determined by the diffusion distance and the contact area between the two liquids that allows the molecules of one liquid to travel to the region of the other to achieve uniform concentration. With other conditions the same, a micromixer that allows a larger contact area between the two liquids will therefore result in a speedier mixing.

8.2 STATIC MIXING ELEMENTS

Static mixing elements mentioned in the previous section are generally protrusions out of the wall in a microchannel. These elements have abrupt changes in their surface orientations such as sharp corners and are put in the path of a flow to cause separation of boundary layers and secondary flow, which lead to vortex generation. When a liquid flowing in a microchannel encounters a static mixing element, provided that the Reynolds number is not in the creep flow regime, separation of boundary layers occurs before and after the element. The separation of boundary layers results in the formation of vortices in the region of separation upstream and downstream of the element as already illustrated in *fig. 3-3a*. The separation length and the size of the vortices vary depending on the Reynolds number of flow. Flow recirculation occurs in the separation regions enhancing the transport of liquid material there. The unsteady reattachment of the flow some distance downstream of the element disturbs the slow moving molecules in the boundary layer, sweeping them to the bulk of the flow. The boundary layer redevelops further downstream. So with a series of static mixing elements arranged along the channel wall, the separation of boundary layers and the reattachments of the flow smooth out the concentration non-uniformities across the flow. Although the effects of introducing static mixing elements in a microchannel have not been investigated in the literature, similar work has been carried out for flow in the macro-scale (Lavellee and Popovich, 1974; Focke, 1983). In fact, introducing some mixing elements in pipes to create turbulence and hence mixing in the flow is a popular method for mixing in chemical engineering applications. It was found that by introducing corrugations along the wall of a channel, an increase in local mass transfer rate of up to four times compared to the flow in an empty channel can be achieved (Focke, 1983).

The introduction of static mixing elements in a flow channel can unfortunately lead to a higher pressure drop along the channel. With a constant pressure source, the introduction of

static mixing elements leads to a reduction in the mean flow velocity in the channel. It is very important that the introduction of static mixing elements does not cause a significant reduction in flow velocity that eventually suppresses the separation of boundary layers and the subsequent generation of vortices. The size of static mixing elements should therefore be relatively small compared to the size of the channel. In this way, their presence results in a larger effect on the enhancement of mixing performance than the reduction in flow velocity. This can also be attained by creative arrangements of static mixing elements in the channel.

8.3 COMPUTER SIMULATIONS

Computer simulations similar to those already performed on micro T-mixers were also performed on cross-shaped micromixers. Fluent 6 was again used for performing the simulations. The simulation algorithm, flow model and material properties of the two mixing liquids used in the simulations were the same as those used for micro T-mixers. 3D solid models of the cross-shaped micromixer having the standard dimensions as shown in *fig. 8-4* with different shapes and numbers of static mixing elements in the mixing channel were constructed. Under each case, simulations of mixing with the Reynolds numbers at 100 and 300 in the mixing channel were performed. Species ⟨a⟩ was specified to enter the cross-shaped micromixer from the middle inlet channel while species ⟨b⟩ was specified to enter from the side-inlet channels. In order to compare the performance enhancement caused by the introduction of static mixing elements, mixing simulations in a cross-shaped micromixer with and without static mixing elements were performed. *Table 8-1* to *8-3* summarize the 16 scenarios (1–16) simulated for various designs of static mixing elements and boundary conditions. In Scenario 1 and 2, the mixing in a cross-shaped micromixer without static mixing element was simulated. Their mixing performances were compared with Scenario 3 and 4 when two rectangular static mixing elements were incorporated in the mixing channel.

In order to evaluate the effects from introducing static mixing elements at the junction, two static mixing elements were incorporated at the junction in Scenario 5 and 6 in additional to those already in the mixing channel. The effects from introducing different numbers and shapes of static mixing elements on mixing performance were investigated in Scenario 7 to 14. An additional static mixing element was introduced in the mixing channel in Scenario 7 and 8 while in Scenario 9 to 14, static mixing elements of different shapes were incorporated. In Scenario 15 and 16, asymmetrical boundary conditions were specified at the two side inlets of the micromixer. The magnitudes of the z velocity components in opposite directions specified at the inlets were 1 and 10 percent of their x velocity components in Scenario 15 and 16 respectively. The mixing performance under each scenario was evaluated by computing the intensity of mixing at the outlet and then comparing these values for different scenarios.

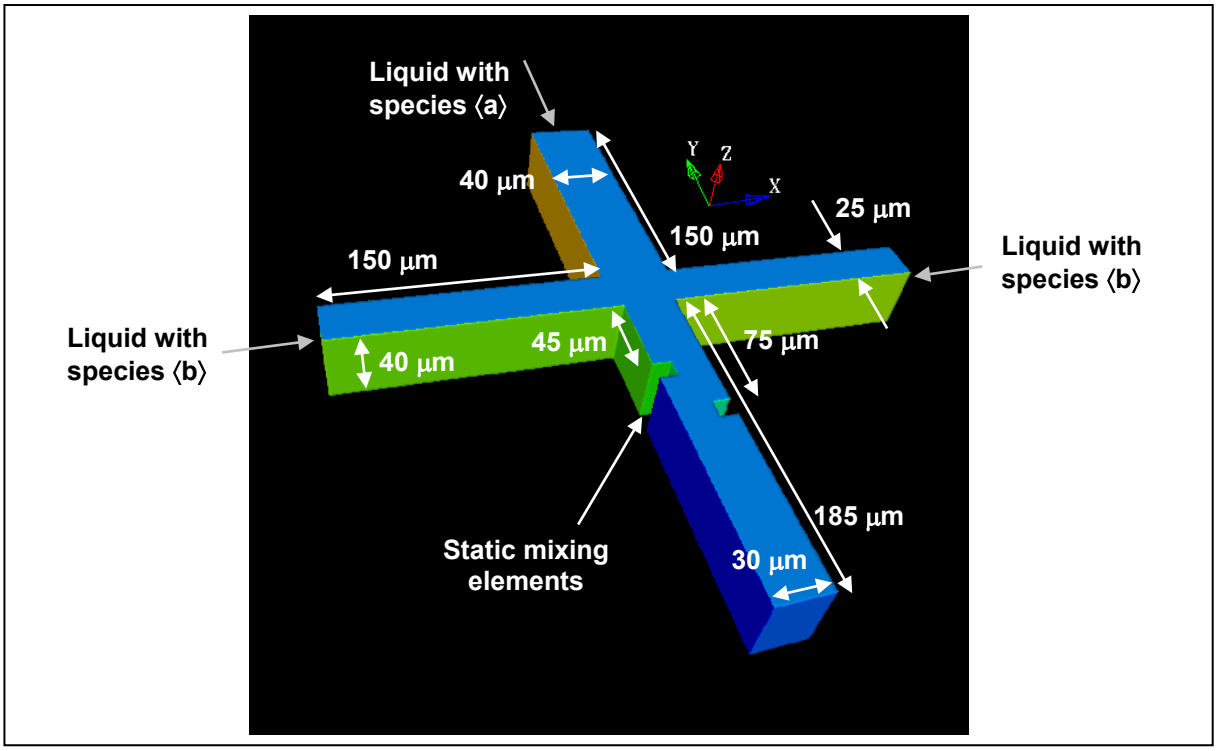

Fig. 8-4 *The dimensions of the 3D solid model of cross-shaped micromixer constructed for mixing simulations, which are also representative of the actual micromixer.*

Reynolds number	Flow rate in mixing channel (μl/s)	Mean flow velocity (m/s)		
		Mixing channel	Middle inlet channel	Side inlet channel
100	3.518	2.93	1.10	0.88
300	10.55	8.79	3.30	2.64

Table 8-1 *Mixing was simulated for each design of the cross-shaped micromixer for two Reynolds number of flow in the mixing channel. The mean flow velocities specified at the inlets and the corresponding flow rate and flow velocity in the mixing channel are shown.*

Scenario	1	2	3	4	5	6	7	8	9	10	11	12	13	14	15	16
Nil	✓	✓														
Rectangular			✓	✓												
[a]Rectangular					✓	✓										
[a,b]Rectangular							✓	✓							✓	✓
[a]Triangular									✓	✓						
[a]Trapezoidal											✓	✓				
[a]Semicircular													✓	✓		
[a,b]Asymmetrical															✓	✓
Re = 100	✓		✓		✓		✓		✓		✓		✓			
Re = 300		✓		✓		✓		✓		✓		✓		✓	✓	✓

[a] *Static mixing elements are introduced at the junction.*
[b] *Three static mixing elements are introduced in the mixing channel.*

Table 8-2 *The 16 scenarios simulated are summarized in the table above. Cross-shaped micromixers with no static mixing elements, with static mixing elements of different shapes and with asymmetrical boundary conditions specified at the side inlets for Reynolds number of 100 and 300 have been simulated.*

Scenario	Side inlet – left		Side inlet – right	
	x velocity component (m/s)	*z* velocity component (m/s)	*x* velocity component (m/s)	*z* velocity component (m/s)
15	2.64	0.0264	-2.64	-0.0264
16	2.64	0.264	-2.64	-0.264

Table 8-3 *The asymmetrical boundary conditions specified at the side inlets for Scenario 15 and 16 involve the presence of z velocity components in the opposite directions for the two inlets. The z velocity components are 1% of the x velocity components in Scenario 15 and 10% of the x velocity components in Scenario 16. The Reynolds number of flow in the mixing channel is 300 in both cases.*

8.4 SIMULATION RESULTS AND DISCUSSIONS

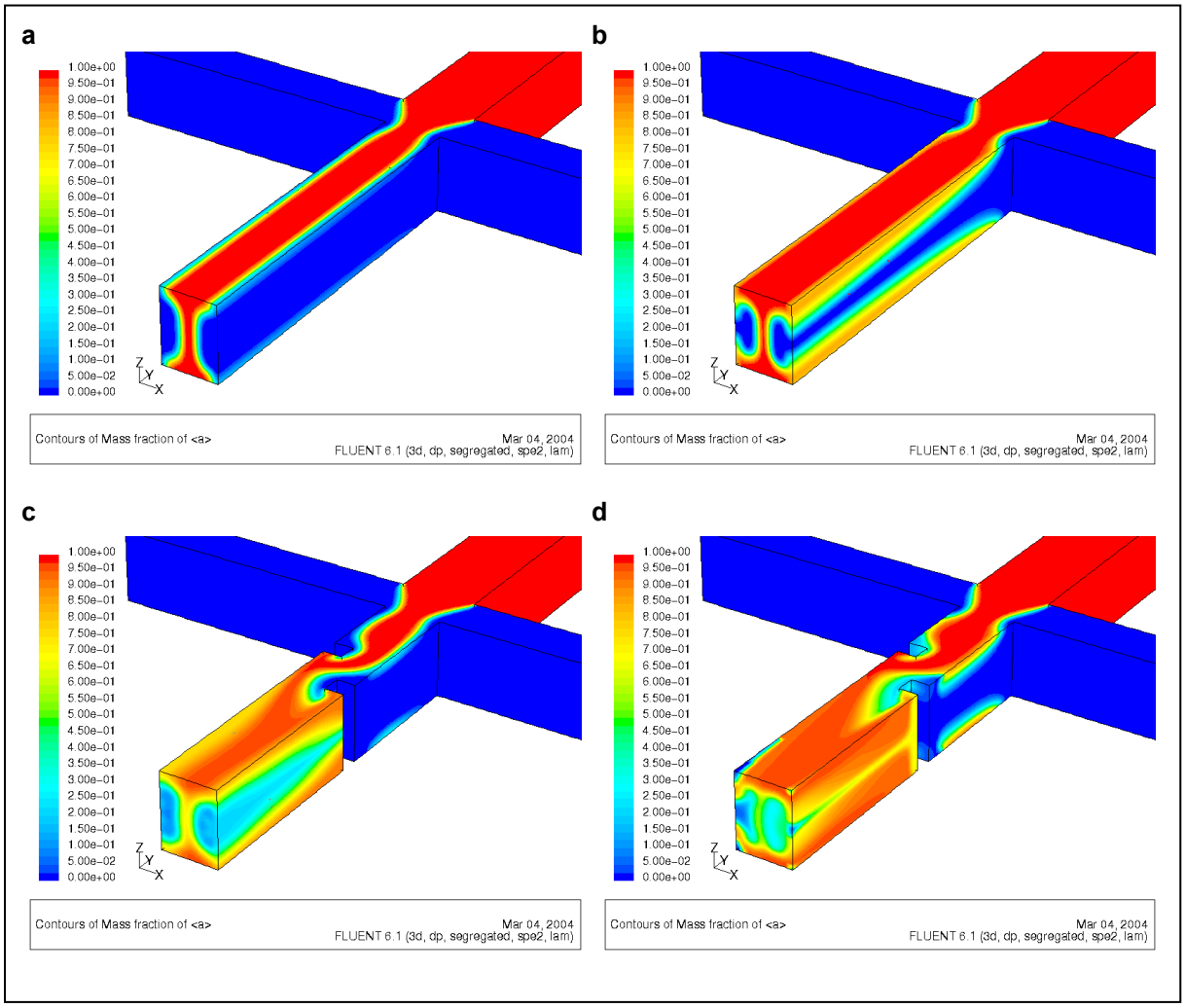

Fig. 8-5 *The mass fraction plots of species ⟨a⟩ in Scenario 1 (a) and Scenario 2 (b) at Reynolds number of 100 and 300 respectively show distinct mass fraction gradient across the outlet face of the micromixer indicating poor mixing. Improvement in mixing performance is achieved with the introduction of 2 static mixing elements in the mixing channel as shown by (c) and (d) for the same Reynolds numbers.*

The mass fraction contour plots of species ⟨a⟩ in Scenario 1 and 2 show extensive segregation of the two species at the outlet. This is indicated by the distinct mass fraction gradient along the mixing channel in *fig. 8-5a* and *8-5b*. The poor mixing performance is due to the absence of static mixing elements in the mixing channel to disrupt the orderly laminar flow and produce vortices in the flow. The mixture flows in the laminar regime and mixing takes place mostly by molecular diffusion, which is unable to fully mix the two liquids due to the relatively wide mixing channel and short residence time of the species. Secondary flow in the

mixing channel due to the change in direction of liquid flow from the side-inlets is more noticeable at higher Reynolds number. It results in the interface of the two liquids at the outlet being more curved at higher Reynolds number. When two static mixing elements are incorporated in the mixing channel in Scenario 3 and 4, the uniformity of the mass fraction at the outlet of the micromixer is improved as shown in *fig. 8-5c* and *8-5d*. This is further confirmed by comparing the intensity of mixing values between Scenario 1 and 3 and between Scenario 2 and 4 as tabulated in *table 8-4*. The static mixing elements cause the two liquids to mix not only by molecular diffusion but also by stretching and folding processes due to the generation of vortices and flow recirculation around the static mixing elements. The distinct difference between the two sets of mass fraction contour plots demonstrates the effectiveness of static mixing elements in speeding up the mixing process in a cross-shaped micromixer. As the amount of vortices generated increases with increasing Reynolds number of flow in the mixing channel, the mixing quality obtained at a higher Reynolds number is better. This is evident by comparing the intensity of mixing values for flow at different Reynolds numbers.

Scenario	Without SMEs		With 2 SMEs	
	1 (Re = 100)	2 (Re = 300)	3 (Re = 100)	4 (Re = 300)
Intensity of mixing	0.2844	0.3707	0.6569	0.7076

Table 8-4 *Comparing the intensity of mixing values between Scenario 1 and 3 for flow at Re=100 and between Scenario 2 and 4 for flow at Re=300, improvement in mixing is evident with the introduction of 2 static mixing elements (SMEs) in the mixing channel.*

Re	Shapes of SMEs	Rectangular	Triangular	Trapezoidal	Semicircular
100	Scenario	5	9	11	13
	Intensity of mixing	0.6631	0.6527	0.6018	0.6083
300	Scenario	6	10	12	14
	Intensity of mixing	0.7260	0.7335	0.7363	0.7186

Table 8-5 *The intensity of mixing values at the outlet of the cross-shaped micromixer for two Reynolds numbers and four different shapes of static mixing elements (SMEs) investigated.*

The enhancement of mixing performance between static mixing elements of different shapes is very similar, implied by the intensity of mixing values for the four shapes of static mixing element investigated. These values are shown in *table 8-5*. A comparison between the intensity of mixing values in *table 8-4* and *8-5* shows that the enhancement in mixing performance caused by changing the shape of static mixing elements is much less profound than the introduction of static mixing elements itself or an increase in the Reynolds number. An even better mixing performance is achieved with the introduction of an additional static mixing element in the mixing channel. This is evident in *table 8-6* between Scenario 5 and 7 and between Scenario 6 and 8. With the introduction of an additional static mixing element, the mixture undergoes further stretching and folding processes that produce an even more uniform mixture. The introduction of static mixing elements at the junction is however not as effective at improving the mixing performance as introducing static mixing elements in the mixing channel. The improvement in mixing performance shown by the intensity of mixing values in *table 8-7* is only marginal. The specification of asymmetrical boundary conditions at the inlets of the micromixer that cause significant improvement in the mixing performance of micro T-mixers was also specified in cross-shaped micromixers. The intensity of mixing values extracted from Scenario 15 and 16 and tabulated in *table 8-8* however show almost identical values with that obtained from Scenario 8 simulated with symmetrical boundary conditions. This shows that cross-shaped micromixers are not sensitive to asymmetry in the flow at their inlets.

Scenario	2 static mixing elements		3 static mixing elements	
	5 (Re = 100)	6 (Re = 300)	7 (Re = 100)	8 (Re = 300)
Intensity of mixing	0.6631	0.7260	0.7281	0.8365

Table 8-6 *The intensity of mixing values at the outlet of a cross-shaped micromixer with 3 static mixing elements in the mixing channel show a significant improvement in mixing performance with every introduction of an additional static mixing element.*

Scenario	Without SMEs at junction		With SMEs at junction	
	3 (Re = 100)	4 (Re = 300)	5 (Re = 100)	6 (Re = 300)
Intensity of mixing	0.6569	0.7076	0.6631	0.7260

Table 8-7 *The improvement in mixing performance achieved as a result of the introduction of static mixing elements (SMEs) at the junction of the cross-shaped micromixer is not significant.*

Scenario	Symmetrical BCs	Asymmetrical BCs	
	8	15	16
Intensity of mixing	0.8365	0.8364	0.8375

Table 8-8 *Virtually no improvement in mixing performance is achieved with the specification of asymmetrical boundary conditions (BCs) at the side inlets of the cross-shaped micromixer.*

Scenario (Re = 100)	1	3	5	7	9	11	13
Pressure difference (bar)	0.293	0.461	0.465	0.599	0.455	0.452	0.441

Scenario (Re = 300)	2	4	6	8	10	12	14	15	16
Pressure difference (bar)	1.437	2.918	2.930	4.151	2.962	2.977	2.540	4.149	4.128

Table 8-9 *The pressure difference between the inlets and outlet of the cross-shaped micromixers of all the scenarios simulated, grouped according to the Reynolds number of flow in the mixing channel.*

The pressure difference between the inlets and outlet of the cross-shaped micromixers obtained from simulations allows the applied pressure required to achieve a certain Reynolds number in experiments to be estimated. The practicality of a micromixer to achieve the observed simulated mixing performance during experiment can thus be determined. The pressure difference values extracted from the simulation results of each scenario are tabulated in *table 8-9*. They show the pressure required to cause a mixture to flow at a Reynolds number of 100 and 300 in the mixing channel with two static mixing elements is generally less than 0.5 bar and 3 bar respectively. When two static mixing elements are introduced in the mixing channel, the pressure requirement is increased 50% at a Reynolds number of 100 and 100% at a Reynolds number of 300. The pressure requirement is increased about 30% when an additional static mixing is introduced in the mixing channel. The pressures required are achievable in practice based on the experimental work done on micro T-mixers.

8.5 FABRICATION AND TESTING

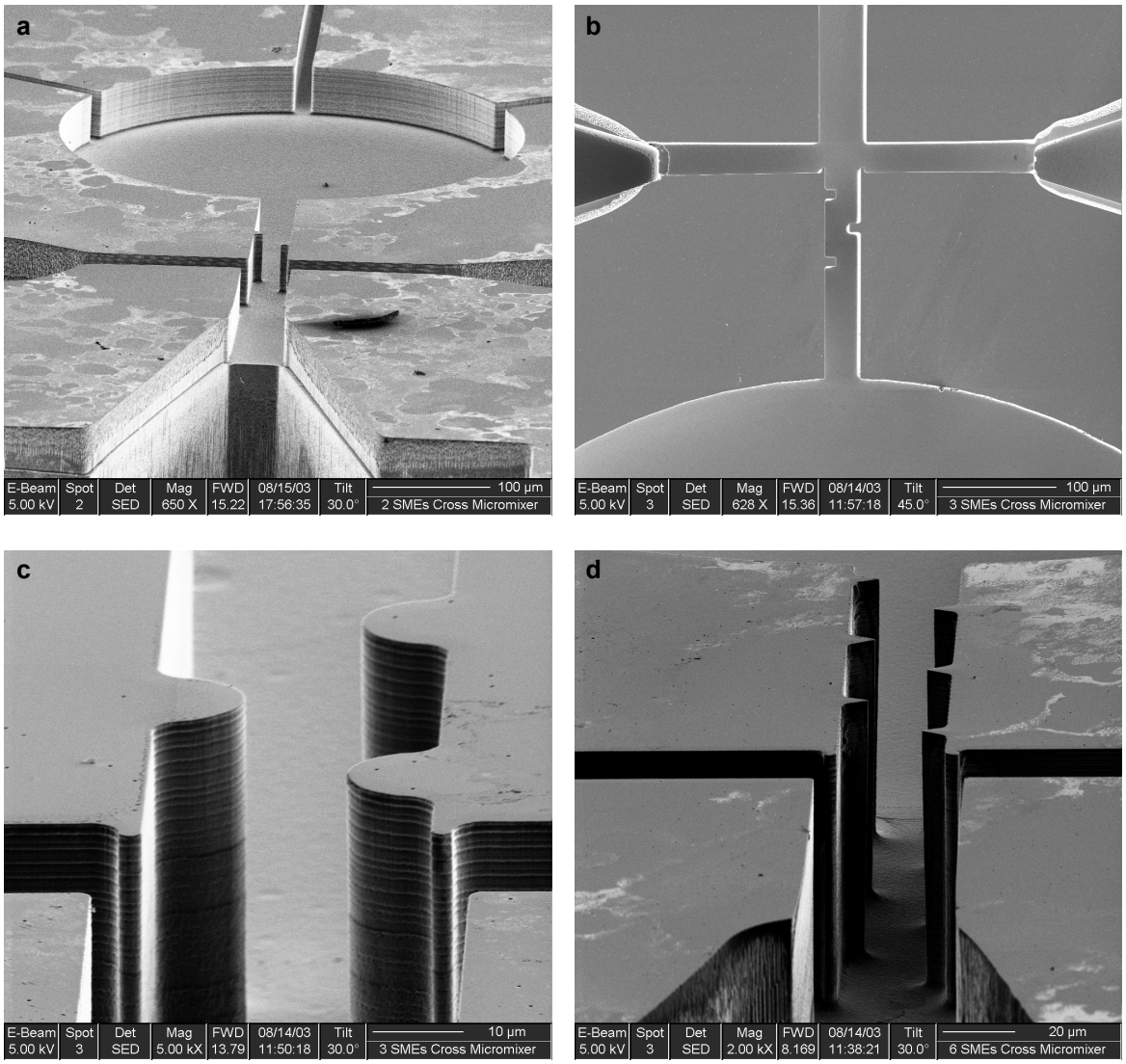

Fig. 8-6 *(a) shows the general appearance of the cross-shaped micromixers produced in this study. It has two triangular static mixing elements in its mixing channel. (b) shows the plan view of a cross-shaped micromixer with rectangular static mixing elements. (c) and (d) show the excellent definition of the static mixing elements produced by DRIE process.*

The fabrication path for the cross-shaped micromixers is very similar to that for the micro T-mixers. A double sided polished wafer with a thickness of 425 µm was used as the substrate of the micromixer. Three photolithography and etch steps were involved in the fabrication process. The patterns of the rectangular inlet reservoirs were first transferred and etched onto the front face of the wafer to a depth of over 200 µm. This was then followed by the etching

of the cross-shaped micromixers, observation chambers and outlet channels in a single etch step. A 12-minute etch produced an etch depth of 41.5 μm when inspected in an electron microscope. A through wafer etching of the inlet ports onto the back face of the wafer was then performed. When the wafer was etched through, the inlet reservoirs on the front were connected to the inlet ports on the back of the wafer. This allowed the liquids to be fed from the back of the micromixer chip while the mixing performance was observed from the front with a microscope fitted with a high speed video camera. The DRIE process that was used to etch the cross-shaped micromixer enabled features with vertical sidewalls and shapes not limited by the silicon crystallographic planes to be produced as shown by the electron micrographs of some cross-shaped micromixers in *fig. 8-6*.

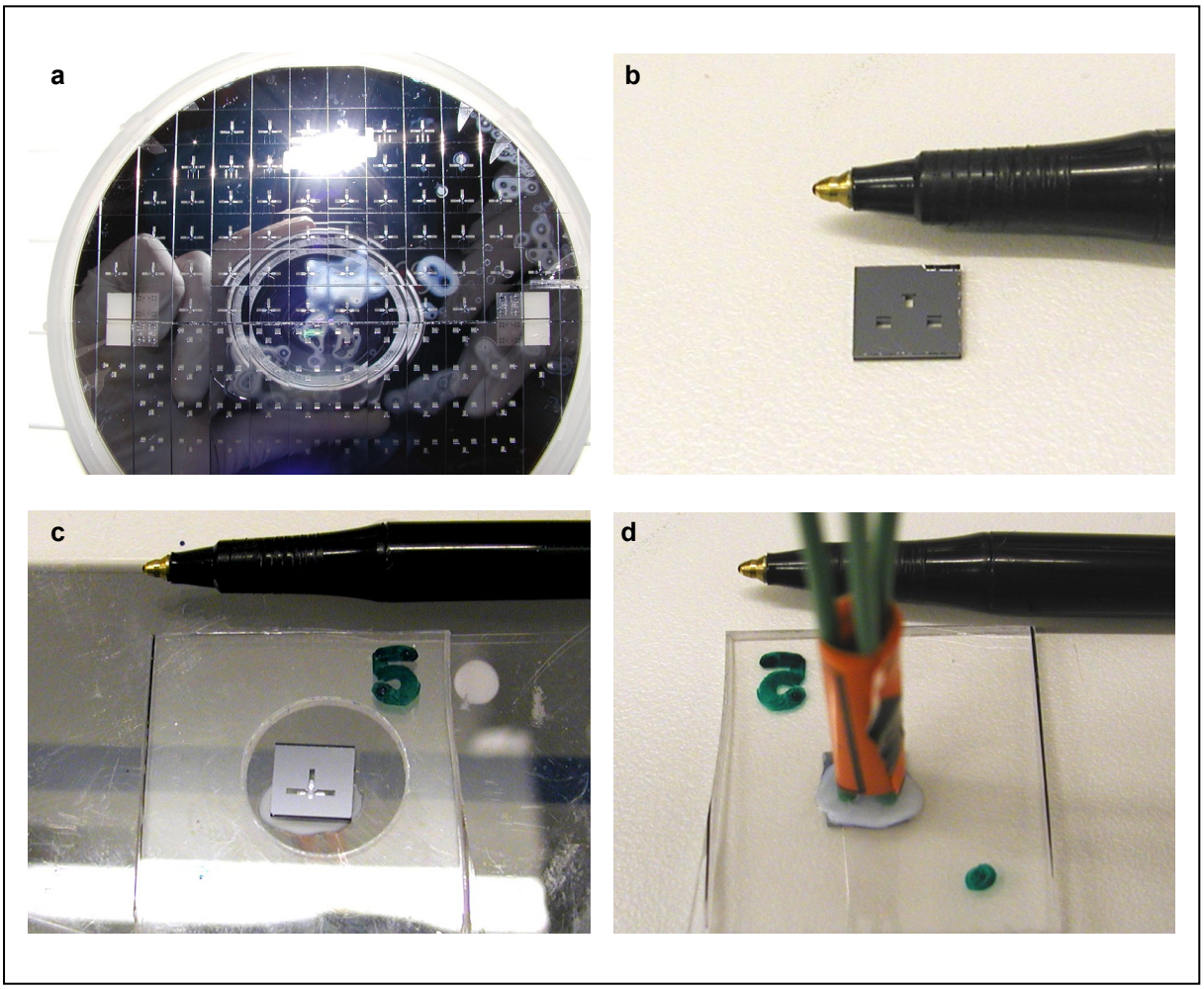

Fig. 8-7 *(a) The wafer assembly containing an array of cross-shaped micromixers was diced into individual chips. (b) The back face of the micromixer chip contains three inlet ports for facilitating liquid entry. (c) The front face of a completed micromixer chip. (d) The back face of a completed micromixer chip with liquid feed tubing.*

The surface within which the array of micromixers was etched was anodically bonded with a Pyrex glass wafer. The wafer assembly was then diced into individual chips so that each of them can be bonded to a clear polystyrene plate that facilitates the connection of liquid feed tubing. A diced wafer assembly with cross-micromixers is shown in *fig. 8-7a*. *Fig. 8-7b* shows the back view of the micromixer. The three inlet ports on the back face form cavities that facilitate the bonding of the micromixer chip to a polystyrene plate and the entry of liquid into the micromixer chip when it is bonded to a polystyrene plate. *Fig. 8-7c* and *8-7d* respectively show the front and back views of a completed micromixer ready for mixing characterization work.

The experiment setup used to characterize the mixing performance in the cross-shaped micromixers was slightly different to that for micro T-mixers. This was because the cross-shaped micromixer was intended to be used as a stopped-flow device. A schematic diagram of the experiment setup is illustrated in *fig. 8-8*. The regulated pressure from a nitrogen gas cylinder was again used as the pressure source for liquid flow in micromixers. Normally closed solenoid valve A in the experiment setup allowed pressure from the nitrogen gas cylinder to be applied onto the liquids in the sample cylinders, while solenoid valve B acted as a pressure relief valve for stopping liquid flow in the micromixer. Although the narrow outlet channels incorporated into the micromixers were means for the micromixer to behave as a stopped-flow device by retarding the flow of mixture out of the micromixer, the narrow outlet channels could not stop the flow. This was only achieved by opening the solenoid valve that was acting as a pressure relief valve. During mixing experiments, solenoid valve A was open to allow pressure to be applied onto the pre-filtered liquids in the sample cylinders, which in turn fed the liquids to the cross-shaped micromixer where mixing was performed. The two liquids used to characterize the mixing performance in cross-shaped micromixers were a commercial blue dye and de-ionized water.

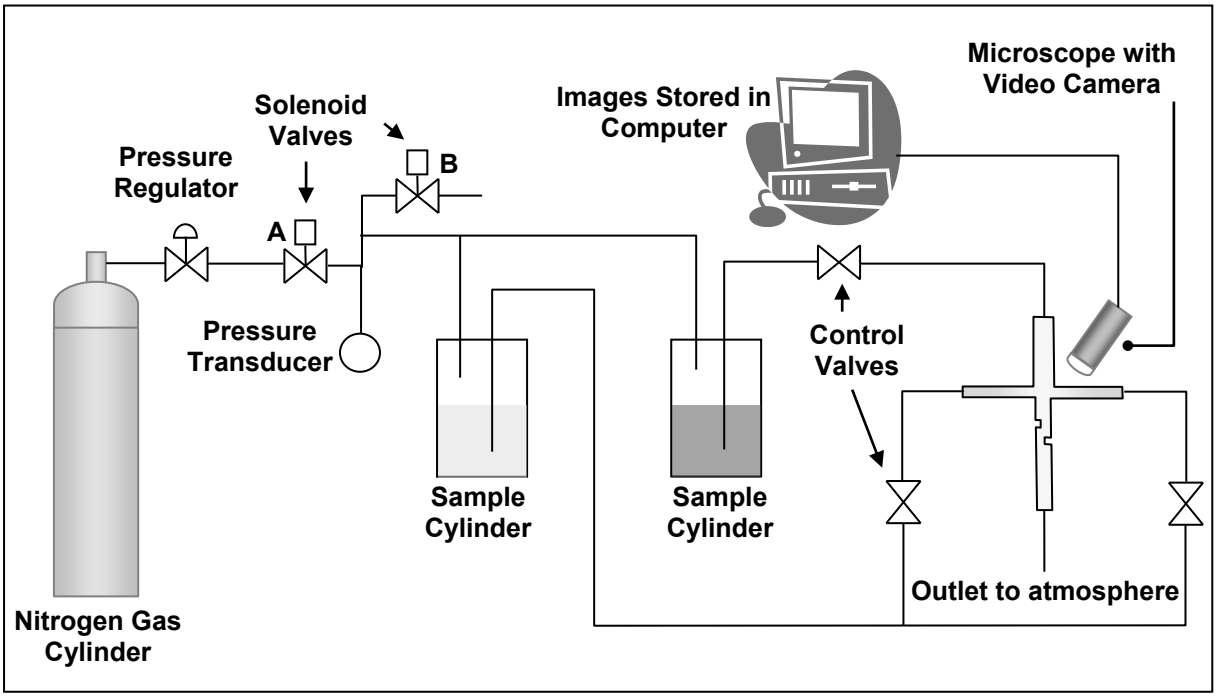

Fig. 8-8 *The experiment set up for characterizing the mixing performance in a cross-shaped micromixers involved the use of two solenoid valves to enable quick application and relief of applied pressure.*

It was intended that the evolution of rapid mixing in the cross-shaped micromixer was observed under a high refresh rate video camera. The camera can be triggered to capture images when the solenoid valve A is opened so that a series of images of mixing in the micromixer can be captured. A Kodak EM high speed monochrome video camera system that was able to capture 1000 frames per second at full resolution of 240×200 pixels was loaned from Engineering and Physical Science Research Council (EPSRC) to carry out the experiment. Due to the high refresh rate of the video camera, the light source of the microscope was unable to provide sufficient amount of light to the camera for any images to be captured. It was also found that the two liquids were not entering the micromixer at the same time. One liquid usually entered before the other. This resulted in the flow being retarded by the flow of liquid in the narrow outlet channels before mixing could take place. When the two liquids eventually collided, the mixture was flowing at a much lower Reynolds number than anticipated. Due to the above reasons, it was not possible to operate the micromixer as intended. The cross-shape micromixers were therefore tested and

characterized in a continuous flow mode, even though the Reynolds number of flow in the micromixer achieved was not as high as achieved in micro T-mixers. The Sony video camera used in the characterization work of the micro T-mixers was again used and the performance of mixing in the cross-shaped micromixers for a range of applied pressures was assessed by comparing the images captured. The volume flow rate in the micromixer at each of these applied pressures was deduced by measuring the time needed to collect 1 ml of the mixture at the outlet of the micromixer. The corresponding Reynolds number of flow in the mixing channel of the micromixer at these applied pressures was then calculated. This enabled the mixing performance observed between micromixers with different designs of static mixing element to be characterized and compared.

8.6 MIXING PERFORMANCE IN A CROSS-SHAPED MICROMIXER

The mixing performances in three cross-shaped micromixers, CM-A, CM-B and CM-C are described here. In CM-A, two semicircular static mixing elements are introduced in the mixing channel. CM-B is similar to CM-A except for the triangular static mixing elements in the mixing channel. In CM-C, six rectangular static mixing elements are incorporated in the mixing channel in additional to two at the junction. Although pressures of up to 10 bar were applied during the mixing experiment, the achievable Reynolds number in the micromixer was however less than 200 due to the flow retarding effect of the three narrow outlet channels. The bulk of the pressure drop occurred along the outlet channels instead of the mixing channel. The mixing performance in CM-A at Reynolds numbers of up to 151 are shown in *fig. 8-9*. It can be observed from the images that complete mixing was not achieved even at the highest Reynolds number attainable in the experiments. At a Reynolds number of 151, a thin striation of blue dye in the middle of the mixing channel can still be seen. Generally, improvement in the uniformity of blue dye concentration at the outlet of the

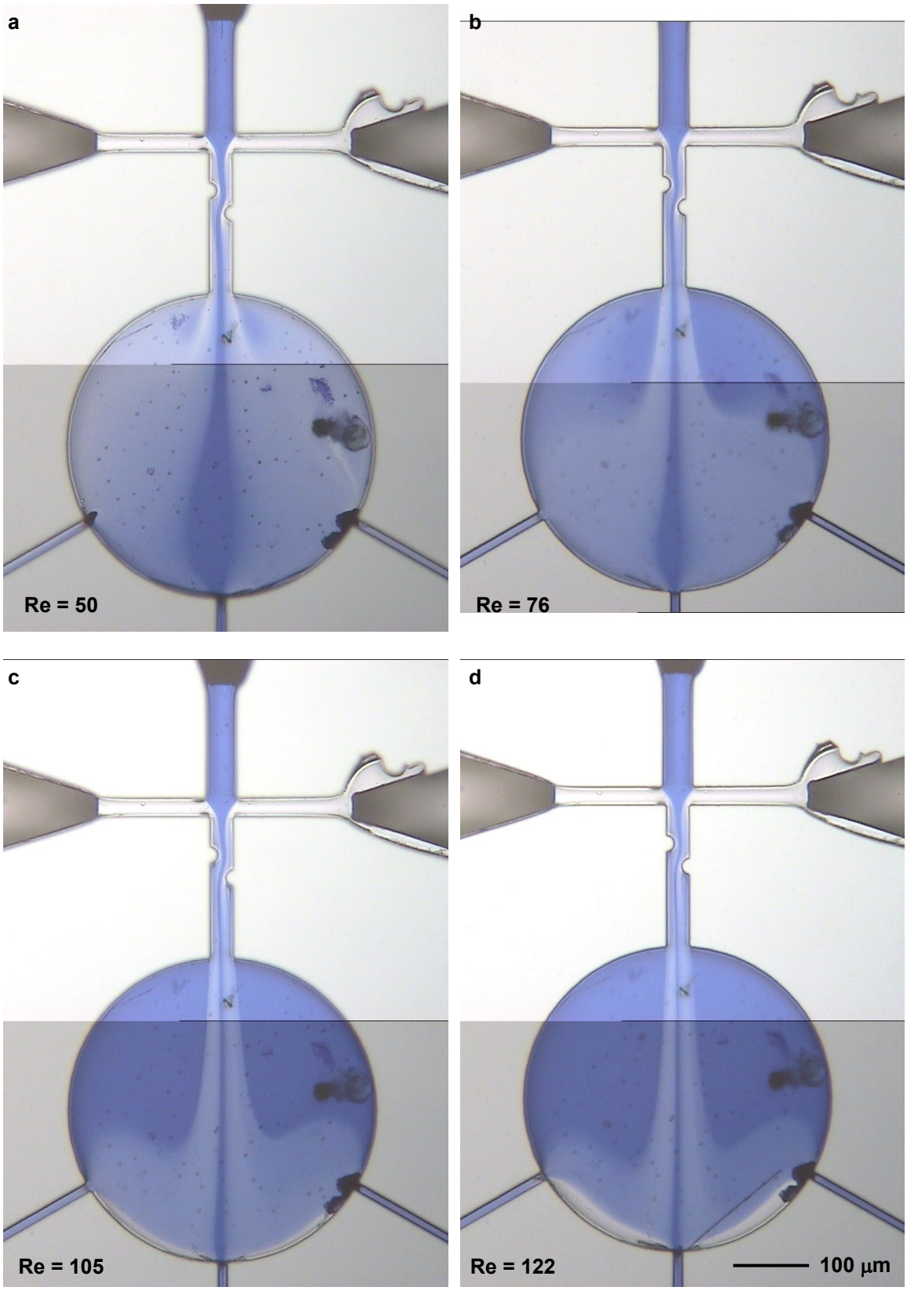
a
Re = 50
b
Re = 76
c
Re = 105
d
Re = 122
100 μm

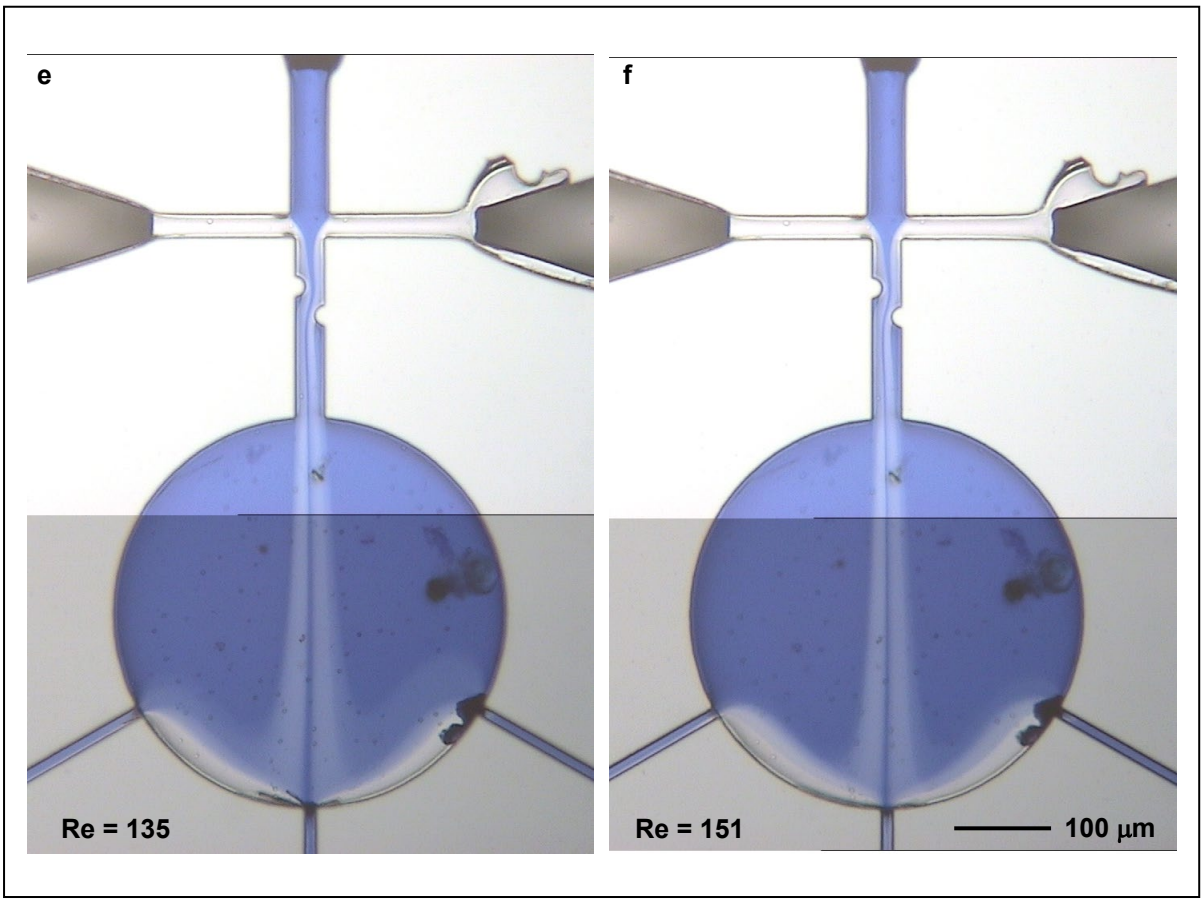

Fig. 8-9 *The images of CM-A captured at different Reynolds number of flow in the mixing channel. At progressively higher Reynolds number, the mixing performance is better as seen from the uniformity of blue dye concentration of the mixture at the end of the mixing channel.*

mixing channel can be observed at progressively higher Reynolds number. At low Reynolds number in the mixing channel as shown by *fig. 8-9a* and *8-9b*, the striation of blue dye from the inlet channel in the middle can be clearly seen with its thickness at about one-third of the width of the mixing channel. The thickness of this striation decreased with increasing Reynolds number as shown by *fig 8-9c* to *8-9f*. The colourless de-ionized water that was sandwiching the blue striation became more coloured at higher Reynolds number, producing a more uniform blue dye concentration at the outlet of the mixing channel.

The observations of mixing in CM-B and CM-C are very similar to those described for CM-A. *Fig. 8-10* and *8-11* show the images of mixing in the micromixers at different Reynolds numbers. Although the static mixing elements introduced in the mixing channel was unable to cause extensive lateral velocity components across the mixing channel to

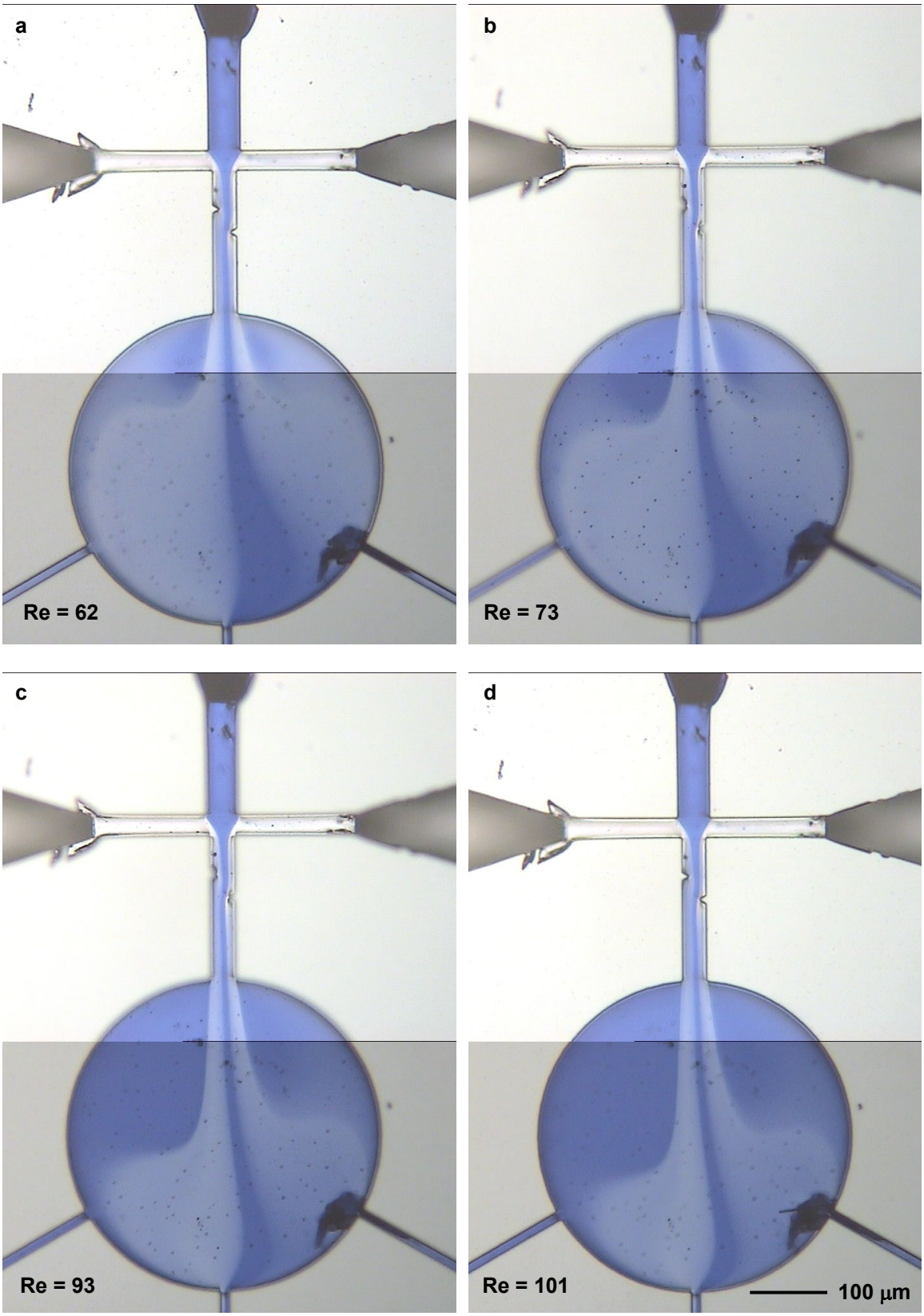

Fig. 8-10 *The mixing in CM-B at different Reynolds number of flow in the mixing channel.*

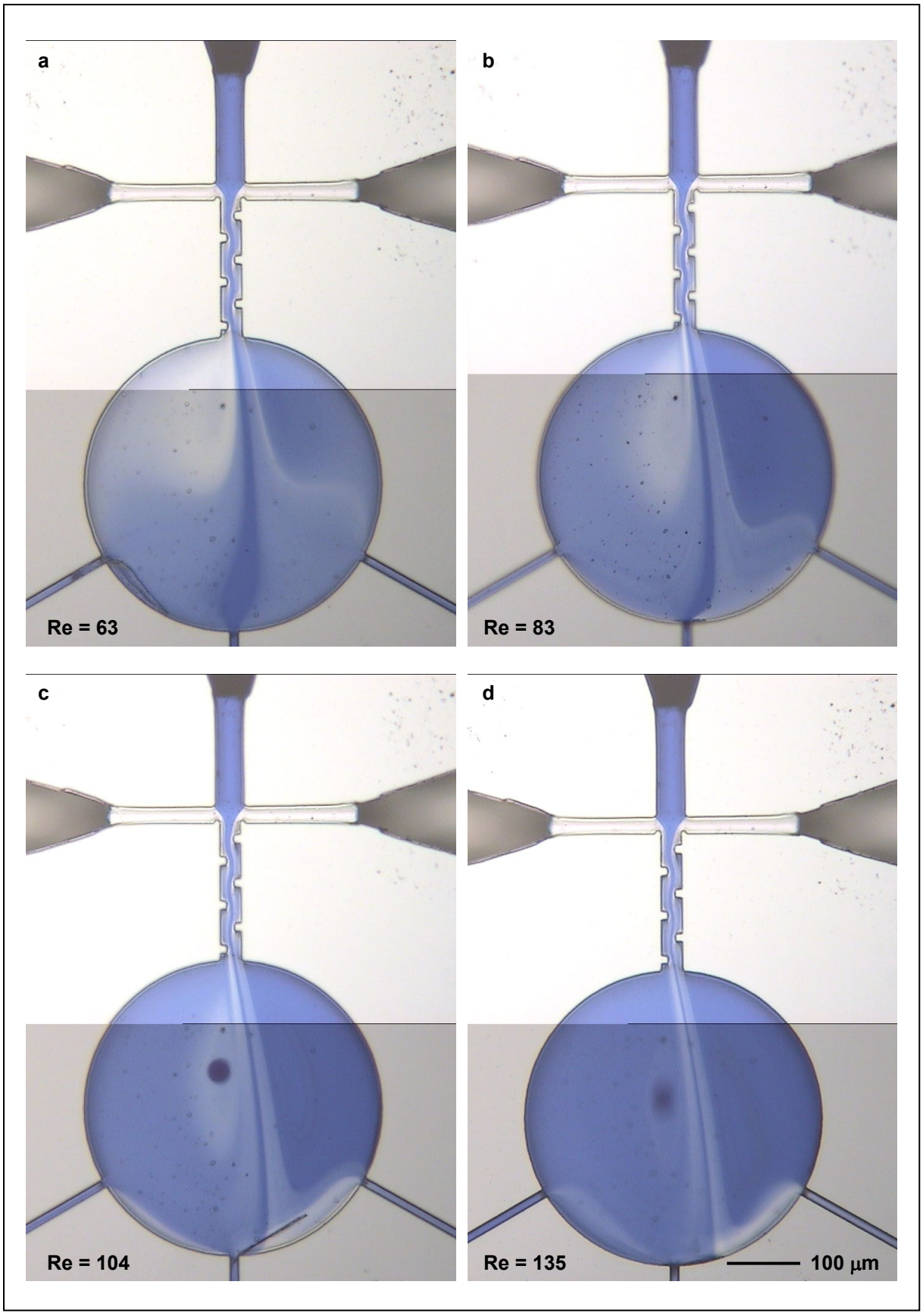

Fig. 8-11 *The mixing in CM-C at different Reynolds number. At higher Reynolds number, the flow recirculation phenomenon at the downstream of each static mixing element results in better mixing.*

achieve good mixing, flow recirculation that resulted in a more uniform blue dye concentration was nevertheless evident downstream of each static mixing element.

The distribution of blue dye concentration in the observation chamber was affected by the location of the narrow outlet channels connected to it. As the outlet channels were connected only to the lower half of the observation chamber, a mixture having different residence times was retained in the observation chamber. A large proportion of the mixture leaving the mixing channel travelled towards the inlets of the narrow outlet channels and was then purged out of the micromixer. A small proportion of the mixture was however trapped in the top left and right regions of the observation chamber. As the mixture in the observation chamber had different residence times, it was not suitable to be used for spectroscopic analysis. The sizes of the microchannels in the cross-shaped micromixers are smaller compared to micro T-mixers. The cross-shaped micromixers are therefore more susceptible to blockage by particles. Particle blockage usually occurred at the inlets to the inlet channels, in the mixing channel and at the inlets to the narrow outlet channels as shown in *fig. 8-12*. Extreme care was therefore taken to ensure cleanliness not only through pre-filtering the liquids used in the experiments, but also when handling the tube fittings to avoid particles being introduced into the system.

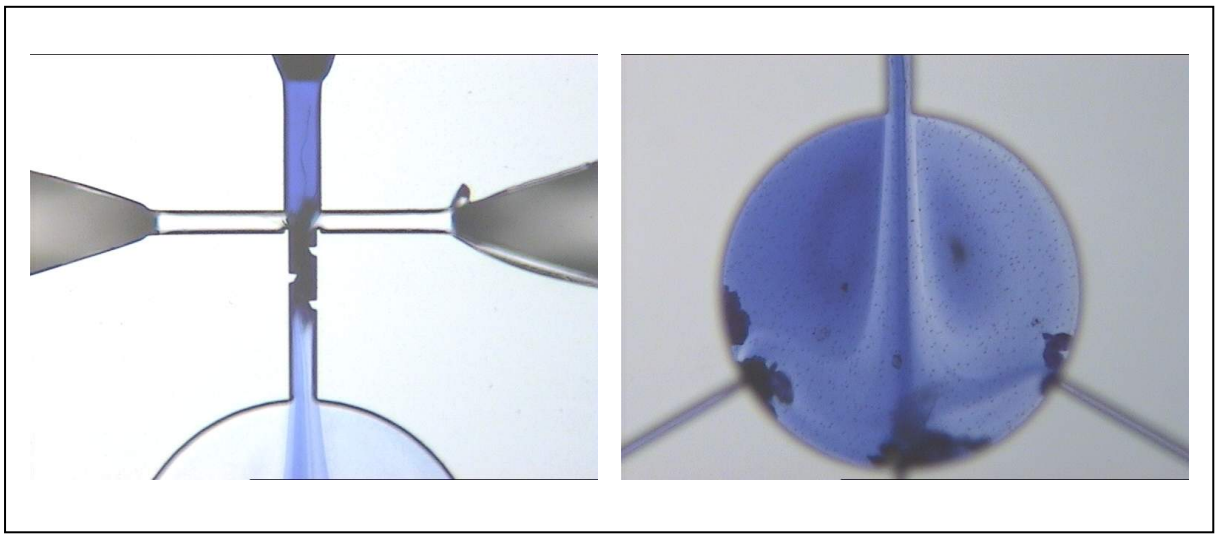

Fig. 8-12 *Blockages in the mixing channel (left) and at the inlet to the narrow outlet channels (right) in the cross-shaped micromixer.*

CLOSURE

The investigation work of mixing in cross-shaped micromixers has been described in detail in this chapter. The cross-shaped micromixers were designed to work as a stopped-flow micromixer by incorporating narrow outlet channels after the observation chamber to retard the flow of liquid when the observation chamber was filled. It was however realized later that ensuring the two liquids to enter and collide at the junction of the micromixer at the same time was not possible. The micromixers were tested in continuous flow mode instead. The inclusion of narrow outlet channels resulted in the Reynolds number of flow attainable in the experiments was much lower than that achieved in micro T-mixers. For the applied pressures of up to 10 bar used in the experiment, the highest Reynolds number achieved was 151. At this Reynolds number, the flow in the micromixer is predominantly laminar. The secondary flow and the generation of vortices around the static mixing elements in the micromixers were not sufficient to ensure a mixture of uniform concentration of the two liquids at the outlet of the mixing channel.

DISCUSSION

9.1 MICRO T-MIXERS

According to the laminar flow theory for flow in rectangular ducts, Reynolds number of flow in a rectangular microchannel varies linearly with the pressure gradient along it. Assuming that in an ideal case, no losses occur in the micro T-mixer at its junction and its inlets and outlet, the Reynolds number – applied pressure relationship is also linear. However, this is not observed in micro T-mixer A, B and C in this study. It can be seen from the graph in *fig. 7-1* that the relationship between the Reynolds number and the applied pressure is linear only for micro T-mixer D but deviates from linearity for micro T-mixer A, B and C at Reynolds number above 400. The slopes of the curves decrease with increasing applied pressure, which indicates that the increase in Reynolds number is progressively less per unit increase in applied pressure at higher pressures. It therefore implies that losses do occur in the micro T-mixers at the locations mentioned and they increase with increasing Reynolds number. The losses in micro T-mixer D are however less significant as the Reynolds numbers of flow in the micro T-mixer is low. At low pressures, the flow velocity in the microchannels is low. Viscous forces dominate in the flow and any perturbation by irregularities and discontinuities in the flow channel is damped out by the viscous forces. Flow is therefore as predicted by the laminar flow theory. At higher pressure, the inertia effects in the flow can no longer be contained by the viscous forces. Secondary flow and vortices are generated around discontinuities in the flow channel such as the junction and the inlet and outlet reservoirs of

the micro T-mixer. These secondary flow and vortices consume part of the energy available for liquid flow, resulting in a lesser increase in flow velocity per unit increase in applied pressure. The fact that the applied pressure is measured from outside of the test chip also results in some inaccuracies as the deviation in the curves in *fig. 7-1* also includes some losses at the entrance to the reservoirs. *Table 9-1* compares the pressure requirements between those predicted by fundamental fluid flow theory and those measured during experiments in Micro T-mixer C for a range of Reynolds numbers in the mixing channel. At low Reynolds number, there are close similarities between the pressure requirements predicted by theory and the actual values. However, at Reynolds numbers greater than 300, the actual pressure required to achieve a certain Reynolds number is greater than that predicted by theory. This can be explained by the extra pressure loss through the via holes that is more significant at higher pressures, but is not accounted for in the design calculations.

Reynolds number	Applied pressure (kPa)	
	Design calculation	Experimental measurement
100	88	78 [a]
200	180	180
300	277	292
400	379	419
500	485	565
600	596	702 [a]

[a] *The values are extrapolated .*

Table 9-1 *A comparison between the estimated pressure requirements at different Reynolds numbers computed from design calculations and the actual pressure requirements measured from experiments in Micro T-mixer C. Note the close agreement between predicted and actual values at low Reynolds numbers. At higher Reynolds numbers, the actual pressure requirements are higher.*

Secondary flow of Prandtl's first kind is set up as a result of centrifugal force when fluid flows in a curved path (Prandtl, 1952). When a fluid is flowing around a bend, the region of flow with a higher flow velocity tends to flow outwards while the slower flow at

the top and bottom walls of the channel tends to flow inwards towards the bend. In a micro T-mixer, this gives rise to a secondary flow patterns at the junction as shown in *fig. 9-1a* where the two streams of liquid from the two side-inlets change direction to flow in the mixing channel. Separation of boundary layers occur at the top of the junction where the two streams change direction, as shown in *fig. 9-1b*. Vortices are set up there, resulting in mixing between the two liquids in that region. The partially mixed solution there is swept by the secondary flow towards the sidewalls of the mixing channel. This results in cross flow as observed in the experiments. This phenomenon is also evident in the computer simulation results of Scenario I when all boundary conditions specified are symmetrical. It can be observed in *fig. 4-5a* that the mass fraction of the liquid around the bend shows some mixing there due to cross flow. Cross flow assists in the mixing process by creating a larger area of contact between the two liquids for mixing.

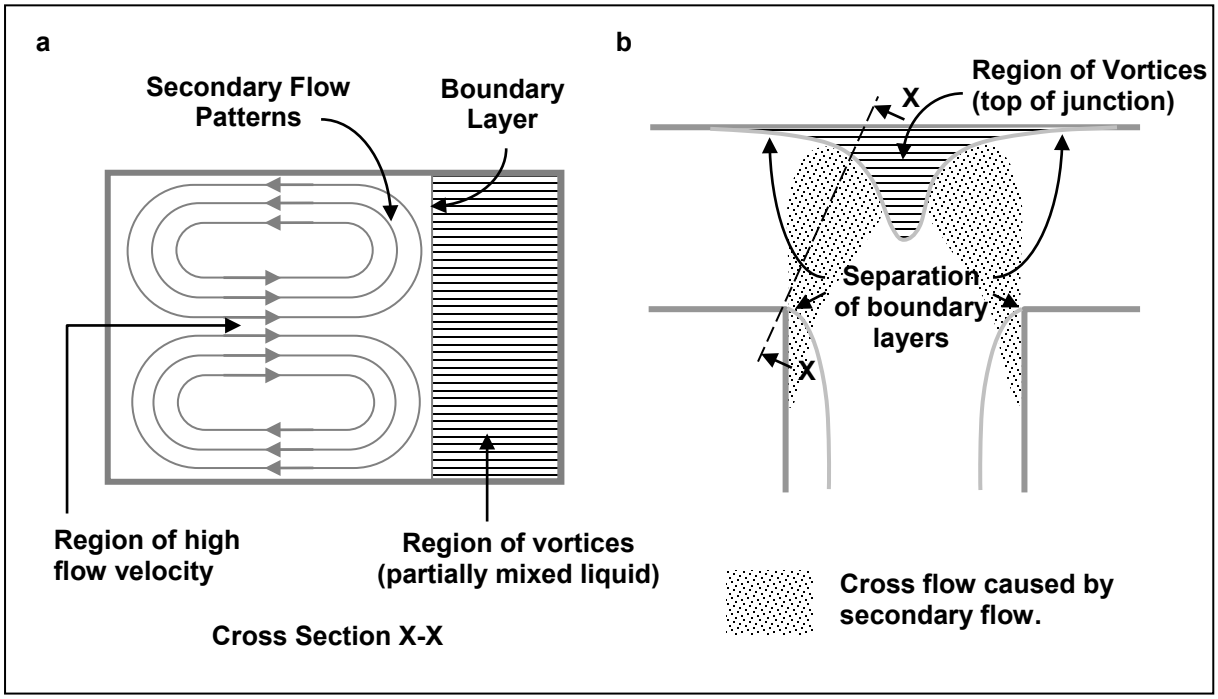

Fig. 9-1 *(a) is the cross-section view of (b) at X–X. The change in flow direction results in secondary flow that sweeps the mixture from the region of partially mixed liquid to the walls of the mixing channels. This gives rise to the cross flow observed in the mixing experiments.*

Computer simulations of mixing in a micro T-mixer for the eight scenarios showed that the enhanced mixing performance in micro T-mixer observed in the experiments was mainly caused by the presence of small *z* velocity components at the inlets. These *z* velocity components create asymmetrical velocity profiles across the depth of the two inlets. If the velocity profiles across the inlets of the micro T-mixer were perfectly symmetrical, no swirling would be generated along the mixing channel as the momentum of the liquid from the left would be equally countered by that from the right. The two liquids will then travel side by side along the mixing channel with very little liquid crossing the centreline to mix with the liquid from the other side. The small amount of liquid that reaches the other side is due to the cross flow phenomenon. In reality, however, perfectly symmetrical velocity profile is seldom obtainable. Many factors can disturb this symmetry such as the presence of some undulations on the surfaces of the microchannel caused by imperfect etching. *Fig. 9-2* shows some undulations on the surfaces of the microchannels in the micro T-mixers. The presence of small protrusions on the bottom and across the left inlet channel for example will introduce a vertical velocity component in the flow as simulated in Scenario IV, V and VIII. When the two liquids collide, the liquid momentums from the two sides are no longer countered equally resulting in swirling flow in the mixing channel that significantly enhances the mixing performance. A small vertical velocity component is sufficient to have significant effect on the mixing performance downstream of the mixing channel as observed in the simulations. The enhancement in mixing performance is however much more significant when the Reynolds number of flow is high. No significant improvement in the mixing performance is observed when the Reynolds number is low as simulated in Scenario V. Other than asymmetrical velocity profile, asymmetrical speed of flow on the inlets and the difference in viscosity of the two liquids can also enhance the mixing performance of the micro T-mixer by enabling the species in one of the liquids to reach the other side of the

mixing channel. Slight difference in the speed of flow can occur in the mixing experiments due to the slightly different paths taken by the liquids before entering the micro T-mixer. For example, one of the liquids passes through an extra tee fitting needed for pressure measurement. The viscosity of the two liquids may also be slightly different. This is however not considered to be the main cause for the rapid mixing achieved in the micro T-mixer in the experiments as the blue dye was diluted with de-ionised water at a ratio of 1:9 before use.

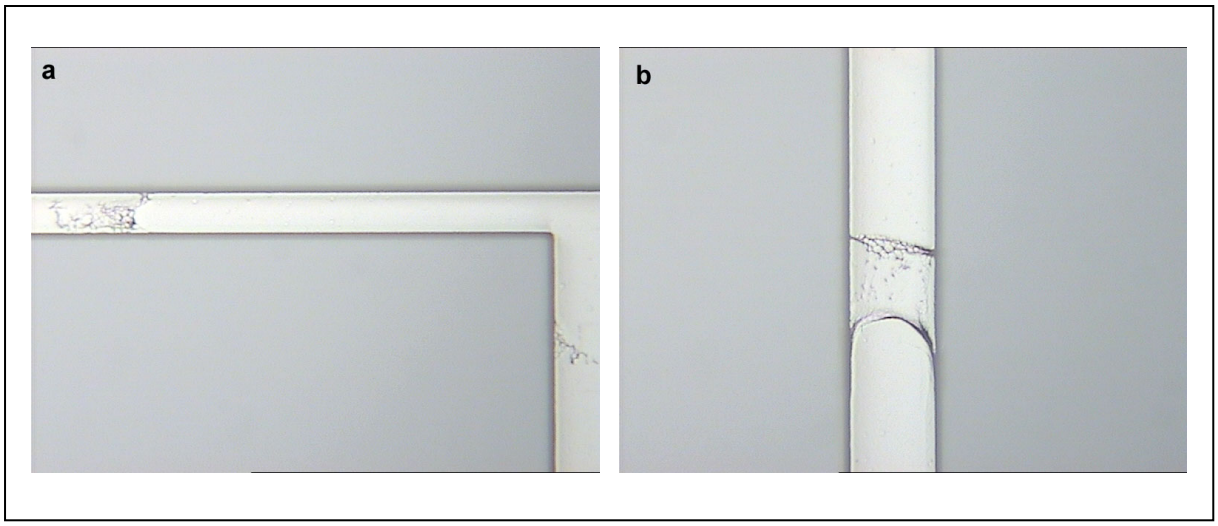

Fig. 9-2 *The micrographs show some of the features that may be present on the surface of the microchannel in the micro T-mixers used in the experiments. These features are caused by imperfect etching associated with the deep reactive ion etching used to produce the micro T-mixers.*

In order to relate the computer simulation results to the experimental results, the mass fraction values for species ⟨a⟩ on the outlet face obtained from Scenario IV were extracted. The mass fraction values at the nodes along the depth at the same position across the mixing channel were summed together to give an arbitrary, total intensity value of species ⟨a⟩. This resembles the intensity of blue dye observed under the microscope in the experiments where the intensity of the blue colour in the images captured reflects the sum of the blue dye species in the horizontal layers of mixture in the mixing channel. *Fig. 9-3* shows a graph of the arbitrary intensity of species ⟨a⟩ across the mixing channel at the outlet face. It can be clearly seen that the intensity of species ⟨a⟩ does not constantly reduce from one side of the mixing channel to the other. There are peaks and troughs in the intensity of species ⟨a⟩ across the

channel and this corresponds well to the striations observed at the upstream of the mixing channel in the experiments. It should also be noted that the ability of the optical microscope to focus on different depths of the microchannel allows the presence of horizontal stratified layer in the microchannel to be detected. *Fig. 9-4* shows the mixing of blue dye and colourless liquid at the same applied pressure with the microscope focusing on different depths. It can be seen that the presence of horizontal stratified layers, not extending completely across the channel, can be brought into focus. This is therefore an additional way of ensuring the good mixing observed in the mixing channels is not just an artefact resulted from the horizontal stratified layers of unmixed liquids.

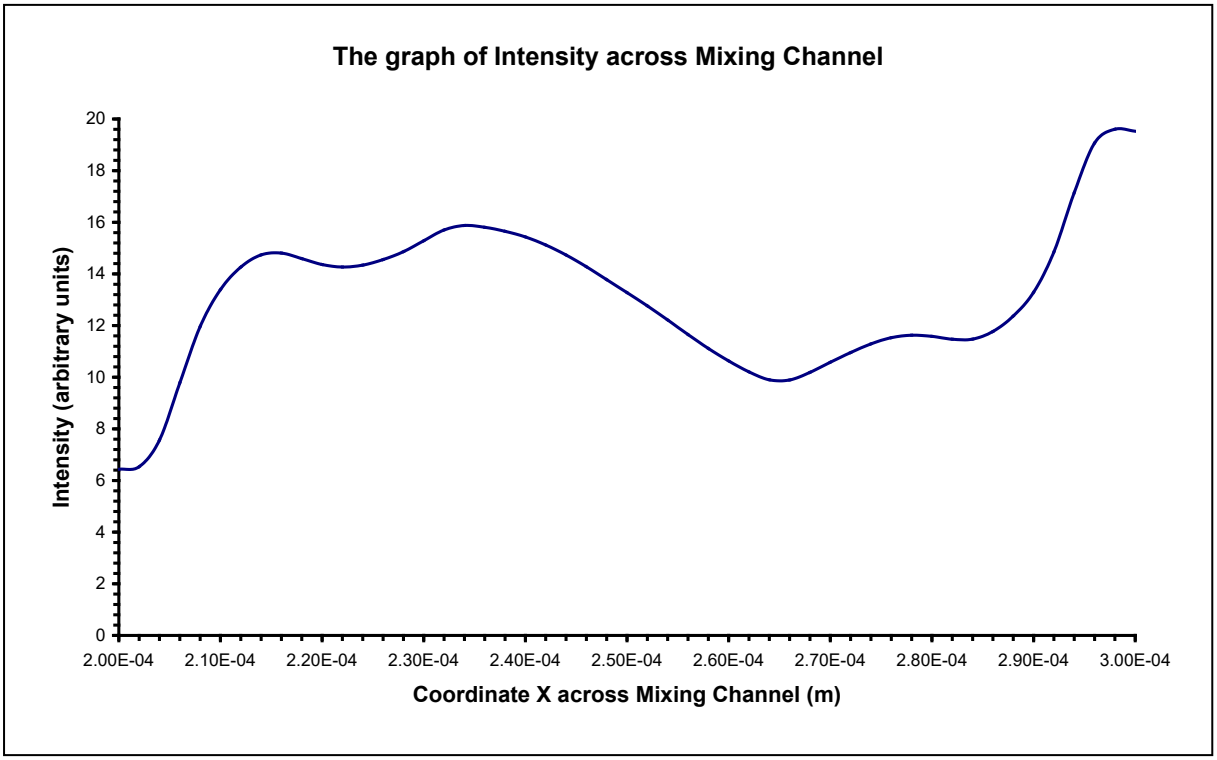

Fig. 9-3 *The graph of intensity of species ⟨a⟩ across the mixing channel at the outlet face based on the simulation result of Scenario IV shows that the concentration of species ⟨a⟩ does not constantly decrease from one side of the channel to the other side but fluctuate across the channel. This is similar to the experimental observation of the presence of striations in the mixing channel.*

Computer simulations of mixing in a micro T-mixer have also been carried out by Kockmann *et al.* (2003), Engler *et al.* (2003) and Hoffmann *et al.* (2003). In their simulations, symmetrical flow conditions were specified at the inlets. The breakdown of

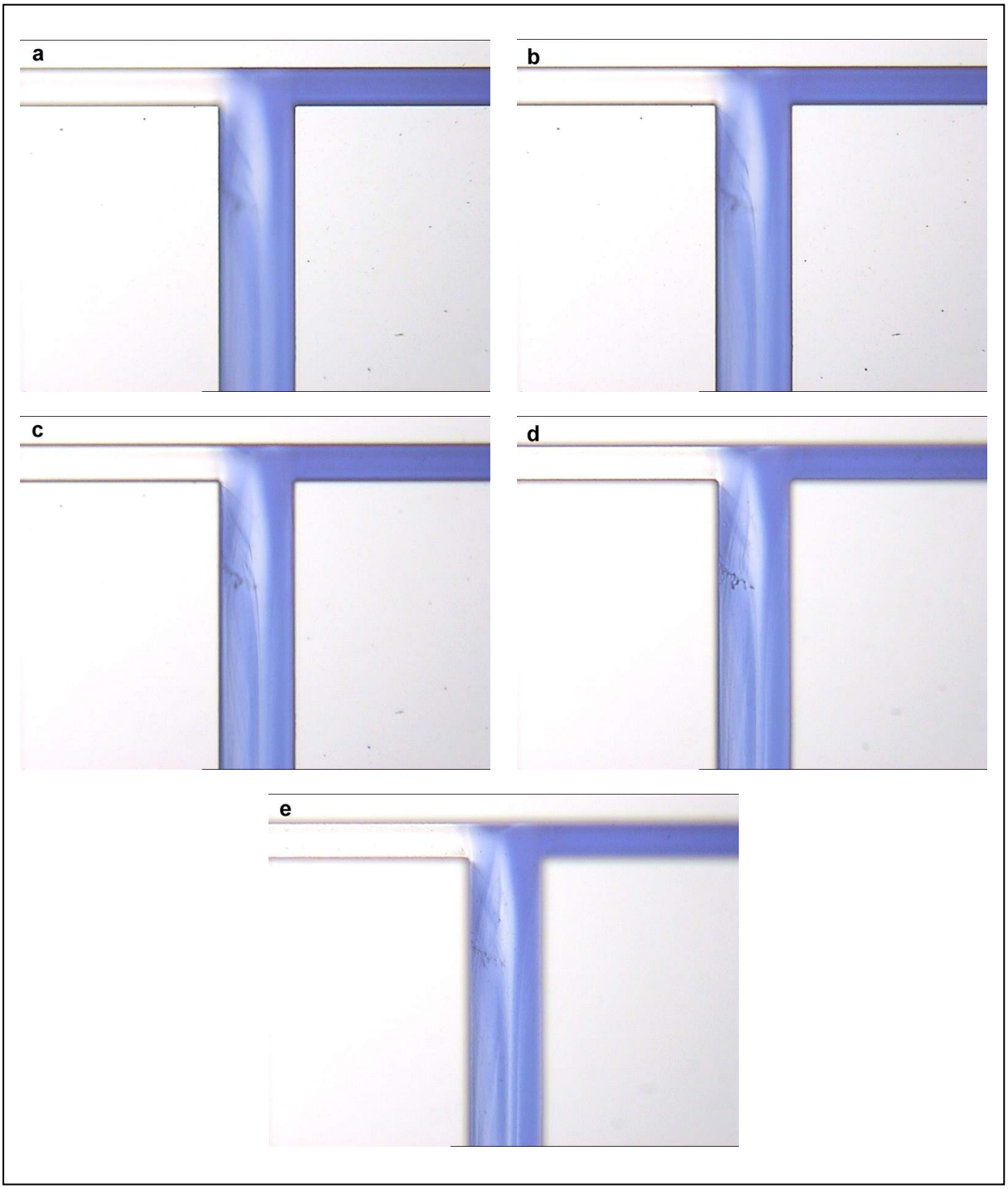

Fig. 9-4 *The micrographs show the mixing process characterized with blue dye and colourless liquid, all at the same applied pressure but with the optical microscope focusing on different depths in the microchannel. (a) to (e) show the mixing process from the top to the bottom of the microchannel. By focusing on different depths, horizontal stratified layers of unmixed liquids not extending completely across the channel can be detected.*

symmetry of flow field at the junction has also been observed by them at high Reynolds number. It was said to happen because the symmetrical flow field tended to instability due to the unstable stagnation point at the junction. In our simulations however, when symmetrical flow conditions were specified, no breakdown of symmetry was observed, even at high Reynolds number. Breakdown of symmetry of flow field similar to that observed by Kockmann *et al.*, Engler *et al.* and Hoffmann *et al.*, described by them as engulfment flow, was only observed in this study when asymmetrical flow conditions were specified. Hoffmann *et al.* also carried out some mixing experiments in a micro T-mixer but having a trapezoidal cross section as opposed to rectangular ones used in this study. Cross flow phenomenon was also observed by them in their mixing experiments.

9.2 CROSS-SHAPED MICROMIXERS

The experimental observations of mixing in cross-shaped micromixers are in close agreement with the results obtained from computer simulations at the same Reynolds number. It is observed that at a Reynolds number of 108, a striation of blue dye from the middle inlet channel is sandwiched between the two streams of de-ionized water from the side-inlets and the variation of blue dye concentration at the outlet is not fully evened out at the outlet of the mixing channel. This is reflected in the computer simulation results at the same Reynolds number. An image showing the mixing progress in a micromixer with semicircular static mixing elements at a Reynolds number of 108 (*fig. 9-5a*) is compared with the corresponding fluid trajectory plots of species ⟨a⟩ and ⟨b⟩ obtained from computer simulation (*fig. 9-5b* and *c*). It can be seen from the fluid trajectory plots that the static mixing elements are not able to produce sufficient lateral transport of liquid species ⟨b⟩ from the two sides of the mixing channel at this Reynolds number, resulting in the presence of a striation of blue dye along the middle of the mixing channel. The fluid trajectory plot of species ⟨a⟩ shows that some of the

liquid species is disturbed by the static mixing elements and are transported to the two sides of the mixing channel resulting in some extent of mixing across the channel.

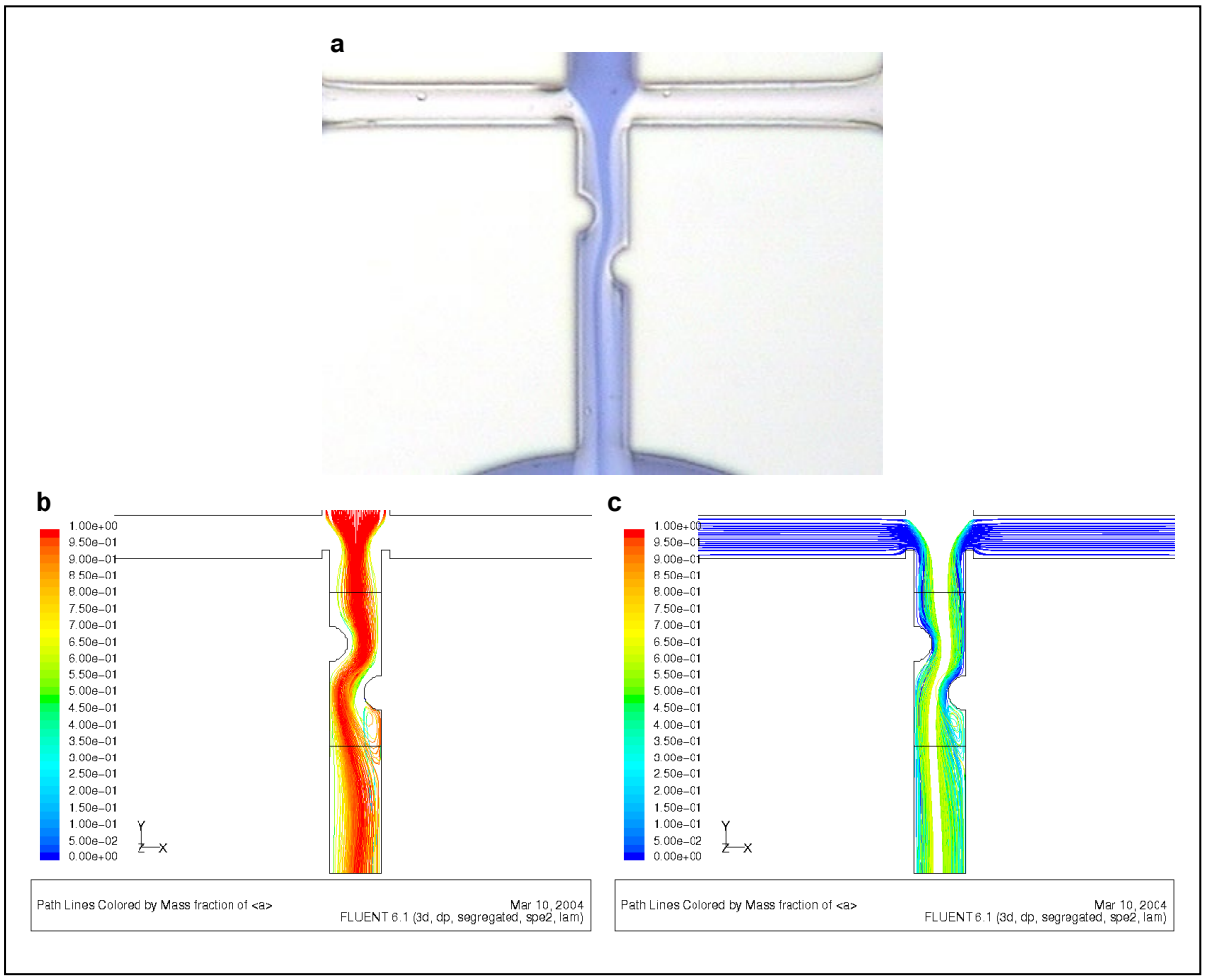

Fig. 9-5 *(a) shows an image of mixing in the cross-shaped micromixer at a Reynolds number of 108. The experimental observation compares closely with the computer simulation results at the same Reynolds number shown by the two fluid trajectory plots of species ⟨a⟩ and ⟨b⟩ in (b) and (c) respectively.*

The extent of mixing of two liquids achieved by a cross-shaped micromixer at the outlet of its mixing channel is not as good as that achieved by a micro T-mixer in this study. It does not however mean that the static mixing elements introduced in the cross-shaped micromixers are not capable of improving mixing performance through the generation of vortices. The cross-shaped micromixers were intended to be used as stopped-flow devices that were thought to be attained by the introduction of narrow outlet channels that could retard the flow of liquid when the observation chamber was filled. This was however not

possible as the two liquids could not be made to enter and collide at the junction at the same time. The cross-shaped micromixers were tested in a continuous flow mode in which the flow velocity of the mixture in the micromixer was suppressed by the narrow outlet channels as a result. The pressure requirement for a micromixer in order to operate at a certain Reynolds number of flow in the experiment far exceeds that predicted by computer simulations at the same Reynolds number. The maximum achievable Reynolds number of flow in the cross-shaped micromixers at applied pressures of up to 10 bar is 151. The uniformity of blue dye concentration at the outlet of the mixing channel at this Reynolds number is nevertheless better than that obtainable in micro T-mixers at the same Reynolds number. The length of the mixing channel must also be considered when comparing the mixing performance between the two micromixers. The length of the mixing channel in micro T-mixers is very much longer than that in cross-shaped micromixers. The residence time of the mixture in the mixing channel of a cross-shaped micromixer at a Reynolds number of 151 is 43 μs, compared to 2.45 ms in micro T-mixer C at the same Reynolds number. The longer residence time in the mixing channel of micro T-mixers allows the two liquids more time to mix, thus resulting in a greater extent of mixing at the outlet of the mixing channel.

The excellent mixing performance observed in micro T-mixers is mainly due to the asymmetrical flow conditions at their inlets. The presence of small z velocity components at the inlets results in swirling flow in the mixing channel and extensive mixing at the outlet. This is however not obtained in cross-shaped micromixers as indicated by the simulation results of Scenario 15 and 16 when asymmetrical boundary conditions were specified at the inlets. The fluid trajectory plot of species ⟨b⟩ from the two side-inlets as shown in *fig. 9-6* indicates limited crossover of the liquid species from one side of the mixing channel to the other side even when the z velocity components are at 10 percent of their x velocity

components. This is very much due to the stabilizing effect of the stream of liquid from the middle inlet channel. Unlike in micro T-mixers where the two colliding streams of liquid are coming from opposite directions, the two streams of liquid coming from both sides are separated by the stream of liquid coming from the middle. Any offset in velocity profile across the two side-inlet channels cannot be translated into swirling flow in the mixing channel as the two streams do not come into contact. The stream of liquid from the middle inlet channel is not sensitive to an offset in velocity profile of the streams from the two side-inlet channels as the two streams are flowing in perpendicular directions to each other.

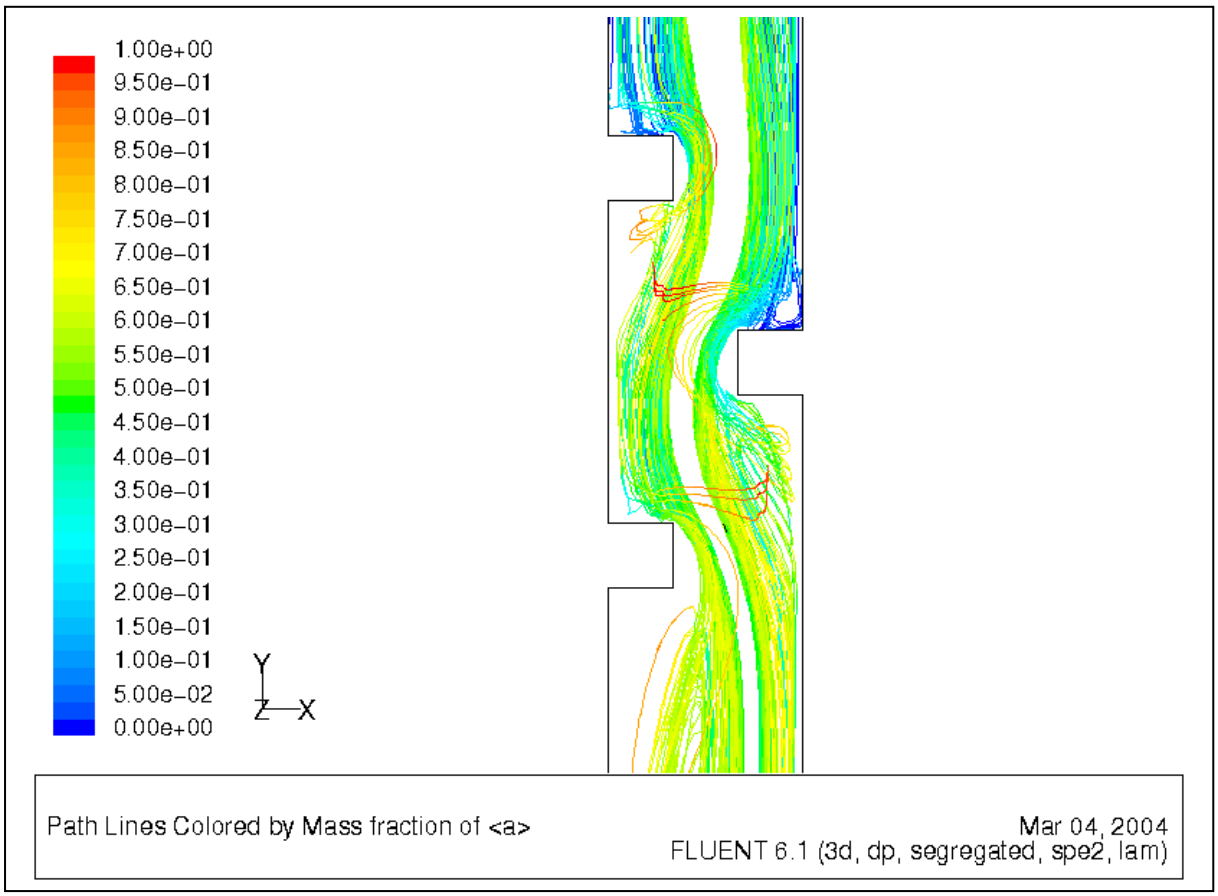

Fig. 9-6 *The fluid trajectory plot of liquid species from the two side-inlet channels shows very limited crossover of liquid from one side of the micromixer to the other side even when asymmetrical boundary conditions are applied at the two side-inlets.*

Cross-flow phenomenon observed in micro T-mixers caused by secondary flow is also observed in cross-shaped micromixers. When the two streams of colourless de-ionized water from the side-inlets change direction of flow at the junction, secondary flow is set up

where some blue dye species are transported to the two sides of the mixing channel through the top and bottom surfaces of the channel following the secondary flow patterns. The transport of blue dye species across the mixing channel due to molecular diffusion is limited compared to that due to secondary flow as the residence time of the mixture in the mixing channel is too short for the dye species to travel across the mixing channel by diffusion. This is evident from the blue colour on both sides of the mixing channel that is more evident at higher Reynolds number of flow.

The operation method of the cross-shaped micromixers investigated in this study is different to that employed by Knight *et al.* (1998) in their cross-shaped micromixers. The micromixers produced by Knight *et al.* employed hydrodynamic focusing of a liquid from the middle inlet channel to obtain a very thin layer of this liquid so that rapid mixing can proceed by means of diffusion. The micromixers fabricated in this study on the other hand harnessed the mixing ability of vortices generated by the inclusion of static mixing elements in the mixing channel. The Reynolds number of flow achieved in this study is about two orders of magnitude larger than that achieved in the micromixers produced by Knight *et al.* The dimensions of the micromixer in this study are larger than those of the micromixer investigated by Knight *et al.* as the main means of mixing is not by diffusion and it is therefore not necessary to achieve a thin film of liquid for rapid diffusion through the use of small dimensions.

9.3 CLOSURE

From the above discussions of all the results obtained from the investigations of mixing in micro T-mixers and cross-shaped micromixers, a few main points can be distilled. It is very common for any system to be designed and operated in such a way that symmetry is ensured. For example, simulation work on mixing in a micro T-mixer performed prior to this study all

specified symmetrical boundary conditions in their systems. The mixing performance obtained with symmetrical boundary conditions at the inlets is poor and this may be discouraging experimental characterization work to be carried out on a micro T-mixer until recently. But in practice, perfect symmetrical conditions are difficult to achieve and some degree of asymmetry is always present. Sensitivity to asymmetry is different for different microfluidics systems as evident from the two micromixers investigated in this study. The sensitivity of a micro T-mixer to asymmetrical conditions at its inlets is particularly high due to the high velocity gradient associated with fluid flow in the microscale even at moderate Reynolds number of just a few hundreds. The high velocity gradient in the fluid flow in the microscale enables rotational flow of high vorticity to be obtained. The fact that the Reynolds number of a liquid flow in the microscale is low and how this has limited the mixing speed achievable in micromixers are now very well appreciated by the MEMS community. But the fact that even at low Reynolds number, the flow velocity in a microchannel and the velocity gradient across it are very high and how this can enhance the mixing performance in a micromixer have yet to be fully exploited.

CONCLUSIONS

10.1 CONCLUSIONS

A blue dye and colourless de-ionized water were used to characterize the mixing performance in micro T-mixers and cross-shaped micromixers fabricated in this study. Due to the possibility of horizontal stratification of unmixed liquids that can give the impression of good mixing when dyes are used for characterization, the mixing results observed in micro T-mixers were further confirmed by the results obtained from mixing two chemical solutions. Design calculations and computer simulations were carried out before experimental work to predict the pressure requirements for a certain Reynolds number of flow in the micromixers as well as to investigate based on theory the improvement of mixing performance from the introduction of static mixing elements in the mixing channel. The mixing times achieved by the micro T-mixers tested are in the range of a millisecond, which is orders of magnitude faster than those achieved by the current micromixers. It is very difficult to attain turbulent flow in microchannels, but rapid mixing is still possible by the generation of secondary flow, swirling flow and vortices in the micromixer. Further computer simulations with asymmetrical boundary conditions were performed in micro T-mixers to gain insight on the mechanisms behind the rapid mixing observed. The presence of small z velocity components in the flow of liquids in the inlet channels, as well as asymmetrical flow velocities at the inlets and dissimilar viscosity of the two liquids results in swirling flow that enhances the mixing performance. This is also assisted by the cross flow phenomenon and the geometry at

the junction that create secondary flow, separation of boundary layers and vortices in the flow. Complete mixing was not observed at the outlet of the mixing channel in cross-shaped micromixers but the introduction of static mixing elements in the mixing channel nevertheless improved the mixing performance. This is evident from the progressively better blue dye uniformity at the outlet of the mixing channel with increasing Reynolds number. The short residence time of the mixture and the relatively low achievable Reynolds number in the cross-shaped micromixer due to the short mixing channel and narrow outlet channels respectively contributed to the less than optimum mixing performance.

The importance of asymmetry in the flow at the inlets of a micro T-mixer cannot be under-estimated. A laminar flow in the microscale is not completely identical to a laminar flow in the macro-scale. Even at laminar flow, the flow velocity in a microchannel can be very high at up to a few metres per seconds. With the small dimensions across the microchannel, flow with very high velocity gradient is produced. Two colliding streams of liquid with their velocity profile offset due to asymmetrical flow conditions at the inlets can therefore produce a swirling flow with significant strength that effects rapid mixing. Due to the difference between the designs of a micro T-mixer and a cross-shaped micromixer, asymmetrical flow conditions at the inlets of a cross-shaped micromixer cannot produce the same effect as obtained in a micro T-mixer. The velocities of the streams of liquid in collision are perpendicular in direction to each other, thus do not generate swirling flow in the mixing channel. In all, this study shows that rapid mixing can be achieved in a micro T-mixer at a Reynolds number between 400 and 500. There is also potential in achieving rapid mixing in a cross-shaped micromixer with some modifications. Mixing times in the range of one millisecond are obtained in micro T-mixers making them suitable for the analysis of fast reactions involving expensive chemicals.

10.2 FUTURE WORK

The excellent mixing performance in the micro T-mixers achieved in this study serves to demonstrate that a micro T-mixer with asymmetrical conditions at its inlets is capable of achieving rapid mixing. The applied pressure used in this study is much higher than those used in other micromixers. However, further modifications can be carried out based upon a micro T-mixer design and exploit the asymmetry flow conditions to cause a stronger swirling flow and improve its efficiency, i.e. achieving rapid mixing at a lower applied pressure. For instance, asymmetry flow field created by intentionally incorporating structures such as a step to induce a larger z velocity component in the flow at one of the inlets to enhance the swirling of the mixture in the mixing channel can be incorporated in the micro T-mixer.

One of the main intentions of the investigation of mixing performance in the micro T-mixers and cross-shaped micromixer is to produce a rapid mixing micromixer for reaction kinetics studies of antibiotics and enzymes. The characterization of mixing between two biological fluids, which could be more viscous and have a smaller diffusivity, should therefore be performed. The adsorption properties of biological molecules on silicon surfaces and the possibility of fouling of the microchannels when the two biological fluids react in the micromixer and how this can be avoided must also be looked at.

The micromixer chips used in this study are made up of a silicon-glass bonded assembly. This allowed straight forward observation of the mixing performance in the micromixers. But when they are used for reaction kinetics studies of antibiotics and enzymes where infrared spectroscopy method is commonly used, a silicon-glass bonded assembly is not acceptable because glass is not transparent to infrared light. A silicon-to-silicon diffusion bonded assembly must be produced as silicon is transparent to infrared light. As the silicon substrate has a very high reflectivity, the external surface of such a micromixer chip around

where the infrared beam is to penetrate the micromixer chip should also be coated with a layer of anti-reflective coating to limit the scattering of the infrared light.

The cross-shaped micromixer requires a number of modifications before it allows rapid mixing to be observed. A longer mixing channel can be designed to increase the residence time of the mixture while the narrow outlet channels can be replaced with equally spaced via holes around the observation chamber so that no dead volume is formed and the bulk of the pressure drop occurs along the mixing channel. A stopped-flow rapid mixing micromixer can probably be achieved with the use of some external control valves after the outlet of the micromixer.

LIST OF REFERENCES

Andersson, H., van der Wijngaart, W., Nilsson, P., Enoksson, P. and Stemme, G. (2001). 'A valve-less diffuser micropump for microfluidic analytical systems'. *Sensor and Actuator B: Chemical*, 72, 259-265.

Bau, H.H., Zhong, J. and Yi, M. (2001). 'A minute magneto hydro dynamic (MHD) mixer'. *Sensors and Actuators B: Chemical*, 79, 207-215.

Beebe, D.J., Adrian, R.J., Olsen, M.G., Stremler, M.A., Aref, H. and Jo, B.H. (2001). 'Passive mixing in microchannels: fabrication and flow experiments'. *Mécanique & Industries*, 2, 343-348.

Blom, M.T., Tas, N.R., Pandraud, G., Chmela, E., Gardeniers, J.G.E., Tijssen, R., Elwenspoek, M. and Berg, A. (2001). 'Failure mechanisms of pressurized microchannels, model and experiments'. *Journal of Microelectromechanical Systems*, 10, (1), 158-163.

Bökenkamp, D., Desai, A., Yang, X., Tai, Y., Marzluff, E.M. and Mayo, S.L. (1998). 'Microfabricated silicon mixers for submillisecond quench-flow analysis'. *Analytic Chemistry*, 70, 232-236.

Bouteille, D. (1973). *Fluid logic control and industrial automation*. New York, John Wiley & Sons.

Clerc, P-A., Dellmann, L., Grétillat, F., Grétillat, M-A., Indermühle, P-F., Jeanneret, S., Luginbuhl, Ph., Marxer, C., Pfeffer, T.L., Racine, G-A., Roth, S., Staufer, U., Stebler, C., Thiébaud, P. and de Rooij, N.F. (1998). 'Advanced deep reactive ion etching: a versatile tool for microelectromechanical systems'. *Journal of Micromechanics and Microengineering*, 8, 272-278.

Cussler, E.L. (1984). *Diffusion: Mass Transfer in Fluid Systems* (p. 15-54). Cambridge, Cambridge University Press.

Elwenspoek, M., Lammerink, T.S.J., Miyake, R. and Fluitman, J.H.J. (1994). 'Towards integrated microliquid handling system'. *Journal of Micromechanics and Microengineering*, 4, 227-245.

Engler M., Föll, C., Kockmann, N. and Woias, P. (2003). 'Investigations of liquid mixing in static micro mixers'. *Proceeding of the 11th European Conference on Mixing, Bamberg, 14-17 October 2003*, 277-284.

Erbacher, C., Bessoth, F.G., Busch, M., Verpoorte, E. and Manz, A. (1999). 'Towards integrated continuous-flow chemical reactors'. *Microchimica Acta*, 131, 19-24.

Eringen, A.C. (1966). 'Theory of micropolar fluids'. *Journal of Mathematics and Mechanics*, 16, (1), 1-18.

Fluitec Documentation No. 11.102 Rev. 1

Focke, W.W. (1983). 'On the mechanism of transfer enhancement by eddy promoters'. *Electrochimica Acta*, 28, (8), 1137-1146.

Gobby, D., Angeli, P. and Gavriilidis, A. (2001). 'Mixing characteristics of T-type microfluidic mixers'. *Journal of Micromechanics and Microengineering*, 11, 126-132.

Gray, J.B. (1986). 'Turbulent radial mixing in pipes'. In V.W. Uhl and J.B. Gray (ed), *Mixing: Theory and Practice Vol. III* (p. 63-131). London, Academic Press.

Hardt, S. and Schönfeld, F. (2003). 'Laminar mixing in different interdigital micromixers: II. Numerical simulations'. AIChE Journal, 49, (3), 578-584.

He, B., Burke, B.J., Zhang, X., Zhang, R. and Regnier, F.E. (2001). 'A picoliter-volume mixer for microfluidic analytical systems'. *Analytical Chemistry*, 73, 1942-1947.

Hessel, V., Hardt, S., Löwe, H. and Schönfeld, F. (2003). 'Laminar mixing in different interdigital micromixers: I. Experimental characterization'. *AIChE Journal*, 49, (3), 566-577.

Hinsmann, P., Frank, J., Svasek, P., Harasek, M. and Lendl, B. (2001). 'Design, simulation and application of a new micromixing device for time resolved infrared spectroscopy of chemical reactions in solution'. *Lab on a Chip*, 1, 16-21.

Hoffmann, M., Raebiger, N., Schlueter, M., Blazy, S., Bothe, D., Stemich, C. and Warnecke, A. (2003). 'Experimental and numerical investigations of T-shaped micromixers'. *Proceedings of the 11th European Conference on Mixing, Bamberg, 14-17 October 2003*, 269-276.

Jansen, H., de Boer, M., Wensink, H., Kloeck, B. and Elwenspoek, M. (2001). 'The black silicon method. VIII. A study of the performance of etching silicon using SF_6/O_2-based chemistry with cryogenical wafer cooling and a high density ICP source'. *Microelectronics Journal*, 32, 769-777.

Judy, J., Maynes, D. and Webb, B.W. (2002). 'Characterization of frictional pressure drop for liquid flows through microchannels'. *International Journal of Heat and Mass Transfer*, 45, 3477-3489.

Karttunen, J., Kiihamäki, J. and Franssila, S. (2000). 'Loading effects in deep silicon etching'. *Proceedings of SPIE's Symposium on Micromachining and Microfabrication Process Technology VI*, Ed. J.M. Karam, J. Yasaitis, SPIE Vol 4174, 90-97, International Society for Optical Engineering, Santa Clara, CA, 18-20 Sept. 2000.

Kiihamäki, J. and Franssila, S. (1999). 'Pattern shape effects and artifacts in deep silicon etching'. *Journal of Vacuum Science Technology A*, 17, (4), 2280-2285.

Kiihamäki, J. (2000). 'Deceleration of silicon etch rate at high aspect ratios'. *Journal of Vacuum Science Technology A*, 18, (4), 1385-1389.

Kiihamäki, J., Kattelus, H. Karttunen, J. and Franssila, S. (2000). 'Depth and profile control in plasma etched MEMS structure'. *Sensors and Actuators A*, 82, 234-238.

Kirshner, J.M. and Katz, S. (1975). *Design theory of fluidic components: Introduction to fluidics*. New York, Academic Press.

Knight, J.B., Vishwanath, A., Brody, J.P. and Austin, R.H. (1998). 'Hydrodynamic focusing on a silicon chip: mixing nanoliters in microseconds'. *Physical Review Letters*, 80, (17), 3863-3866.

Koch, M., Chatelain, D., Evans, A.G.R. and Brunnschweiler, A. (1998). 'Two simple micromixers based on silicon'. *Journal of Micromechanics and Microengineering*, 8, 123-126.

Koch, M., Schabmueller, C.G.J., Evans, A.G.R. and Brunnschweiler, A. (1999a). 'Micromachined chemical reaction system'. *Sensors and Actuators A: Physical*, 74, 207-210.

Koch, M., Witt, H., Evans, A.G.R., Brunnschweiler, A. (1999b). 'Improved characterization technique for micromixers'. Journal of Micromechanics and Microengineering, 9, 156-158.

Kockmann, N., Föll, C. and Woias, P. (2003). 'Flow regimes and mass transfer characteristics in static micro mixers'. *Proceeding of SPIE 4982*, 319-329.

Kricka, L.J. (2001). 'Microchips, microarrays, biochips and nanochips: personal laboratories for the 21st century'. *Clinica Chimica Acta*, 307, 219-223.

Lärmer, F. and Schilp A. (1992). 'Method for anisotropically etching silicon'. *German Patent* DE4241045.

Lavallee, H.C. and Popovich, A.T. (1974). 'Fluid flow near roughness elements investigated by photolysis method'. *Chemical Engineering Science*, 29, 49-59.

Li, H.Q., Roberts, D.C., Steyn, J.L., Turner, K.T., Yaglioglu, O., Hagood, N.W., Spearing, S.M. and Schmidt, M.A. (2004). 'Fabrication of a high frequency piezoelectric microvalve'. *Sensors and Actuators A: Physical*, 111, 51-56.

Liu, R.H., Stremler, M.A., Sharp, K.V., Olsen, M.G., Santiago, J.G., Adrian, R.J., Aref, H. and Beebe, D.J. (2000). 'Passive mixing in a three-dimnensional serpentine microchannel'. *Journal of Microelectomechanical Systems*, 9, (2), 190-197.

Mala, G.M., Li, D. and Dale, J.D. (1997a). 'Heat transfer and fluid flow in microchannels'. *International Journal of Heat and Mass Transfer*, 40, (13), 3079-3088.

Mala, G.M., Li, D., Werner, C., Jacobasch, H.J. and Ning, Y.B. (1997b). 'Flow characteristics of water through a microchannel between two parallel plates with electrokinetic effects'. *International Journal of Heat and Fluid Flow*, 18, (5), 489-496.

Mala, G.M., Yang, C. and Li, D. (1998). 'Electrical double layer potential distribution in a rectangular microchannel'. *Colloids and Surfaces A: Physicochemical and Engineering Aspects*, 135, 109-116.

Mala, G.M. and Li, D. (1999). 'Flow characteristics of water in microtubes'. *International Journal of Heat and Fluid Flow*, 20, 142-148.

McAuley, S.A., Ashraf, H., Atabo, L., Chambers, A., Hall, S., Hopkins, J. and Nicholls, G. (2001). 'Silicon micromachining using a high-density plasma source'. *Journal of Physics D: Applied Physics*, 34, 2769-2774.

Mengeaud, V., Josserand, J. and Girault, H.H. (2002). 'Mixing processes in a zigzag microchannel: finite element simulations and optical study'. *Analytical Chemistry*, 74, 4279-4286.

Munson, B.R., Young, D.F. and Okiishi, T.H. (1998). Fundamentals of Fluid Mechanics (p. 505). New York, John Wiley & Sons, Inc.

Neu, H.C. (1992). 'The crisis in antibiotic resistance', *Science*, 257, 1064-1072.

Niu, X. and Lee, Y. (2003). 'Efficient spatial-temporal chaotic mixing in microchannels', *Journal of Micromechanics and Microengineering*, 13, 454-462.

Ottino, J.M. (1989). *The kinematic of mixing: stretching, chaos, and transport* (p. 1-17). Cambridge, Cambridge University Press.

Papautsky, I., Brazzle, J., Ameel, T. and Frazier, A.B. (1999). 'Laminar fluid behaviour in microchannels using micropolar fluid theory'. *Sensors and Actuators A: Physical*, 73, 101-108.

Park, S.J., Kim, J.K., Park, J., Chung, S., Chung, C. and Chang, J.K. (2004). 'Rapid three-dimensional passive rotation micromixer using the breakup process'. *Journal of Micromechanics and Microengineering*, 14, 6-14.

Peng, X.F. and Peterson, G.P. (1995). 'The effect of thermofluid and geometrical parameters on convection of liquids through rectangular microchannels'. *International Journal of Heat and Mass Transfer*, 38, (4), 755-758.

Peng, X.F. and Peterson, G.P. (1996). 'Convective heat transfer and flow friction for water flow in microchannel structures'. *International Journal of Heat and Mass Transfer*, 39, (12), 2599-2608.

Prandtl, L. (1952). *Essentials of Fluid Dynamics* (p.145-148, Chapter III). London, Blackie and Son Ltd.

Regenfuss, P., Clegg, R.M., Fulwyler, M.J., Barrantes, F.J. and Jovin, T.M. (1985). 'Mixing liquids in microseconds'. *Review of Scientific Instruments*, 56, (2), 283-290.

Ren, L., Qu, W. and Li, D. (2001a). 'Interfacial electrokinetic effects on liquid flow in microchannels'. *International Journal of Heat and Mass Transfer*, 44, 3125-3134.

Ren, L., Li, D. and Qu, W. (2001b). 'Electro-viscous effects on liquid flow in microchannels'. *Journal of Colloid and Interface Science*, 233, 12-22.

Roder, H. and Shastry, M.C.R. (1999). 'Methods for exploring early events in protein folding'. *Current Opinion in Structural Biology*, 9, 620-626.

Rubenstein, K. (2003). *Microfluidics: second generation technologies driving commercial opportunities*. Westborough, Drug and Market Development Publications.

Schwesinger, N., Frank, T. and Wurmus, H. (1996). 'A modular microfluid system with an integrated micromixer'. *Journal of Micromechanics and Microengineering*, 6, 99-102.

Shaw, C.T. (1992). *Using computational fluid dynamics* (p. 1-8). New York, Prentice Hall.

Toegl, A., Kirchner, R., Gauer, C. and Wixforth, A. (2003). 'Enhancing results of microarray hybridizations through microagitation'. *Journal of Biomolecular Techniques*, 14, 197-204.

Tohyama, O., Kohashi, M., Yamamoto, K. and Itoh, H. (1996). 'A fibre-optic silicon pressure sensor for ultra-thin catheters'. Sensors and Actuators A: Physical, 54, 622-625.

Towner, K.J. (1995). 'Mechanisms of Acquired Resistance' In D. Greenwood (ed), *Antimicrobial Chemotherapy* (p. 147-158). Oxford, Oxford University Press.

Tsai, J. and Lin, L. (2002). 'Active microfluidic mixer and gas bubble filter driven by thermal bubble micropump'. *Sensors and Actuators A: Physical*, 97-98, 665-671.

Tuckerman, D.B. and Pease, R.F.W. (1981). 'High performance heat sinking for VLSI'. *IEEE Electron Device Letters*, 2, (5), 126-129.

Urbanek, W., Zemel, J.N. and Bau, H.H. (1993). 'An investigation of the temperature dependence of Poiseuille numbers in microchannel flow'. *Journal of Micromechanics and Microengineering*, 3, 206-209.

Veenstra, T.T., Lammerink, T.S.J., Elwenspoek, M.C. and van den Berg, A. (1999). 'Characterization method for a new diffusion mixer applicable in micro flow injection analysis systems'. *Journal of Micromechanics and Microengineering*, 9, 199-202.

Vivek, V., Zeng, Y. and Kim E.S. (2000). 'Novel acoustic-wave micromixer'. *Proceedings of the IEEE Micro Electro Mechanical Systems (MEMS)*, 668-673.

Voldman, J., Gray, M.L. and Schmidt, M.A. (2000). 'An integrated liquid mixer/valve'. *Journal of Microelectromechanical Systems*, 9, (3), 295-302.

Wang, B.X. and Peng X.F. (1994). 'Experimental investigation on liquid forced-convection heat transfer through microchannels'. *International Journal of Heat and Mass Transfer*, 37, Suppl. 1, 73-82.

White, F. (1999). *Fluid Mechanics*. Singapore, WCB McGraw-Hill.

Xiao, Z., Chen, M., Wu, G., Zhao, C., Zhang, D., Hao, Y., Zhang, G. and Li, Z. (1999). 'Silicon micro-accelerometer with mg resolution, high linearity and large frequency bandwidth fabricated with two mask bulk process'. *Sensors and Actuators A: Physical*, 77, 113-119.

Xu, B., Ooi, K.T., Wong, N.T. and Choi, W.K. (2000). 'Experimental investigation of flow friction for liquid flow in microchannels'. *International Communication of Heat and Mass Transfer*, 27, (8), 1165-1176.

Yang, C. and Li, D. (1998). 'Analysis of electrokinetic effects on the liquid flow in rectangular microchannels'. *Colloids and Surfaces A: Physicochemical and Engineering Aspects*, 143, 339-353.

Yang, C., Li, D. and Masliyah, J.H. (1998). 'Modeling forced liquid convection in rectangular microchannel with electrokinetic effects'. *International Journal of Heat and Mass Transfer*, 41, 4229-4249.

Yang, Z., Matsumoto, S., Goto, H., Matsumoto, M. and Maeda, R. (2001). 'Ultrasonic micromixer for microfluidic systems'. *Sensors and Actuators A: Physical*, 93, 266-272.

Yi, M. and Bau, H.H. (2003). 'The kinematics of bend-induced mixing in micro-conduits'. *International Journal of Heat and Fluid Flow*, 24, 645-656.

Zdeblick, M.J., Barth, P.W. and Angell, J.B. (1990). 'Microminiature fluidic amplifier'. *Technical Digest IEEE Solid-State Sensor and Actuator Workshop*.

APPENDIX A

For a steady incompressible fluid flowing in a horizontal closed channel of constant and arbitrary cross section at a mean velocity $\bar{u}$, the head loss H in a channel of length L due to the frictional effects in the fluid is given by the following expression.

$$H = \frac{fL}{d}\frac{\bar{u}^2}{2g} \tag{A-1}$$

Considering Bernoulli equation with energy loss between the two ends of this channel, the equation can be simplified to equation A-2.

$$-\frac{\Delta p}{\rho g} = H \tag{A-2}$$

where Δp is the pressure difference between the ends of the channel evaluated by $p_o - p_i$. Substituting A-2 into A-1 and simplifying the resulting equation, the following expression is obtained.

$$f = -\frac{2d\Delta p}{\rho L\bar{u}^2} \tag{A-3}$$

The friction constant, C, for a laminar flow is defined by the following relationship, $\mathrm{C} = f \times \mathrm{Re}$. Substituting equation 3-1 for the Reynolds number in the expression yields

$$f = \frac{\mathrm{C}\mu}{\rho\bar{u}d} \tag{A-4}$$

Equating equations A-3 and A-4 and rearranging the expression, an expression for the mean flow velocity as a function of pressure difference can be obtained.

$$\bar{u} = -\frac{2d^2 \Delta p}{\mu C L} \tag{A-5}$$

From the continuity equation, the volume flow rate in the channel, Q is given by $A\bar{u}$. Therefore, equation A-5 can be modified to give a relationship between the pressure difference between two ends of the channel and the volume flow rate in it.

$$Q = -\frac{2Ad^2}{\mu C}\frac{\Delta p}{L} \tag{A-6}$$

Equation A-6 can also be expressed as shown in equation 3-7 by assuming that the pressure gradient, dp/dx, along the channel is constant equal to Δp/L in equation A-6.

The friction coefficient is a function of the cross sectional geometry of the channel and for a rectangular cross-section, the friction constants are given in *Table A-1* for cross-sections of different aspect ratios b/a (White, 1999).

b/a	0	0.05	0.1	0.125	0.167	0.25	0.4	0.5	0.75	1.0
C	96.00	89.91	84.68	82.34	78.81	72.93	65.47	62.19	57.89	56.91

Table A-1 *The friction constants for a channel with a rectangular cross-section of different aspect ratios.*

For a circular channel, the friction constant is 64. Substituting this and an expression for the cross sectional area of the channel into equation 3-7 gives the well-known Hagen-Poiseuille equation for steady incompressible laminar flow in a channel of circular cross-section.

$$Q = -\frac{\pi d^4}{128\mu}\frac{\mathrm{d}p}{\mathrm{d}x} \tag{A-7}$$

APPENDIX B

A 40 mM solution of dichloroacetyl phenol red was prepared by stirring 28 mgs of phenol red with 10 μl of dichloroacetylchloride and 15 μl of triethylamine in 2 ml of acetonitrile for approximately 14 hours. The chemicals used were obtained from Aldrich. For use in the mixing experiments, the 40 mM stock solution was diluted with 1 ml acetonitrile and 2 ml 10 mM pH 5.5 phosphate buffer.

The second order rate constant for hydroxide ion induced hydrolysis is approximately 7×10^4 $M^{-1}s^{-1}$. This gives, for example, a half-time for hydrolysis of 100 μs in 0.1M NaOH. The rate constant for hydrolysis was measured at pH values from 4 to 8 in a Phillips PU 8720 UV/VIS spectrometer. The appearance of phenol red product was detected at 560 nm. The total hydrolysis rate is comprised of a component from neutral water and a component from hydroxide ion. The neutral water rate was subtracted from the hydroxide-induced values and the slope of the plot of the first order rate constants against hydroxide ion concentration is the second order rate constant for hydrolysis.